

In presenting this thesis in partial fulfillment of the requirements for an advanced degree at Idaho State University, I agree that the Library shall make it freely available for inspection. I further state that permission for extensive copying of my thesis for scholarly purposes may be granted by the Dean of the Graduate School, Dean of my academic division, or by the University Librarian. It is understood that any copying or publication of this thesis for financial gain shall not be allowed without my written permission.

Signature \_\_\_\_\_

Date \_\_\_\_\_

Copyright (2022) W. Brad Baxter

Environmental Change in Postglacial Alaska: a 14,000-year lacustrine record of water balance  
and nutrient cycling in the Matanuska-Susitna Valley

by

W. Brad Baxter

A thesis

submitted in partial fulfillment

of the requirements for the degree of

Master of Science in the Department of Geosciences

Idaho State University

Spring 2022

To the Graduate Faculty:

The members of the committee appointed to examine the thesis of W. BRAD BAXTER find it satisfactory and recommend that it be accepted.

---

Dr. Bruce Finney,  
Major Advisor

---

Dr. Glenn Thackray,  
Committee Member

---

Dr. Katherine Reedy,  
Graduate Faculty Representative

## *Acknowledgements*

Contributions to this project from the following individuals and grants not only made this project possible but created an enjoyable research environment. In acknowledgement, I would like to thank:

Dr. Bruce Finney, Idaho State University Departments of Geosciences and Biology, for being a supportive graduate advisor who was invested in this project and always happy to answer my questions. Thanks for being readily available to discuss project details, lending continued support throughout this process, and for fostering an enjoyable learning environment in the lab and in the field.

Dr. Lesleigh Anderson, USGS Geoscience and Environmental Change Science Center, Denver CO, for being a helpful collaborator who offered feedback on my ideas and project deliverables, and for keeping us organized in the lab and in the field.

Dr. Mark Shapley, Continental Scientific Drilling Facility, University of Minnesota, for teaching me fundamental skills in limnological investigation and for giving thoughtful feedback throughout this process.

Dr. Million Hailemichael, Idaho State University, for analyzing the samples to provide the data needed for this analysis, and for instructing me in various lab procedures.

Dr. Glenn Thackray and Dr. Katherine Reedy of Idaho State University for being supportive and invested committee members.

Richard Pelltier, USGS, for teaching me many useful lab and GIS procedures, and for making great contributions to the sample preparation required for this project.

Laura Strickland, USGS, for identifying sediment macrofossils, sampling materials for radiocarbon dating, and for teaching me the basics of macrofossil ID and sampling.

The U.S. Geological Survey Climate Research and Development Program through the Past Perspectives of Water in the West Project for primary funding of this project. The Geslin Research Award for funding my field work and lab analyses, and the Center for Ecological Research and Education for funding my lab work and isotope analyses.

Lastly, I would like to thank my family for their encouragement throughout this process, and all my friends at ISU for creating a fun experience and for reminding me to get out of the lab once and a while.

## TABLE OF CONTENTS

<b>List of Figures.....</b>	<b>vi</b>
<b>List of Tables.....</b>	<b>vii</b>
<b>List of Symbols.....</b>	<b>viii</b>
<b>Thesis Abstract.....</b>	<b>ix</b>
<b>i. Introduction.....</b>	<b>1</b>
<b>ii. Geologic Background.....</b>	<b>2</b>
<b>iii. References Cited in Introduction.....</b>	<b>5</b>
<b>Chapter 1: Postglacial hydroclimatic change in southern Alaska.....</b>	<b>7</b>
<b>1. Abstract.....</b>	<b>7</b>
<b>1.1 Introduction.....</b>	<b>7</b>
1.1.1 Paleohydrological Application of Finger Lake $\delta^{18}\text{O}$ .....	8
<b>1.2 Study Location.....</b>	<b>10</b>
<b>1.3 Methods.....</b>	<b>11</b>
1.3.1 Sediment Sampling and Chronology.....	11
1.3.2 Stable Isotope Analysis.....	12
<b>1.4 Results.....</b>	<b>13</b>
1.4.1 Sediment Description.....	13
1.4.2 Sedimentation and Geochronology.....	14
1.4.3 Isotopic Compositions.....	14
<b>1.5 Discussion.....</b>	<b>15</b>
1.5.1 Deglaciation and Climate Reversals in the Matanuska-Susitna Valley (13.7-9 ka BP)...	15
1.5.2 Cyclone-Modulated changes in Water Balance.....	20
1.5.3 Hydroclimatic Variability through the Middle Holocene (2-8 ka BP).....	23
1.5.4 Climate in the Late-Holocene (2 ka BP - Present).....	26
<b>1.6 Conclusion.....</b>	<b>28</b>
<b>1.7 Figures.....</b>	<b>30</b>
<b>1.8 References Cited in Chapter 1.....</b>	<b>38</b>

<b>Chapter 2: Ecological recovery in postglacial Alaska.....</b>	<b>44</b>
<b>2. Abstract.....</b>	<b>44</b>
<b>2.1 Introduction.....</b>	<b>45</b>
<b>2.2 Methods.....</b>	<b>46</b>
2.2.1 Study Location.....	46
2.2.2 Sediment Sampling and Chronology.....	47
2.2.3 Organic Isotope ( $\delta^{13}\text{C}$ , $\delta^{15}\text{N}$ ) Analysis.....	47
<b>2.3 Results.....</b>	<b>48</b>
2.3.1 Sediment Description.....	48
2.3.2 Sedimentation and Geochronology.....	49
2.3.3 Isotopic Compositions.....	50
<b>2.4 Discussion.....</b>	<b>50</b>
2.4.1 Climatic Influence on Lake Carbon Cycling.....	51
2.4.2 Nitrogen Cycling.....	52
2.4.3 Late-glacial Productivity.....	53
2.4.4 Carbon and Nitrogen Cycling throughout the Holocene.....	56
2.4.5 Changes in Loess Supply Inferred from Sediment Lithology.....	58
<b>2.5 Conclusion.....</b>	<b>60</b>
<b>2.6 Figures.....</b>	<b>62</b>
<b>2.7 References Cited in Chapter 2.....</b>	<b>70</b>
<b>Appendix.....</b>	<b>74</b>
A. LOI Tables.....	74
B. Carbonate $\delta^{18}\text{O}$ and $\delta^{13}\text{C}$ Tables.....	78
C. Sediment organic $\delta^{15}\text{N}$ and $\delta^{13}\text{C}$ Tables.....	81
D. Age Data.....	86

List of Figures

Chapter 1. Postglacial hydroclimatic change in southern Alaska: a carbonate isotope perspective on water balance over the last 14,000 years

Figure 1 Map of the Study Lake..... 30  
Figure 2 Finger Lake  $\delta^2\text{H}$  vs.  $\delta^{18}\text{O}$ ..... 31  
Figure 3 Downcore Sediment Characteristics..... 33  
Figure 4 Sediment Age Model..... 34  
Figure 5 Time Series of Carbonate Isotope Compositions..... 35  
Figure 6 Comparison of Finger Lake  $\delta^{18}\text{O}$  with Other Records..... 36  
Figure 7 Carbonate Isotopes for the Medieval Warm Period and Little Ice Age..... 37

Chapter 2. Ecological recovery in postglacial Alaska: a sedimentary isotope record of productivity and catchment processes following deglaciation of the Matanuska-Susitna Valley

Figure 1 Map of the Study Lake..... 62  
Figure 2 Downcore Sediment Characteristics..... 63  
Figure 3 Sediment Age Model..... 65  
Figure 4 Organic Isotope vs. C/N Regressions..... 66  
Figure 5 Time Series of Organic Sediment Proxies..... 67  
Figure 6 Time Series Comparison of Organic and Carbonate Isotopes..... 68  
Figure 7 Core Lithology and Fluxes..... 69

List of Tables

Chapter 1. Postglacial hydroclimatic change in southern Alaska: a carbonate isotope perspective on water balance over the last 14,000 years

Table 1 Age Control Through the Core..... 32

Chapter 2. Ecological recovery in postglacial Alaska: a sedimentary isotope record of productivity and catchment processes following deglaciation of the Matanuska-Susitna Valley

Table 1 Age Control Through the Core..... 64

## List of Symbols

$\delta$	Lowercase Delta
$\text{‰}$	Permil

Environmental Change in Postglacial Alaska: a 14,000-year lacustrine record of water balance  
and nutrient cycling in the Matanuska-Susitna Valley

Thesis Abstract–Idaho State University (2022)

Stable isotope analysis of lake sediments was applied to provide a record of environmental changes in south-central Alaska following deglaciation from the Last Glacial Maximum. This record reveals unique insights on climate variability from the water-balance perspective, including abrupt climate reversals in the late-glacial period, with water supply lowest in the early Holocene and generally increasing towards the present. Significant Holocene changes in regional moisture supply correspond with inferred changes in atmospheric circulation over the North Pacific. These alterations in water balance appear to be highly influential on nutrient sourcing to the lake basin through time, indicating the impact of climate change on carbon and nitrogen exchanges between terrestrial and aquatic systems.

Key Words:

Stable Isotope Analysis

Limnology

Climate Variability

Glaciation

Water Balance

Aleutian Low

Nutrient Cycling

## *i. Introduction.*

Climate evolution following deglaciation from the Last Glacial Maximum featured dynamic regional variability recently superimposed on global warming trends. Paleoclimate records across North America exhibit regional heterogeneity in ecological responses to climate forcings throughout the postglacial period, complicating our understanding of climate variability. The complex geography of Alaska combined with highly variable seasonal insolation and a considerable latitudinal gradient together create a suite of unique conditions making local responses to climate forcing quite variable. Records across Alaska demonstrate varied ecological responses to climate events including millennial-scale reversals (Kaufman et al., 2004; Kokorowski et al., 2008; Yu et al., 2008; Bigelow et al., 2019) and multidecadal-scale oscillations (e.g., Aleutian Low cyclonic system, Anderson et al., 2005; Bailey et al., 2018) throughout the late Quaternary Period. Despite their environmental influence across the North Pacific and western North America, the spatiotemporal character of these events is overall poorly constrained in sparse records of inconsistent chronological control. Adequate spatial coverage of thoroughly dated, multiproxy climate records is lacking but essential for characterizing regional climate evolution. Furthermore, in order to address events of different timing and character, suitable records must be sensitive to low- (millennial-scale) and high-frequency (decadal-scale) climate variability. In response, this thesis produces a high-resolution, multiproxy record spanning the postglacial interval for the Matanuska-Susitna Valley of south-central Alaska.

Climate reconstructions for this record rely on stable isotope analysis of carbonate sediments from Finger Lake (61°36'18"N, 149°16'53"W), an aquatically productive lake that produces authigenic carbonate sediments. Carbonate isotopes of  $\delta^{18}\text{O}$  and  $\delta^{13}\text{C}_{\text{DIC}}$  are used as

proxies of paleohydrology from a water balance perspective, and sedimentary organic  $\delta^{15}\text{N}$  and  $\delta^{13}\text{C}_{\text{org}}$  are applied as proxies of nutrient cycling and productivity in the lake basin and catchment. Together, these isotopic compositions are compared with sediment C/N ratios, and calcite and organic matter content to gain a holistic perspective on paleoenvironmental change in south-central, coastal Alaska where no similar record exists. Discussion of the Finger Lake climate record is organized into 2 chapters: Chapter 1 concerns the carbonate isotope record and climatic insights offered by  $\delta^{18}\text{O}$  and  $\delta^{13}\text{C}_{\text{DIC}}$ , and Chapter 2 explores the organic isotope record and environmental information gained from  $\delta^{15}\text{N}$ ,  $\delta^{13}\text{C}_{\text{org}}$ , C/N ratios, and sediment organic and calcium carbonate content.

## ***ii. Geologic Background.***

Lake sediments from the Matanuska-Susitna Valley are advantageous for producing extensive, high-resolution (decadal-centennial scale) climate reconstructions due to the basin's hydrogeology and geomorphological history. Groundwater-bedrock interactions in the valley create hard water conditions in many lakes of the valley, which may become supersaturated in carbonate-forming ions by various processes (Kelts & Hsü, 1978). Upon supersaturation, cations of  $\text{Ca}^{2+}$  or  $\text{Mg}^{2+}$  dissolved in lake water bond with anions of  $\text{CO}_3^{2-}$  and  $\text{HCO}_3^-$  to form carbonate precipitates such as calcite or aragonite, which are collectively termed authigenic carbonates (Last, 1982). Authigenic calcite ( $\text{CaCO}_3$ ), or micrite (loosely referred to here as carbonate), forms in isotopic equilibrium with the lake water, indiscriminately locking the oxygen isotopic compositions of lake water and carbon isotopic compositions of dissolved inorganic carbon into carbonate precipitates (Shapley et al., 2005; Horton et al., 2015). Consequently, authigenic carbonate lake sediment preserves historical lake  $\delta^{18}\text{O}$  and inorganic

$\delta^{13}\text{C}$  roughly at the time the sediments are deposited and are thus archived in a sedimentary sequence. These former lake water isotopic compositions can be quantified with mass spectrometry and are hence, useful proxies of water conditions in paleoclimate analysis.

Previous studies have applied lacustrine carbonates to reconstruct the isotopic composition of lake water as proxies of climate (e.g., Stuiver, 1970; Leng & Marshall, 2004; Anderson et al., 2005). The hydrogeology of the Matanuska-Susitna Valley is known to support the precipitation of authigenic carbonates in many of its lakes, as calcium bicarbonate ion loading of groundwaters can be found in many lakes of the valley (Moxham and Eckhart, 1956). The presence of carbonate-precipitating lakes with varying hydrologies in the Matanuska-Susitna Valley allows for reconstructions and comparisons of historical lake-water isotopic compositions with relevance to past precipitation, evaporation, and atmospheric circulation (Anderson et al., 2016). Given that most of these lakes formed during deglaciation, their sediments provide extensive isotope histories that often reach deglaciation in the late-Pleistocene.

The broad availability of extensive lacustrine carbonate records in the Matanuska-Susitna Valley permits investigation of climate variability throughout the late Quaternary Period, including local expressions of events consistent with the recognized chronologies of the Younger Dryas stadial and Holocene Thermal Maximum, which are poorly characterized across Alaska (Kaufman et al., 2004; Kokorowski et al., 2008). Additionally, the sedimentation rates of many lakes in the valley enable high resolution records capable of detecting high-frequency climate variability throughout the Holocene. The high-latitude location of the Matanuska-Susitna Valley, confined latitudinally by the Talkeetna mountains to the north and Chugach mountains to the south, and proximity to the Gulf of Alaska combine to subject the region to a complex suite of climate forcings, making the climatic history of the region important to characterize for

elucidating local responses to synoptic climate systems. Finger Lake was chosen for coring in this study because of its carbonate-bearing quality and closed-basin hydrology which results in an evaporation-sensitive isotopic signal and specific paleohydrological insights that are explored in Chapter 1.

### *iii. References Cited in Introduction and Background.*

- Anderson, L., Abbott, M., Finney, B., and Burns, S., 2005, Regional atmospheric circulation change in the North Pacific during the Holocene inferred from lacustrine carbonate oxygen isotopes, Yukon Territory, Canada: Quaternary Research, doi: 10.1016/j.yqres.2005.03.008.
- Anderson, L., Berkelhammer, M., Barron, J.A., Steinman, B.A., Finney, B.P., and Abbott, M.B., 2016, Lake oxygen isotopes as recorders of North American Rocky Mountain hydroclimate: Holocene patterns and variability at multi-decadal to millennial time scales: Global and Planetary Change, v. 137, p. 131–148, doi:10.1016/j.gloplacha.2015.12.021.
- Bailey, H. L., et al., 2018, Holocene atmospheric circulation in the central North Pacific: A new terrestrial diatom and  $\delta^{18}\text{O}$  dataset from the Aleutian Islands: Quaternary Science Reviews, v. 194, p. 27-38, doi:10.1016/j.quascirev.2018.06.027.
- Bigelow, N.H., Reuther, J.D., Wallace, K.L., Saulnier-Talbot, É., Mulliken, K., and Wooller, M.J., 2019, Late-Glacial Paleocology of the Middle Susitna Valley, Alaska: Environmental Context for Human Dispersal: Frontiers in Earth Science, v. 7, p. 43, doi:10.3389/feart.2019.00043.
- Horton, T. W., Defliese, W. F., Tripathi, A. K., & Oze, C., 2016, Evaporation induced  $^{18}\text{O}$  and  $^{13}\text{C}$  enrichment in lake systems: A global perspective on hydrologic balance effects: Quaternary Science Reviews, v. 131, p. 365-379.
- Kaufman, D. S., Ager, T. A., Anderson, N. J., Anderson, P. M., Andrews, J. T., Bartlein, P. J., ... & Wolfe, B. B., 2004, Holocene thermal maximum in the western Arctic (0–180 W): Quaternary Science Reviews, v. 23(5-6), p. 529-560.
- Kelts K., Hsü K.J., 1978, Freshwater Carbonate Sedimentation: Springer, New York, NY, doi: 10.1007/978-1-4757-1152-3\_9
- Kokorowski, H. D., Anderson, P. M., Mock, C. J., & Lozhkin, A. V., 2008, A re-evaluation and spatial analysis of evidence for a Younger Dryas climatic reversal in Beringia: Quaternary Science Reviews, v. 27(17-18), p. 1710-1722.
- Lasher, G. E., Abbott, M. B., Anderson, L., Yasarer, L., Rosenmeier, M., & Finney, B. P., 2021, Holocene hydroclimatic reorganizations in northwest Canada inferred from lacustrine carbonate oxygen isotopes: Geophysical Research Letters, v. 48(16), p. e2021GL092948.
- Laws, E. A., Popp, B. N., Bidigare, R. R., Kennicutt, M. C., & Macko, S. A., 1995, Dependence of phytoplankton carbon isotopic composition on growth rate and  $[\text{CO}_2]_{\text{aq}}$ : theoretical considerations and experimental results: Geochimica et cosmochimica acta, v. 59(6), p. 1131-1138.

- Leng, M. J., & Marshall, J. D., 2004, Palaeoclimate interpretation of stable isotope data from lake sediment archives: *Quaternary Science Reviews*, v. 23(7-8), p. 811-831.
- Moxham, R.M., and Eckhart, R.A., 1956, Marl Deposits in the Knik Arm Area Alaska: *Geological Survey Bulletin* 1039-A, p. 4–17.
- Shapley, M., Ito, E., and Donovan, J., 2005, Authigenic calcium carbonate flux in groundwater-controlled lakes: Implications for lacustrine paleoclimate records: *Geochimica et Cosmochimica Acta*, v. 69, p. 2517–2533, doi: 10.1016/j.gca.2004.12.001.
- Stuiver, M., 1970, Oxygen and carbon isotope ratios of fresh-water carbonates as climatic indicators: *Journal of Geophysical Research*, v. 75(27), p. 5247-5257.
- Yu, Z., Walker, K.N., Evenson, E.B., and Hajdas, I., 2008, Lateglacial and early Holocene climate oscillations in the Matanuska Valley, south-central Alaska: *Quaternary Science Reviews*, v. 27, p. 148-161, doi:10.1016/j.quascirev.2007.02.020.

***Chapter 1: Postglacial hydroclimatic change in southern Alaska: a carbonate isotope perspective on water balance over the last 14,000 years***

***1. Abstract.***

Regional hydroclimatic adjustments through time are becoming increasingly important to characterize for better understanding modern climate. The isotopic compositions of carbonate lake sediment can be useful tools for paleohydrological reconstruction, however, carbonate lake records are often discontinuous in Alaska. This study explores climate variability throughout the postglacial period by providing the longest continuous  $\delta^{18}\text{O}$  record for a carbonate P–E lake in south central Alaska. Finger Lake, in the Matanuska-Susitna Valley, contains a ~13,700-year record that reveals an erratic climate following deglaciation, including abrupt reversals during the Pleistocene- Holocene transition including local climate expressions correlative with the Bølling-Allerød warming, the Younger Dryas chronozone, and the Holocene Thermal Maximum. A potential reorganization of atmospheric circulation ~10 ka seemingly initiates changes in water balance that continue throughout the Holocene and appear to be modulated by cyclonic activity over the North Pacific. A sustained decrease in  $\delta^{18}\text{O}$  that initiated ~2000 AD reflects a period of increased P–E in south-central Alaska likely enhanced by Aleutian Low intensification.

***1.1 Introduction.***

The unknown impacts associated with amplified warming at high latitudes (Graversen et al., 2008; Cohen et al., 2014) and increased cyclonic alteration of moisture supply in the North Pacific (Winski et al., 2017) make hydroclimatic variability across the North Pacific a topic of

increasing interest (Osterberg et al., 2017; Broadman et al., 2020; Lasher et al., 2021). Records of hydroclimatic adjustments through time provide insights on potential hydrological controls and forcing mechanisms and are therefore crucial for characterizing the spatiotemporal nature of regional climate change. Carbonate bearing lakes offer detailed hydrological proxies and are commonly sought for investigation of hydroclimatic variability (eg., Anderson et al., 2005; 2016; Gonyo et al., 2012; Steinman et al., 2016), but the breadth of these reconstructions are often limited by the distribution and ages of such sites. Records across the North Pacific region document notable climate events from late-Wisconsinan throughout the postglacial period (Fisher et al., 2008; Davies et al., 2011), but these records are rarely continuous in Alaska (Kaufman et al., 2003; Kokorowski et al., 2008), leaving the regional influence of noteworthy climate events poorly constrained.

This study applies carbonate isotope analysis on a lake formed during the last deglaciation to reconstruct changes in hydroclimate over the last ~ 13.7 ka (13,7000 cal. yr before present (BP)) in south-central Alaska. Since carbonate lakes are relatively rare in Alaska, this record offers the longest continuous  $\delta^{18}\text{O}$  sequence for an evaporation-sensitive coastal lake, Finger Lake (61°36'18"N, 149°16'53"W) in the Matanuska-Susitna Valley (Figure 1), enabling a water balance perspective on changes in hydroclimate throughout the postglacial.

### *1.1.1. Paleohydrological Application of Finger Lake $\delta^{18}\text{O}$ .*

The integrity of Alaska's glaciated mountains, fjords, and densely vegetated coastal ecosystems are highly sensitive to changes in hydroclimate, which are traceable through the isotopic compositions of authigenic lacustrine carbonate (Stuiver, 1970; Leng & Marshall, 2004). The preservation of lake-water  $\delta^{18}\text{O}$  and dissolved inorganic carbon  $\delta^{13}\text{C}$  ( $\delta^{13}\text{C}_{\text{DIC}}$ ) in carbonate precipitates archives hydrological changes throughout the lake history (Horton et al., 2016).

However, as previous studies recognize, the paleoenvironmental information provided in carbonate  $\delta^{18}\text{O}$  is dependent on lake hydrology (Ito, 2001; Anderson et al., 2016; Kjellman et al., 2022). Lake basins with minimal outflow and prolonged water retention are subjected to evaporative losses and  $\delta^{18}\text{O}$  enrichment in residual water by fractionation (Leng & Marshall, 2004). The  $\delta^{18}\text{O}$  of endogenic carbonate from these lakes is directly linked with changes in water balance (Horton et al., 2016), and reflects source water compositions elevated by evaporative enrichment, or changes in P–E (Anderson et al., 2016). Contemporary  $\delta^2\text{H}$  and  $\delta^{18}\text{O}$  compositions in Finger Lake define a water line ( $\delta^2\text{H} = 4.7 * \delta^{18}\text{O} - 52$ ) that deviates to the right of the Global Meteoric Water Line (GMWL,  $m=8$ , Figure 2), indicating Finger Lake is sensitive to evaporative enrichment of  $\delta^{18}\text{O}$  (Anderson et al., 2016) from its source values.

Lake  $\delta^{18}\text{O}$  baselines upon which evaporative processes alter, are dictated by a culmination of environmental and fractionation controls on isotopic composition, beginning with water source (Ito, 2001). Lakes receive recharge from precipitation either directly through lake surface receipt and runoff or indirectly from groundwater. The isotopic baseline of lake water can therefore largely be attributed to the  $\delta^{18}\text{O}$  of precipitation ( $\delta^{18}\text{O}_{\text{precip}}$ ). Variance in  $\delta^{18}\text{O}_{\text{precip}}$  is expected with season due to temperature controls on evaporation and condensation events along moisture transport trajectories (Dansgaard, 1964). Therefore, the seasonal contributions to total annual precipitation and the isotopic compositions of local precipitation can greatly affect the isotopic baseline for lake water.

A local meteoric water line (LMWL) composed from an event-based precipitation dataset spanning 13 years in Anchorage by Bailey et al. (2019), exhibits precipitation trends slightly altered ( $y = 7.2 x - 11$ ) from global meteoric values. In this region, contributions to annual precipitation are largest in the warm season (May–September) which average 56% ( $n=69$ ) of the

annual total (WRCC, 2009). The average meteoric  $\delta^{18}\text{O}$  input (non-weighted) to the lake is around  $-15.5\text{‰}$  (Bailey et al., 2019),  $\sim 1.5\text{‰}$  below the period of record mean for Finger Lake of  $-13.00 \pm 0.04\text{‰}$  indicating Finger Lake water is enriched from source compositions. The enriched Finger Lake  $\delta^{18}\text{O}$  in combination with its high deviance from meteoric water compositions (Figure 2) indicates evaporative enrichment is likely driven by extended water retention in the lake basin (Leng & Marshall, 2004). Variations in Finger Lake  $\delta^{18}\text{O}$  therefore largely reflect changes in the P–E balance through time.

Consistent with  $\delta^{18}\text{O}$  modification, fractionation associated with degassing of  $\text{CO}_2$  during evaporation can enrich residual DIC and cause  $\delta^{13}\text{C}_{\text{DIC}}$  to vary in phase with  $\delta^{18}\text{O}$  in evaporative lake basins (Horton et al., 2016). The presence or absence of covariation throughout the sediment record may therefore offer a metric for hydrological controls on  $\delta^{13}\text{C}_{\text{DIC}}$ . The  $\delta^{18}\text{O}$  vs.  $\delta^{13}\text{C}_{\text{DIC}}$  regression (Figure 2) displays a weak positive relationship for the period of record ( $r^2=0.25$ ,  $n=204$ ), but  $\delta^{13}\text{C}_{\text{DIC}}$  largely covaries with  $\delta^{18}\text{O}$  during many visible excursions. Deviations from the covariation trend may reflect additional modification to  $\delta^{13}\text{C}_{\text{DIC}}$  irrespective of  $\delta^{18}\text{O}$  including fractionation from biological  $\text{CO}_2$  uptake, and contributions to the DIC pool including carbonate saturation and  $\text{CO}_2$  respired in the watershed (Gu et al., 1998; Finney et al., 2012; Horton et al., 2016). Given these controls on carbonate isotope compositions, the following sections explore post-glacial climate throughout the Finger Lake sedimentary sequence.

## ***1.2 Study Location.***

The Matanuska-Susitna Valley in south-central Alaska is situated adjacent to the Gulf of Alaska and confined latitudinally by the Talkeetna and Chugach mountains, subjecting it to maritime climate influence and topographical constraints. The valley displays a glacial overprint

with surficial deposits remnant of Quaternary glacial outwash and diamicton, which act as a productive aquifer and permeable subsurface (Kikuchi, 2013). Groundwater generally flows from the Talkeetna and Chugach Mountain foothills along a southwestward water table gradient to the Cook Inlet (Moran & Solin, 2006; Kikuchi, 2013). Subterranean flow interacts with calcareous deposits in the valley leading to carbonate ion loading of groundwater, high in calcium bicarbonate-type solutes that match many lakes in the valley, indicating the importance of groundwater in lake recharge (Moran & Solin, 2006). Inflow of carbonate ion-rich groundwater generates conditions in groundwater-fed lakes that continuously fuel the precipitation of endogenic carbonates (Moxham & Eckhart, 1956). Furthermore, many lakes in the valley were formed in lowlands by glacial retreat (Kopczynski et al., 2017), producing sediments dating back to the late-glacial period. Finger Lake is framed by glacial and alluvial deposits (Kikuchi, 2013) and has a large volume ( $6,934,634 \text{ m}^3$ ) basin with an average depth of 4.7 m and surface area of 146.5 ha ( $1,465,000 \text{ m}^2$ , ADFG, 2013) that produces micrite (authigenic lime mud) sediments. The sedimentation of carbonate and the late-glacial formation of Finger Lake create a limnological record of sufficient temporal extent and resolution to evaluate hydroclimatic change of varying frequency throughout the post-glacial period.

### ***1.3 Methods.***

#### *1.3.1 Sediment Sampling and Chronology.*

A 664 cm-long sediment core was taken through the ice in April 2016, on a carbonate-bearing shelf of Finger Lake in  $\sim 1.6$  m water depth (Figure 1). A piston-corer with polycarbonate tubing was used to preserve the sediment-water interface and upper core stratigraphy. Deeper sediments were cored with a Livingstone piston-corer in 7 overlapping drives. Sediment cores

were scanned for magnetic susceptibility, sectioned, photographed, and described. The cores were then analyzed at regular increments for compositional properties including water content, bulk density, and organic and calcium carbonate content quantified by the loss-on-ignition (LOI) method at 550° and 950°C. Age control for the sedimentary sequence places isotopic excursions into a temporal context and is informed by  $^{210}\text{Pb}$  dating in the upper sediments and 10 AMS  $^{14}\text{C}$  dates on terrestrial macrofossils and charcoal sampled throughout the sediment profile and calibrated using IntCal 13 by Reimer et al. (2013). Sediment ages were modeled to non-dated depths using linear interpolation that was referenced with the Bayesian age-depth interpolation developed by Blaauw and Christen (2011).

### 1.3.2 Stable Isotope Analysis.

Sedimentary isotopic compositions were quantified with a Delta V Advantage Stable Isotope Ratio Mass Spectrometer (IRMS) in the Idaho State University Stable Isotope Laboratory. Results are presented in delta notation ( $\delta$ ), given by the equation  $\delta \text{ element } (\text{‰}) = [(R \text{ sample} - R \text{ standard}) / R \text{ standard}] * 1000$  where, for the element of interest, “R” is the ratio of heavy to light isotopes (e.g.,  $^{18}\text{O}/^{16}\text{O}$ ), and “standard” is the Vienna Peedee Belemnite (VPDB) for O and C. Delta values are reported in deviations permil (‰) from the standards. In preparation for analysis of O and inorganic C isotopes, 2 cm<sup>3</sup> volumetric samples were sieved at 30  $\mu\text{m}$  with high-purity deionized water to isolate the fine-grained fraction for analysis. Samples were then homogenized and reacted with phosphoric acid to measure isotopic ratios from the CO<sub>2</sub> product with a GasBench II front end coupled to the IRMS.

## ***1.4 Results.***

### *1.4.1 Sediment Description.*

The Finger Lake sediments consist mainly of varying proportions of CaCO<sub>3</sub> to organic matter, together accounting for ~28 to 87% of the total sediment composition with residual mineral content constituting ~13 to 72% throughout the lake record. Core stratigraphy features a thin bedded (3-10 cm) strata of white-pale yellow carbonate layers interleaved with gray-grayish brown to olive brown-black organic layers with diffuse to indistinct contacts throughout the core (0-664 cm). Some notable breaks in the layered bedding occur as more massive, homogeneous sections at 228-242 cm, 351-358 cm, and 380-387 cm, all ranging from dark gray to very dark grayish brown in color. A spike in magnetic susceptibility at 390 cm (Figure 3) indicates the presence of a cryptotephra within a 7 cm dark gray band. Radiocarbon dating through this section of the core places the tephra within the timing uncertainty of the Watana Tephra (~3900 <sup>14</sup>C yr BP; Wallace et al., 2014). The sediment color slowly transitions downcore from a general green-gray chroma from 37-201 cm, to darker grays down to 290 cm where the core transitions to gray-brown until 334 cm. Below this level, sediments darken to very dark gray before transitioning to lighter shades of brown-tan from 509-557 cm where sediments continue to lighten downcore to tan-white before ending in gray gravelly sand at the core base.

Throughout the core, variability in LOI data reveals compositional changes in coherence with the visual descriptions. Sediment organic composition ranges from 5 to 56.8% and correlates with intervals of darker color. CaCO<sub>3</sub> content ranges from 5 to 80% and is highest on average in the lower 108 cm where color ranges from pale-yellow to white. Organic content is generally higher between 250 and 556 cm with mean percent organic content averaging 31.7%, but falling to 15.1% from 0-250 cm and 13.8% from 556-664 cm. Conversely, CaCO<sub>3</sub> content

decreases from 50% at 0-250 cm, to 26.9% at 250-556 cm, before increasing to 53.3% from 556-664 cm. The transition to higher organic matter content in the mid-section of the core is reflected by darkened color and less evident contacts with carbonate laminations. The heightened CaCO<sub>3</sub> content above and below the organic-rich middle section are consistent with their overall lighter sediment color. LOI residuals reflect the mineral and opal content of the sediment and vary ~20-35% without any obvious downcore trends. Terrestrial macrofossils sampled throughout the Livingstone drives reflect the prevalence of *Alnus sp.*, *Betula sp.*, *Picea mariana*, and *Picea glauca* in the catchment. Aquatic macrofossils are abundant throughout the core and include leafy plant material and trace ostracode remains and *Chara spp. oogonia* and stem casts.

#### 1.4.2 Sedimentation and Geochronology.

The age model displays considerable changes in sedimentation rate downcore (Figure 4). Sedimentation rate is overall highest in the upper 200 cm (~1,900 years), with recent years dated by <sup>210</sup>Pb accumulation demonstrating the highest sedimentation rates averaging at 0.14 cm/year that decrease downcore to the lowest rates below 500 cm (~7 ka) ranging from 0.031 to 0.021 cm/year in the oldest sediments. A basal age sample could not be obtained, and the basal age was extrapolated from the age model to cal. 13.7 ka from the nearest AMS date of 13,100 ± 220 cal. years BP (Table 1) to represent the latest time of deglaciation in this part of the valley.

#### 1.4.3 Isotopic Compositions.

Carbonate δ<sup>18</sup>O and δ<sup>13</sup>C<sub>DIC</sub> display both high-frequency variability and prolonged excursions throughout the lake history. δ<sup>18</sup>O values are significantly enriched above average meteoric compositions, with a mean of -13.0 ± 0.1‰ throughout the period of record. Above 100 cm, δ<sup>18</sup>O mainly falls below the record mean reaching a minimum value of -14.4‰ at 72 cm. Overall δ<sup>18</sup>O values between 100 cm to ~350 cm display intermediate values, then largely exceed

the record mean between 350 cm to 660 cm but subsequently decline, reaching the record minimum of -14.4‰ at 664 cm.  $\delta^{13}\text{C}_{\text{DIC}}$  remains below the record mean of  $2.37 \pm 0.1\text{‰}$  from 0-100 cm and 600-664 cm while mostly enriched above the record mean from 100-490 cm and displaying variable oscillations between 490-600 cm. As discussed,  $\delta^{13}\text{C}_{\text{DIC}}$  and  $\delta^{18}\text{O}$  show moderate positive correlation.

## ***1.5 Discussion.***

### *1.5.1 Deglaciation and Climate Reversals in the Matanuska-Susitna Valley (13.7-9 ka BP).*

The sedimentary sequence provides a detailed record of hydroclimatic transitions following the Wisconsinan. The presence of coarse basal sediments in Finger Lake are interpreted as glaciolacustrine deposits and suggest Finger Lake formed in the wake of glacial retreat, receiving input from a proximal glacier. Finger Lake is located slightly north of the Matanuska-Knik suture zone inferred from clast provenance (Kopczynski et al., 2017), and was likely formed by a slowly retreating Matanuska lobe thought to collapse in place, forming many stagnation deposits and kettle lakes in the valley (Kopczynski et al., 2017). The age of basal deposits in Finger Lake is extrapolated to 13.7 ka (age uncertainty represented in Figure 4), which is generally consistent with the estimated time for glacial retreat from the valley lowlands and precedes the estimated entry of the Matanuska lobe to the Matanuska Valley between  $13,650 \pm 130$  cal. years BP and  $13,350 \pm 90$  cal. years BP, constrained by AMS ages on sedge seeds in the Matanuska Glacier Bog (Ager, unpublished data; Kopczynski et al., 2017). A basal age of 13.7 ka is further supported by planktonic foraminiferal records in the Gulf of Alaska, with the last documented increase of inferred freshwater input ending  $\sim 13.9$ -13.7 ka (Davies et al., 2011).

Isotopic compositions in the basal carbonates exhibit the lowest values in  $\delta^{18}\text{O}$  and  $\delta^{13}\text{C}_{\text{DIC}}$  for the period of record at -14.4‰ and -1.9‰ respectively (Figure 5). The low isotopic compositions likely reflect relatively high lake inflow from a depleted glacial meltwater source. However, groundwater samples throughout the valley influenced by the glacier-fed Matanuska River have  $\delta^{18}\text{O}$  values of -20.0 and -21.3‰ (Kikuchi, 2013). Therefore, the record minimum  $\delta^{18}\text{O}$  values, falling at the base of the core, display significant enrichment above glacial sources and even modern meteoric water. The basal  $\delta^{18}\text{O}$  therefore suggests that the lake's hydrology and hydroclimate conditions were such that evaporative enrichment became influential shortly after lake formation. Similarly, the low  $\delta^{13}\text{C}_{\text{DIC}}$  during lake formation likely reflects slight enrichment of the DIC pool from evaporation. Quickly following deglaciation in the valley, colonization of *Artemisia* and *Salix* shrubs and *Cyperaceae* is suggested by pollen accumulation in Hundred Mile Lake of the upper Matanuska Valley (Yu et al., 2008), and Hidden Lake of the Kenai Peninsula (Ager, 1983). The presence of these taxa but the persistence of cool temperatures and low percent organic matter of ~10% suggest local vegetation was likely constricted to a dwarf shrub and herb tundra.

Isotopic compositions rise following deglaciation, indicating the increasing effects of evaporation on the P–E water balance, likely reflecting a continuation of the climatic warming that deglaciated the valley. The warming trend falls within the late Bølling-Allerød interstadial chronology recognized across the Northern Atlantic (Dansgaard et al., 1993; Buizert et al., 2014). Impacts of this warming are expressed elsewhere in Alaska, including the Arctic Foothills north of the Brooks Range by relatively high peat production and *Populus* shrub abundance from ~15-13 ka (Mann et al., 2002), and the Gulf of Alaska as a shift in biogenic marine sediments to increased opal concentrations and  $\delta^{18}\text{O}$  depletions from glacial meltwater runoff from ~14.6-13

ka (Davies et al., 2011; Addison et al., 2012). In addition to the isotopic enrichments in Finger Lake, increasing *Betula* pollen in the upper Matanuska Valley by ~13 ka (Yu et al., 2008) and on the Kenai Peninsula as early as 13.7 ka, reflect warmer conditions than the preceding shrub-dominated period (Ager, 1983). These warming expressions in coastal southern Alaska coinciding with the Bølling-Allerød timing support the potential control of poleward heat transfer on abrupt climatic warming (Praetorius & Mix, 2014) across the Pacific and Atlantic basins.

The late-Pleistocene warming trend slowed by ~13.3 ka, followed by an abrupt reversal at ~12.3 ka featuring a ~1.6‰ depletion in  $\delta^{18}\text{O}$  by ~11.8 ka, which is generally tracked by  $\delta^{13}\text{C}_{\text{DIC}}$ . This negative excursion correlates with an ~2‰  $\delta^{18}\text{O}$  depletion in Hundred Mile Lake in the Matanuska Valley centered on ~12.3 ka (Yu et al., 2008). The similar  $\delta^{18}\text{O}$  depletion in Finger Lake and Hundred Mile Lake, which have vastly different hydrologies, suggest that a temperature induced control on  $\delta^{18}\text{O}$  is a probable mechanism. The depleted excursion suggests an intense cooling affected the region within the Younger Dryas chronozone, with age constraint provided from the nearest dated, underlying sample of  $13,102 \pm 220$  cal. years BP (terrestrial wood and leaf-like fragments, Table 1). The estimated timing of this local cooling is generally coincident with ecological expressions documented elsewhere in Alaska that coincide with the Younger Dryas chronozone (Kokorowski et al., 2008), with climatic cooling thought to be driven by thermohaline disturbance in the North Atlantic (Alley, 2000; Praetorius & Mix, 2014). The potentially late expression of this cooling event may be due to dating resolution and age uncertainties. Additionally, the Finger Lake record may under-represent the duration of the period due to sampling resolution and low sedimentation rates over this interval.

Cooling signals coincident with the Younger Dryas chronozone across Alaska were synthesized by Kokorowski et al. (2008) on a common high-resolution time scale to suggest the cooling featured asynchronous proxy expressions across the state. Records from the interior display *Artemisia* dominance and stream incision in the Arctic Foothills (Mann et al., 2002) suggesting increased aridity. Conversely, simultaneous moist conditions along the southern coast are indicated by muskeg and lacustrine pollen records yielding a continued dominance of *Betula* through this interval, with cold temperatures likely suppressing growth to a dwarf *Betula* tundra including ferns and sedges (Heusser, 1995; Ager, 1983). The potential coupling of the Younger Dryas stadial to a thermohaline disturbance may have made coastal areas in Alaska more sensitive to temperatures and inland areas more sensitive to moisture supply caused by altered sea surface temperatures (SSTs) in the North Pacific. Decreased SSTs and a southerly pressure gradient (Kokorowski et al., 2008) may have encouraged cooler summers in southern coastal Alaska. The negative poleward latent heat flux from a cooler North Pacific, linked with an enhanced high-pressure zone over the interior (Kokorowski et al., 2008), would have induced the dry conditions documented for interior Alaska (e.g., Abbott et al., 2000; Bigelow & Edwards, 2001) and increased Arctic Sea ice extent (Praetorius et al., 2018), cooling the Arctic by sea-ice albedo feedbacks (Gaglioti et al., 2017; Praetorius et al., 2018).

Amelioration from the regional cooling is evidenced by an  $\sim 3\%$  increase in  $\delta^{18}\text{O}$  over 1,100 years representing increasing effects of evaporative enrichment during the terminal-Pleistocene warming. This warming is thought to be driven by orbital variations increasing summer insolation (Berger, 1978; 1991; Yin & Berger, 2011), and leads to the record maximum  $\delta^{18}\text{O}$  of  $-10.7\%$  by  $\sim 10.6$  ka. This intense level of enrichment is likely a consequence of high summer temperature as a control on both elevated baseline  $\delta^{18}\text{O}$  and further enrichment by

enhanced water loss to evaporation, marking the local expression of the Holocene Thermal Maximum (HTM, *i.e.*, Hypsithermal). The HTM is best described as a period of increased summer temperature maxima (Bova et al., 2021), with temperatures modeled from pollen transfer functions in Icy Bay estimating summer temperatures 3°C greater than the coldest periods of the Holocene (Heusser et al., 1985). The increased summer temperatures would have enhanced lake surface evaporation, aided by drier conditions as suggested by lower lake levels for interior Alaska (Abbott et al., 2000; Barber & Finney, 2000) and the Yukon (Pompeani et al., 2012) which may have similarly affected south-central Alaska.

A hot HTM in southeastern Beringia is fairly coincident with HTM expressions concentrated in the northern regions as faunal range extensions (McCulloch & Hopkins, 1966; Nelson & Carter, 1987) and expansion of *Populus balsamifera* range (Brubaker et al., 1983; Edwards et al., 1985; Mann et al., 2002). However, the apparent peak in HTM enrichment in Finger Lake at ~11-10.2 ka is significantly shorter than the typical expressions of similar warming elsewhere in Alaska of 9-11 ka (Kaufman et al., 2004). Although dating resolution adds uncertainty (Figure 4), the sustained warmth is supported by peak insolation (Berger, 1978) persisting through the ~10 ka depletion (Figure 5), suggesting the duration of the HTM warm interval may be underrepresented in  $\delta^{18}\text{O}$  as a proxy of water balance. Since Finger Lake  $\delta^{18}\text{O}$  is sensitive not only to thermal changes but also changes in moisture supply, the depletion beginning ~10 ka likely reflects increased precipitation during the HTM in southern Alaska.

Increasing evidence suggests a significant shift in moisture supply occurred across the North Pacific in the early Holocene, consistent with the Finger Lake  $\delta^{18}\text{O}$  decline from earlier peak HTM values. The depletion likely reflects climatic wetting, as multiple lakes across the North Pacific display a significant shift in moisture supply in the early Holocene.  $\delta^{18}\text{O}$

fluctuations in Squanga Lake in the southwest Yukon (interpreted as an open-basin lake today) for the early Holocene (~11-10 ka) were nearly 3‰ higher than post-9 ka and display the onset of depletion at ~10 ka (Lasher et al., 2021). Similarly, an early Holocene  $\delta^{18}\text{O}$  depletion event is reported for Hundred Mile Lake (interpreted as an open basin) at ~10 ka (Yu et al., 2008). The comparatively enriched  $\delta^{18}\text{O}$  prior to ~10 ka in these throughflow lake systems suggest the early HTM may have been sufficiently arid for open-basin lakes to demonstrate an evaporative signal. The subsequent decreased adjustments to Squanga and Hundred Mile Lakes' mean isotopic compositions at ~10 ka suggest significant increases in water supply, which correlate with increased rates of water level rise inferred from peat slab accumulation in Jigsaw Lake on the Kenai Peninsula (Berg et al., 2022).

Climate wetting ~10 ka across the region is further supported by the proliferation of *Alnus* pollen ~9 to 10 ka in the Matanuska Valley (Yu et al., 2008), Susitna Valley (Bigelow et al., 2019), Kenai Peninsula (Ager, 1983; Broadman et al., 2020), and Prince William Sound (Heusser, 1995), and *Populus* appearance on the Kenai Peninsula by 10.3 ka (Ager, 1983). The regional wetting would have diluted the evaporative  $\delta^{18}\text{O}$  signal driven by HTM heat, potentially resulting in underrepresentation of the HTM duration in Finger Lake  $\delta^{18}\text{O}$ . The HTM depletion in  $\delta^{18}\text{O}$  is tracked by that of  $\delta^{13}\text{C}_{\text{DIC}}$  with the initiation of an ~1.5‰ decrease by 10.6 ka at the height of the HTM, likely reflecting an increased input of respired carbon from the watershed during increased inflow. Furthermore, climatic wetting appears to be a significant characteristic of the HTM across the North Pacific but brings to question the potential mechanism.

### *1.5.2 Cyclone-Modulated changes in Water Balance.*

Regional changes in moisture supply such as the inferred early Holocene wetting event in the North Pacific are thought to accompany cyclonic activity as a control on moisture source.

$\delta^{18}\text{O}$  from the Mount Logan ice core ( $\delta^{18}\text{O}_{\text{ML}}$ ) in Yukon, Canada incorporates high altitude meteoric  $\delta^{18}\text{O}$ , free from P–E influence, and is interpreted to reflect  $\delta^{18}\text{O}_{\text{precip}}$ . The effects of moisture trajectory on Rayleigh distillation (Rozanski et al., 2013) make  $\delta^{18}\text{O}_{\text{ML}}$  a useful proxy of changes in atmospheric circulation (Fisher et al., 2004; 2008). The Finger Lake  $\delta^{18}\text{O}$  depletion centered on  $\sim 10$  ka correlates with a  $\sim 3\%$  depletion in the  $\delta^{18}\text{O}_{\text{ML}}$  backed by high deuterium excess and Na accumulation, together indicating a shift to meridional circulation and distal moisture sourcing. Such transitions in atmospheric circulation are thought to be influenced by the intensity and position of the Aleutian Low (AL) pressure anomaly, where stronger AL intervals correspond with negative North Pacific pressure anomalies and eastward centering, typically featuring meridional transport of southerly air masses (Anderson et al., 2005; 2016; Fisher et al., 2008) to southern Alaska where orographic interactions with the coastal mountains increase winter precipitation. By contrast, anomalously weak AL intervals assume a westward centering and more zonal delivery of drier air masses to southern Alaska, decreasing moisture availability (Mock et al., 1998; Rodionov et al., 2007; Malcomb & Wiles, 2013). Therefore, the effects of AL intensity on regional moisture supply impact local water balance and can drive changes in Finger Lake  $\delta^{18}\text{O}$ .

Under anomalously strong AL intervals, increased moisture supplied by the delivery of southerlies to the Yukon and southern Alaska, or increased P–E in those regions, dilutes the evaporative  $\delta^{18}\text{O}$  signal in Finger Lake resulting in depletions. Conversely, anomalously weak AL intervals decrease P–E in the region and cause the effects of evaporation on Finger Lake  $\delta^{18}\text{O}$  to become more pronounced, leading to  $\delta^{18}\text{O}$  enrichment. Although the AL is mainly a winter-time anomaly (Rodionov et al., 2007), increased winter precipitation is likely a strong control on Finger Lake  $\delta^{18}\text{O}$  depletion since evaporation is negligible under ice cover and spring

snowmelt contributes significantly to groundwater and lake input. However,  $\delta^{18}\text{O}$  is likely driven not only by changes in the local P–E, but also adjustments to the input  $\delta^{18}\text{O}_{\text{precip}}$  driven by atmospheric circulation, similar to that determined for Sunken Island Lake by Broadman et al. (2020).  $\delta^{18}\text{O}$  shifts in evaporation-sensitive basins like Finger Lake are expected to accompany changes in moisture trajectories (Anderson et al., 2016), however, the positive relationship between Finger Lake  $\delta^{18}\text{O}$  and  $\delta^{18}\text{O}_{\text{ML}}$  likely suggests circulation controls on water balance and  $\delta^{18}\text{O}_{\text{precip}}$  together complement shifts in Finger Lake  $\delta^{18}\text{O}$  both by influencing the input  $\delta^{18}\text{O}$  and amount.

The significant changes in hydrological proxies across the North Pacific region correlative with  $\delta^{18}\text{O}_{\text{ML}}$  depletion suggest a shift in atmospheric circulation modulated by cyclonic activity was likely responsible for affecting hydroclimate across much of the region at  $\sim 10$  ka. The importance of AL activity after 10 ka may reflect the end of signal overwhelming by intense climatic reversals in the lateglacial, or may reflect the onset of AL variability following suppression throughout the LGM. Increased surface albedo from North American ice sheets likely created a dense, atmospheric trough that displaced cyclonic activity in the North Pacific to the west (Bartlein et al., 2015; Lasher et al., 2021), forcing the dominance of zonal flow prior to 10 ka which would make any cyclonically driven P–E effects on lake  $\delta^{18}\text{O}$  easily overwhelmed by the dramatic climate reversals that ensued throughout the Pleistocene-Holocene transition. Eventually, sufficient warming during the HTM may have melted residual Cordilleran ice to dissipate or weaken the high-pressure zone by  $\sim 10$  ka. The dissipation of a trough above the cordillera around 10 ka may have enabled the AL to migrate eastward in its strong position, increasing meridional circulation and causing climatic wetting across southern Alaska and the Yukon. Resumption of AL activity no longer suppressed by Cordilleran ice may have resulted in

overall wetter climate throughout the Holocene in contrast to drier conditions in the lateglacial across the region.

### *1.5.3 Hydroclimatic Variability through the Middle Holocene (2-8 ka BP).*

Holocene temperatures in Alaska following the HTM optimum likely cooled as summer insolation decreased (Berger, 1978; Heusser et al., 1985), and isotopic excursions throughout this interval are likely driven by the continued influence of atmospheric circulation on P–E. By ~9.2 ka, carbonate isotopic compositions appear to reflect an adjusted mean climate state, demonstrating decreased variability of ~1‰ fluctuations from the record mean  $\delta^{18}\text{O}$ , with covariation in  $\delta^{13}\text{C}_{\text{DIC}}$  ~50% ( $r^2=0.54$ ). At ~8.4 ka, both  $\delta^{18}\text{O}$  and  $\delta^{13}\text{C}_{\text{DIC}}$  initiate a pronounced decrease of ~1 and 3‰ respectively, likely driven by increased moisture supply to the region under anomalously strong cyclonic activity (AL), decreasing the impact of evaporative enrichment and increasing supply of dissolved  $\text{CO}_2$  from the watershed (Finney et al., 2012). Increased moisture supply at this time is further supported by the appearance of *Picea* pollen at ~8 ka in Hundred Mile Lake (Yu et al., 2008) and on the Kenai Peninsula (Ager, 1983), suggesting the wet period indicated by the isotopic depletions permitted the establishment of spruce, likely invading from interior Alaska where they were already present (Ager, 1983). Comparing this event to regional paleoisotope records indicates a change in moisture supply ~8 ka across the North Pacific region.

A significant shift in moisture supply inferred from the  $\delta^{18}\text{O}$  of Squanga Lake in the Yukon (Lasher et al., 2021) is nearly concordant with Finger Lake at ~8 ka, where the Squanga Lake depletion trend initiated at ~10 ka appears to stabilize with overall lower  $\delta^{18}\text{O}$  for the remainder of the Holocene. Similarly, the isotopic compositions in Finger Lake are elevated above the period of record mean in the early Holocene but undergo a significant transition to

near-mean values at 8 ka.  $\delta^{18}\text{O}_{\text{ML}}$  does not indicate a strong shift to meridional flow at this time (Fisher et al., 2008), which may result from age uncertainties between the Mount Logan and Finger Lake chronologies, or may suggest a less intense, yet strong AL increased moisture supply from a more proximate source  $\sim$ 8 ka. In support of an AL control, lake-level reconstructions in western North America suggest the onset of an arid period in Wyoming (Shuman et al., 2017) is simultaneous with the 8 ka depletion in Finger Lake, consistent with the operation of an intense cyclone over the North Pacific that supplied moisture to southern Alaska at the expense of mid-latitude North America. Alternatively, the  $\sim$ 8 ka depletion may reflect cooling at a similar time to the 8.2 ka cooling event recognized across the North Atlantic region (Thomas et al., 2007), but little evidence supports a similar event elsewhere in Alaska. Regardless of the control, the  $\sim$ 8 ka depletion reflects a shift from overall drier climate to increased moisture around 8 ka in southern Alaska.

Successive variations in moisture supply are indicated by significant enrichment events centered on  $\sim$ 4.7 and  $\sim$ 3.6 ka, which correlate with periods of higher  $\delta^{18}\text{O}_{\text{ML}}$  indicating the dominance of zonal circulation, or anomalously weak AL stages. Similarly, the enrichment at 4.7 ka aligns with inferred zonal flow from  $\delta^{18}\text{O}$  in Jellybean Lake in the Yukon (Anderson et al., 2005), further supporting a circulation control on decreased P–E during a short interval of increased aridity. In the Aleutian Islands,  $\delta^{18}\text{O}$  of Heart Lake on Adak supports the occurrence of weak-stage AL events at  $\sim$ 4.7 and  $\sim$ 3.6 ka, when moisture source became more proximate given inferred westerlies and northerlies sourced from the Bering Sea (Bailey et al., 2018).

A dramatic overall increase in  $\delta^{13}\text{C}_{\text{DIC}}$  of  $\sim$ 5.3‰ reflects considerable modifications to the DIC pool throughout the middle Holocene. The  $\delta^{13}\text{C}_{\text{DIC}}$  enrichment generally tracks  $\delta^{18}\text{O}$  to reflect evaporative enrichment of DIC (Horton et al., 2016) but at a higher magnitude for carbon

with additional enrichment possible by increased productivity, perhaps even benthic plant production enabled by lake sediment infill over time.

A period of weak Asian Monsoon and La Niña conditions reported by Morrill et al. (2003; 2004) centered on 4.2 ka and responsible for widespread drought on the western margin of the Pacific, correlates with  $\delta^{18}\text{O}_{\text{ML}}$  depletions and inferred meridional flow (Fisher et al., 2008) and a weak depleted event ( $\sim -12.8\%$ ) separating enrichment peaks in Finger Lake from  $\sim 4.5$  to 3.7 ka (Figure 6). The respective expressions of the culminated Pacific oscillation events at 4.2 ka suggests the event likely affected the hydroclimate of south-central Alaska by increasing or at least restoring moisture supply between the noted weak AL events. Within this  $\sim 4.2$  interval, the Watana Tephra was detected by magnetic susceptibility in the sediment core. The associated Watana ashfall was reported to decrease aquatic and terrestrial productivity in the Susitna Valley  $\sim 4$  ka (Bigelow et al., 2019), but any potential effects of the Watana ashfall on local evaporation potential are either nonexistent or complement AL effects on P–E for the interval.

A significant depletion of  $\sim 1.1\%$  in Finger Lake occurred from 3.6–3 ka, with a prolonged duration resembling isotope excursions in the late-glacial. The  $\delta^{18}\text{O}$  depletion is suggestive of a dramatic adjustment to regional climate, likely representing increased moisture supply and cooling, as it correlates with advances of several glacial termini in southern Alaska. This increase in glacial activity across the coastal cordillera is thought to represent the early Neoglaciation centered on  $\sim 3.2$  to 2.9 ka (Barclay et al., 2009), and correlate with other inferred advances for the Bering and McCarty glaciers at 3.6 ka (Calkin et al., 2001) and wetting inferred from pollen records (Ager, 1983; Heusser, 1995). The correlation of these events with signs of meridional circulation in  $\delta^{18}\text{O}_{\text{ML}}$  (Fisher et al., 2008), and decreased solar insolation by orbital

forcing (Berger, 1978), suggest regionally increased P–E from a strong AL. These changes may have culminated in glacial advances across the region. By 2.2 ka, potential weak AL activity causes enriched values in Finger Lake and Mount Logan  $\delta^{18}\text{O}$  (Fisher et al., 2008), decreasing precipitation in southern Alaska when glacial activity appears to decrease.

#### *1.5.4 Climate in the Late-Holocene (2 ka BP - Present).*

In the more recent sediment history (last ~2000 years), consistent oscillations in  $\delta^{18}\text{O}$  and  $\delta^{13}\text{C}_{\text{DIC}}$  are detected at multidecadal to decadal scales. Correlation between the respective elements is lowest ( $r^2=0.33$ ) in this interval due to high-frequency variability. Further comparisons with regional records for this period indicate fluctuations up to ~1.5‰ in Finger Lake positively correlate with up to ~5‰ fluctuations in  $\delta^{18}\text{O}_{\text{ML}}$  at the multidecadal scale by ~2.2 ka (Figure 6). By ~1.8 ka, Finger Lake  $\delta^{18}\text{O}$  begins to vary in phase with  $\delta^{18}\text{O}$  of Jellybean Lake in addition to Mount Logan (Figure 6), suggesting cyclonic activity continues to affect regional P–E into the late Holocene. The increased correlations between Finger Lake  $\delta^{18}\text{O}$  and that of Mount Logan and Jellybean Lake may reflect an intensification of AL cyclicity by 2 ka enhancing its influence and increasing synchronicity amongst the respective records. The long-term decrease in  $\delta^{18}\text{O}$  following the HTM and sustained values near -13.0‰ from ~10 ka to present reflect an increased delivery of moisture in the early Holocene consistent with an inception of meridional flow reported by Fisher et al. (2008), both reflecting an adjustment to a wetting hydroclimate in southern Alaska.

High-frequency oscillations in Finger Lake  $\delta^{18}\text{O}$  shift around ~1.1 ka by an ~2‰ increase in  $\delta^{18}\text{O}$  and a ~2.5‰ enrichment in  $\delta^{13}\text{C}_{\text{DIC}}$  lasting until ~890 cal. years BP (Figure 7), reflecting increased evaporative enrichment during the Medieval Warm Period. Increased temperatures are inferred from glacial recession of land-terminating glaciers centered on ~850 cal. years BP

(Calkin et al., 2001), consistent within chronologic uncertainty between the records. Other changes in glacier mass balance across southern Alaska are generally correlative with shifts in Finger Lake  $\delta^{18}\text{O}$ , supporting claims of a linkage between ocean-atmosphere moisture regimes and glacier mass balance in the North Pacific (Bitz & Battisti, 1999; Wiles et al., 2004).

From 750 cal. years BP (1250 AD) to 100 cal. years BP (1850 AD) the  $\delta^{18}\text{O}$  of Finger Lake largely fluctuates below the period of record mean (Figure 7), indicating cool and wet conditions during the Little Ice Age (LIA), when most glaciers in southern Alaska reached their maximum termini (Barclay et al., 2009) with equilibrium lines descending up to 200 m (Calkin et al., 2001). The mean in  $\delta^{18}\text{O}$  for this LIA interval decreases to -13.5‰ from the record mean of -13.0‰, reflecting local cooling induced by a southerly polar front as inferred from suppressed AL-type activity recorded in Mount Logan (Fisher et al., 2004). Records from Jellybean Lake (Anderson et al., 2005) and Kepler Lake (hydrologically open) in the Matanuska Valley (Gonyo et al., 2012) show relatively enriched  $\delta^{18}\text{O}$  during the LIA, suggesting a more proximal moisture source and less  $^{18}\text{O}$  rainout during zonal transport. This change in atmospheric circulation ends the positive correlation between Finger Lake and these records. The record divergence during the LIA likely results from the sensitivity of Finger Lake to ambient temperature as a control on evaporation potential; decreased evaporative enrichment from cold temperatures in the LIA likely decreased the  $\delta^{18}\text{O}$  mean for this interval, with variability superimposed on the decline likely driven by subdued changes in moisture supply from a suppressed AL.

The end of the LIA in 100 cal. years BP (1850 AD) coincides with a large decline in  $\delta^{18}\text{O}_{\text{ML}}$  and the resumption of meridional circulation enabled by the northward recession of the Polar Front (Fisher et al., 2004) and an enhanced flux of tropical heat. This depletion in  $\delta^{18}\text{O}_{\text{ML}}$

is met with an enrichment in Finger Lake  $\delta^{18}\text{O}$  in contrast to the mainly positive relationship earlier in the Holocene and may reflect a re-adjustment of the Finger Lake  $\delta^{18}\text{O}$  baseline to increasing temperatures. High resolution sampling (0.5 cm) from 1600 AD to present reveals an increase in the frequency of isotopic oscillations at the multidecadal-decadal scale by ~1690 AD. The increasing rate of oscillations may be a result of local P–E sensitivity to AL intensification observed by Osterberg et al. (2017). However, this increased frequency of oscillations is met with decreased variance in  $\delta^{18}\text{O}$  of less than 1‰ from the record mean into the present. It is doubtful the decreased variance in Finger Lake reflects a lack of AL control over local P–E, as instrumented indices suggest the opposite (Trenberth & Hurrell, 1994; Winski et al., 2017). Instead, decreased  $\delta^{18}\text{O}$  variance in Finger Lake is likely driven by shifting cyclonic strength amidst the dominance of meridional circulation, with the steady decline in  $\delta^{18}\text{O}$  since ~2000 AD reflecting a sustained increase in moisture supply by AL intensification (Winski et al., 2017), and overall increasing P–E in south-central Alaska.

### ***1.6 Conclusion.***

The Finger Lake isotope record reveals a highly variable early postglacial climate interval featuring a cold, glacial climate at ~13.7 ka followed by abrupt climate reversals during the Pleistocene-Holocene transition. These include increasing isotopic enrichment coincident with the late Bølling-Allerød warming, isotopic depletions coincident with the later portion of the Younger Dryas chronozone, and isotopic enrichment to record maximum  $\delta^{18}\text{O}$  from ~11-10.5 ka during the local expression of the Holocene Thermal Maximum. The HTM expression may be underrepresented in  $\delta^{18}\text{O}$  due to significant climatic wetting driven by a distinct reorganization of atmospheric circulation ~10 ka, inferred from correlations with proxies of  $\delta^{18}\text{O}$  of unmodified

precipitation (Fisher et al., 2008; Lasher et al., 2021). The comparison of variability in meteoric  $\delta^{18}\text{O}$  with  $\delta^{18}\text{O}$  from the P-E perspective allows a more holistic assessment of past changes in atmospheric circulation, which reflect a significant relationship between circulation and water balance in southern Alaska throughout the Holocene. The initial increase in meridional circulation at  $\sim 10$  ka is followed by high-frequency moisture variability throughout the Holocene, likely modulated by ocean-atmosphere forcing. Local hydroclimatological expressions of the Little Ice Age featured a temporary decrease in average  $\delta^{18}\text{O}$ , likely reflecting cold temperatures caused by a southerly polar front. Increasing  $\delta^{18}\text{O}$  following the LIA represents an adjustment of lake  $\delta^{18}\text{O}$  to elevated temperatures and a decreasing trend initiated  $\sim 2000$  AD demonstrates the currently increasing P-E in south-central Alaska as moisture supply is seemingly increasing into the present day.

1.7. Figures.

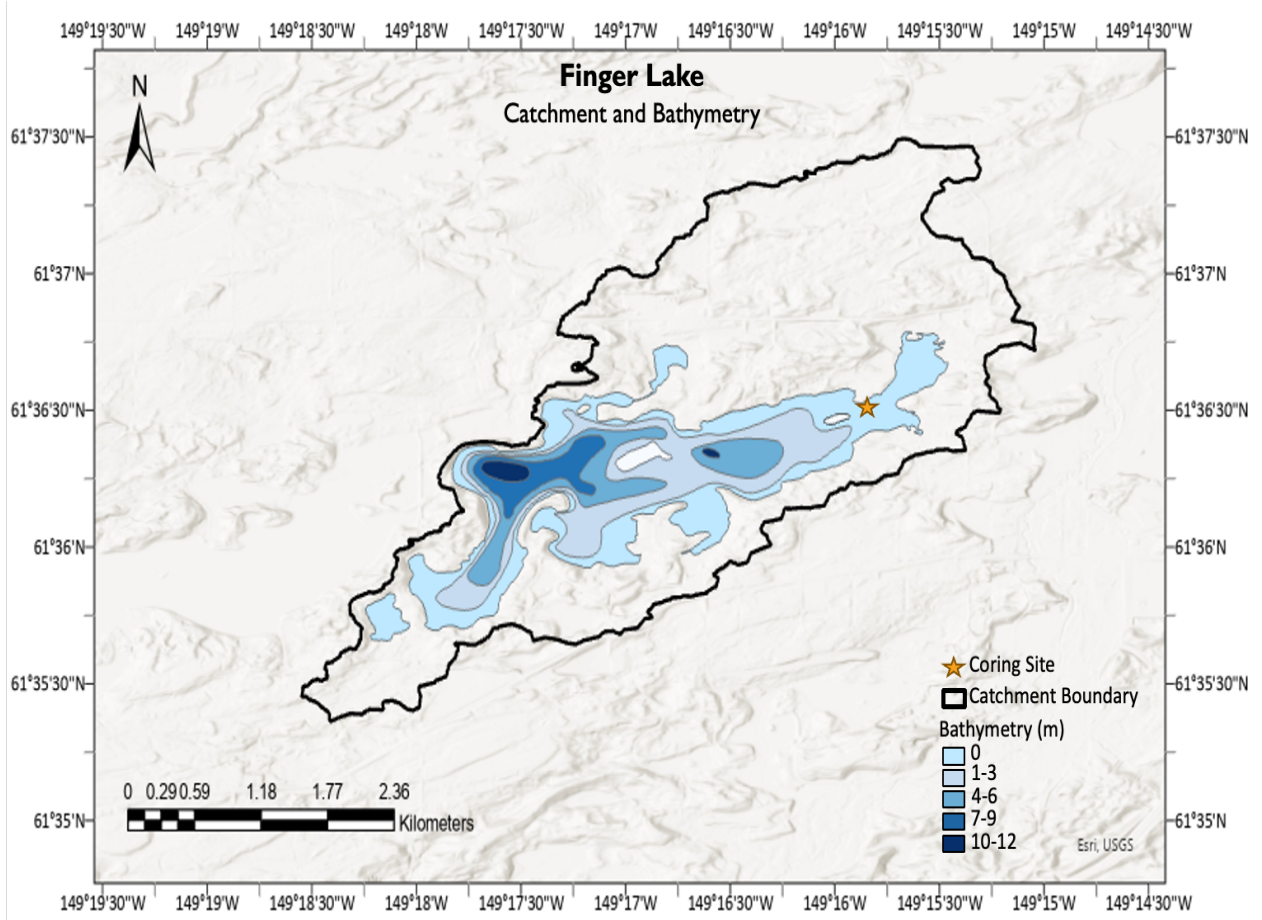


**Figure 1.** Map of the study location depicting the bathymetry of Finger Lake and the low-relief catchment. The coring site is depicted by an orange star (bathymetric contours and catchment boundary by R. T. Pelltier).

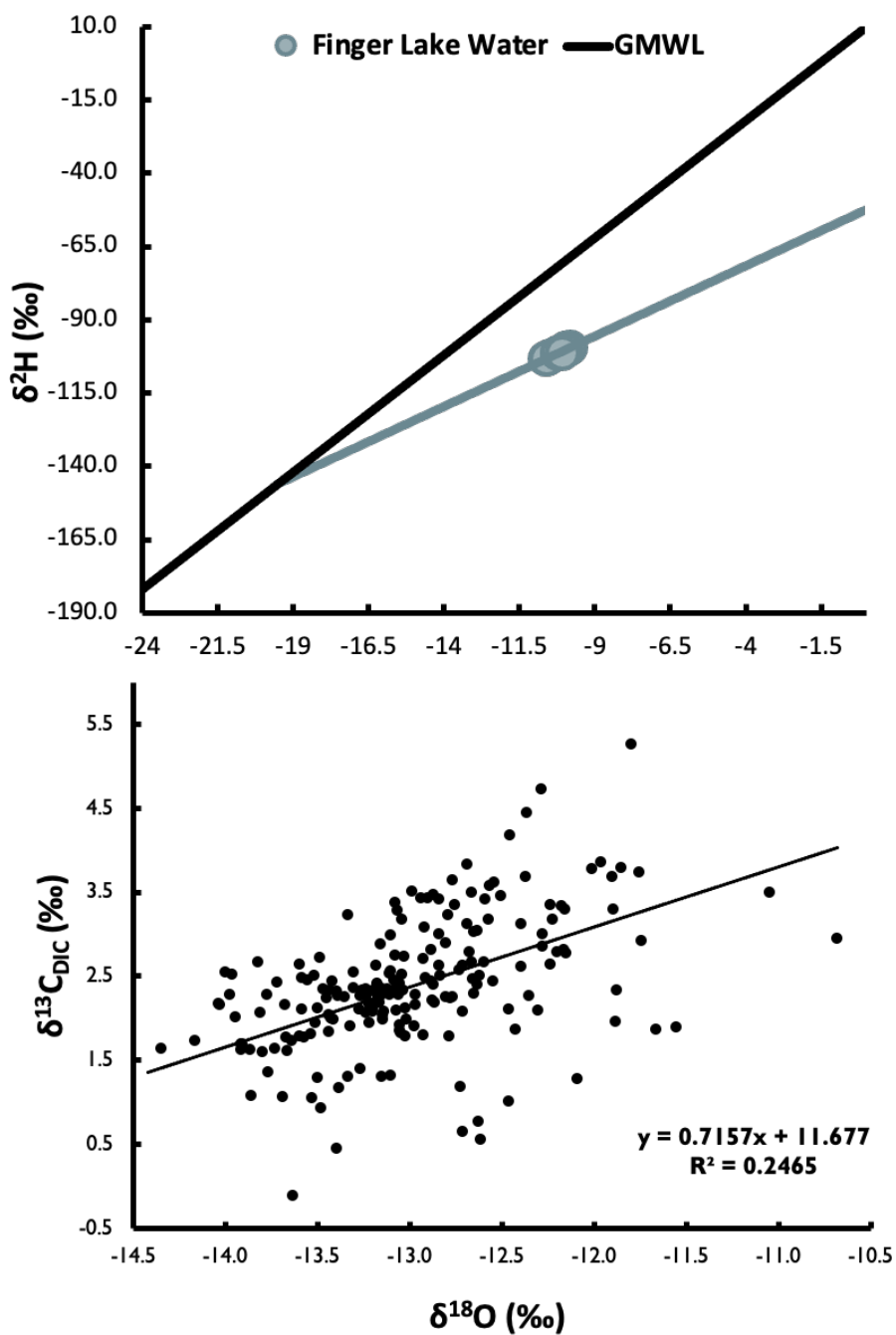


**Figure 2.** (Top) Finger Lake  $\delta^2\text{H}$  vs.  $\delta^{18}\text{O}$  samples represented by blue dots, plotted against the local meteoric water line (LMWL) in gray and the global meteoric water line (GMWL) in black. (Bottom)  $\delta^{13}\text{C}_{\text{DIC}}$  vs.  $\delta^{18}\text{O}$  regression for the period of record.

Core-Drive-Depth	Depth	Material	<sup>14</sup> C AGE	±	1-Sigma	Cal. Years	Error of	Lab/Date
	(cm)					BP	Mean	
A16-D2-29.0 cm	48	Bark fragments	430	15	494-506	500	6	WHOI 7/26/2021
A16-D2-93.0 cm	112	1 woody fragment, 1 bud, 4 broad-leaf type fragments	1100	25	958-1053	1000	47.5	WHOI 7/26/2021
A16-D2-138.5 cm	157.5	Numerous leaf fragments	1210	20	1075-1164	1126	44.5	WHOI 7/26/2021
A16-D3-52-53cm	226	Black tissue, possibly charcoal	1800	170	1535-1923	1730	388	LLNL 9/1/2018
A16-D5-36-37cm	370	Black tissue, possibly charcoal	3400	60	3568-3719	3650	151	LLNL 8/1/2018
A16-D5- 56 cm	390	Watana Tephra			3700-4085	3900	385	
A16-D5-94 cm	428	6 broadleaf fragments picked, 1 Alnus/Betula sp. seed	4400	40	4950-5040	4970	45	WHOI 7/26/2021
A16-D6-38 cm	445	1 Alnus/Betula sp. seed, 1 Picea sp. needle base, 1 Pinaceae needle fragment	4670	40	5321-5463	5400	70.5	WHOI 7/26/2021
A16-D7-14-15cm	509	Wood	6245	30	7162-7245	7200	83	LLNL 8/1/2018
A16-D7-72 cm	566	Woody leaf scar	8170	75	9013-9143	9130	65	WHOI 8/5/21
A16-D8-76 cm	650	Wood and leaf-type fragments	11200	220	12895-13303	13102	204	WHOI 8/5/21

*Table 1. Radiocarbon sample depths, dated material, and age errors.*

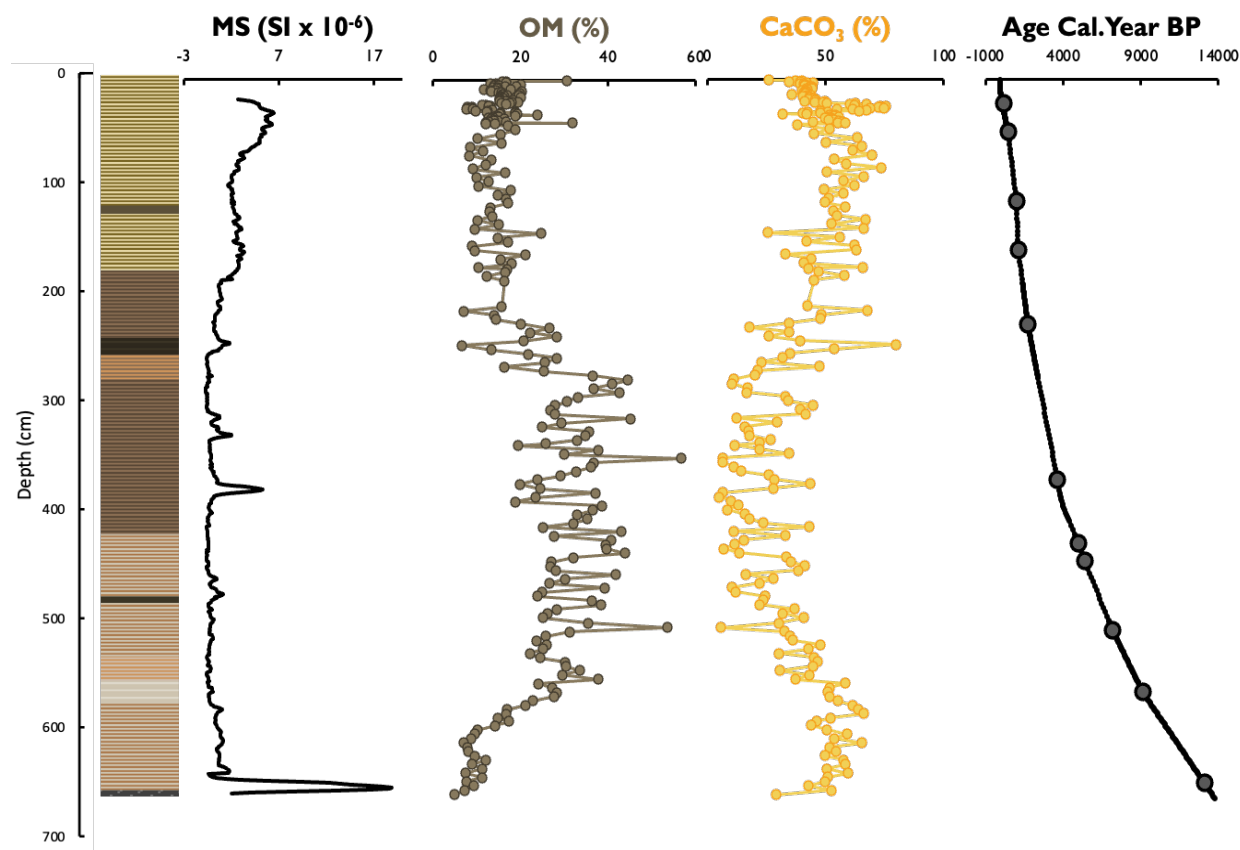


**Figure 3.** Initial sediment analyses with depth down core. (Left to right) simplified diagram of core lithology representing primary lithologic units and associated descriptions below, sediment magnetic susceptibility (SI), organic matter content (OM), calcite content ( $\text{CaCO}_3$ ), and ages in calibrated years before present (1950 AD) with black dots representing dated samples and the black line representing the linear interpolation of ages to non-dated depths.

**Lithologic Key.**

Thin bedded (3-10 cm) marl, green-gray chroma	Gyttja, olive brown-black	Organic-rich, thin bedded (3-10 cm) sediments, gray-brown to very dark gray	Thin bedded (3-10 cm) marl, tan-white	Glaciolacustrine Gravelly Sand
---	---------------------------	---	---------------------------------------	--------------------------------

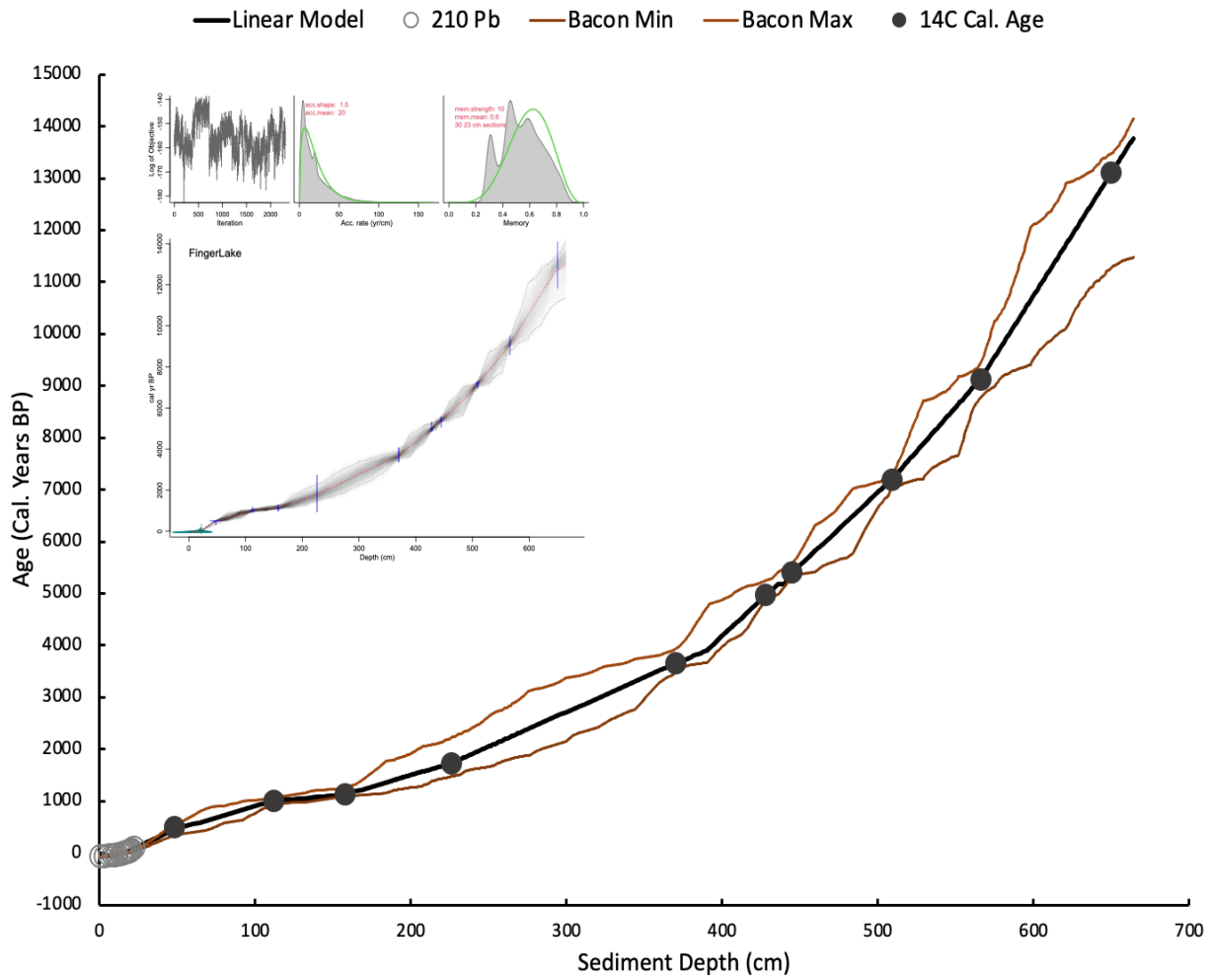


**Figure 4.** Sediment Age Model. Black-filled circles represent radiocarbon dated terrestrial macrofossils sampled throughout the sediment column. Gray hollow circles represent <sup>210</sup>Pb dated sediments in the upper core. The thick black curve represents the age model defined by linear interpolation. The red curves represent the maximum and minimum age models generated by Bayesian interpolation using the R package BACON by Blaauw and Christen (2011). The inset graph generated by BACON displays age uncertainty.

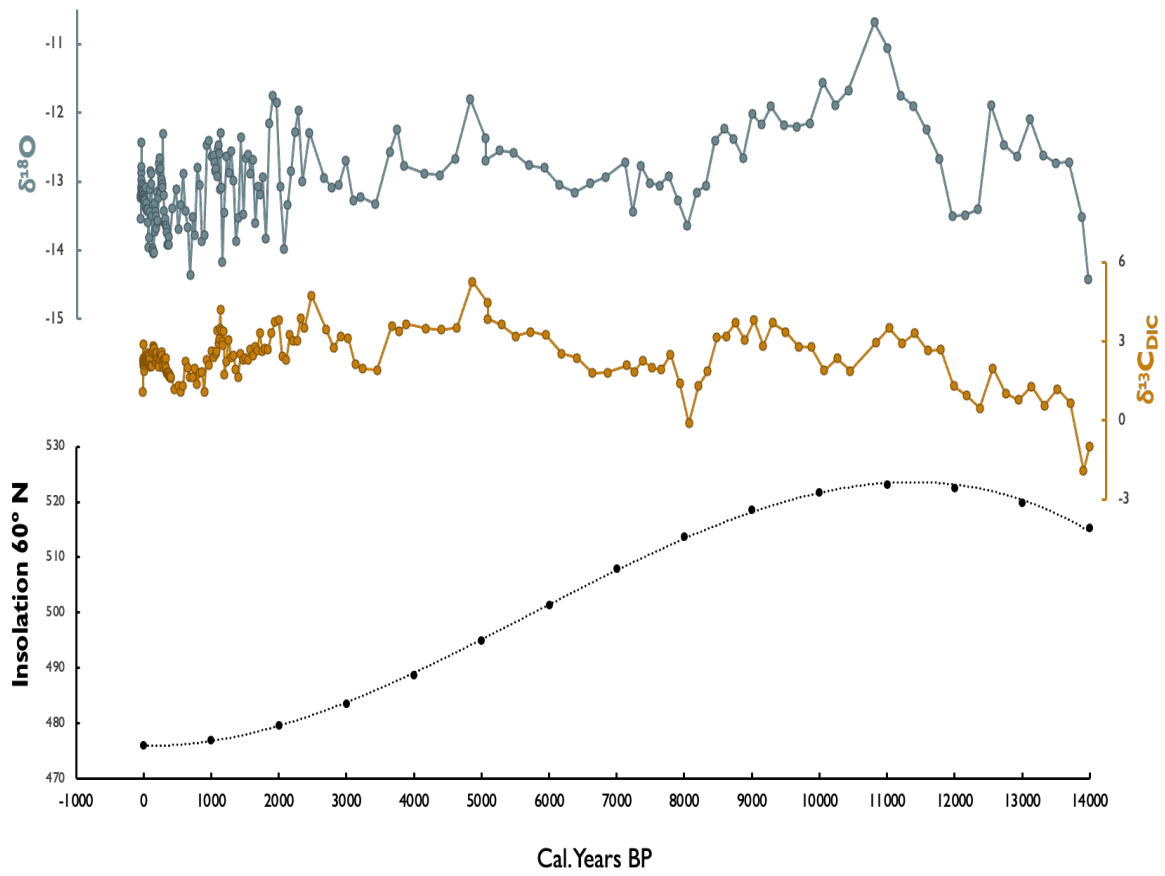


**Figure 5.** Carbonate  $\delta^{18}\text{O}$  (blue),  $\delta^{13}\text{C}_{\text{DIC}}$  (orange), and June insolation at  $60^\circ\text{N}$  from Berger, 1978 (black) plotted with sediment age in years before present for the period of record.

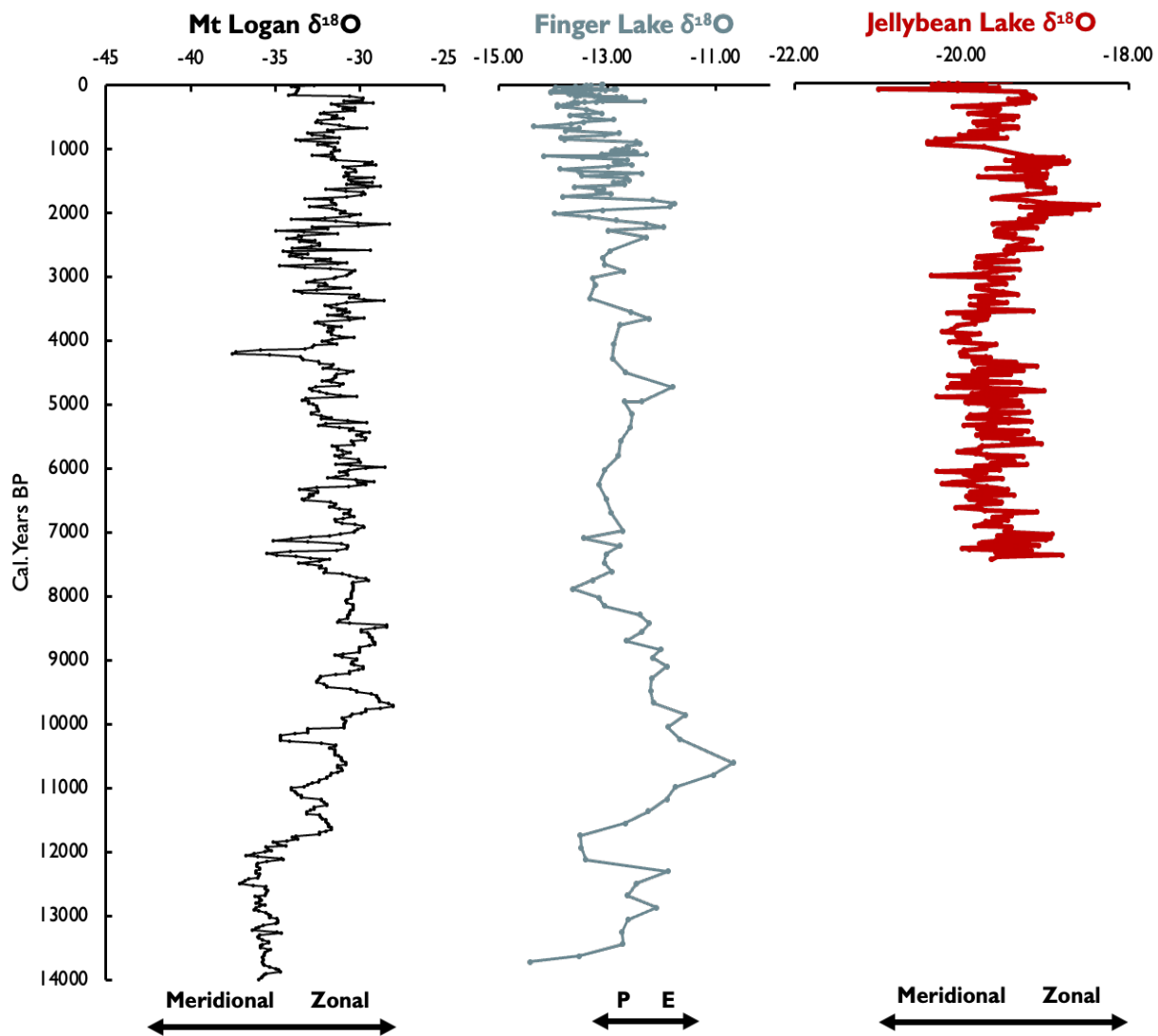


*Figure 6. Comparison of  $\delta^{18}\text{O}$  from Mount Logan ice core in the Yukon (black) from Fisher et al. (2004;2008), Finger Lake (blue), and Jellybean Lake in the Yukon (red) from Anderson et al. (2005).*

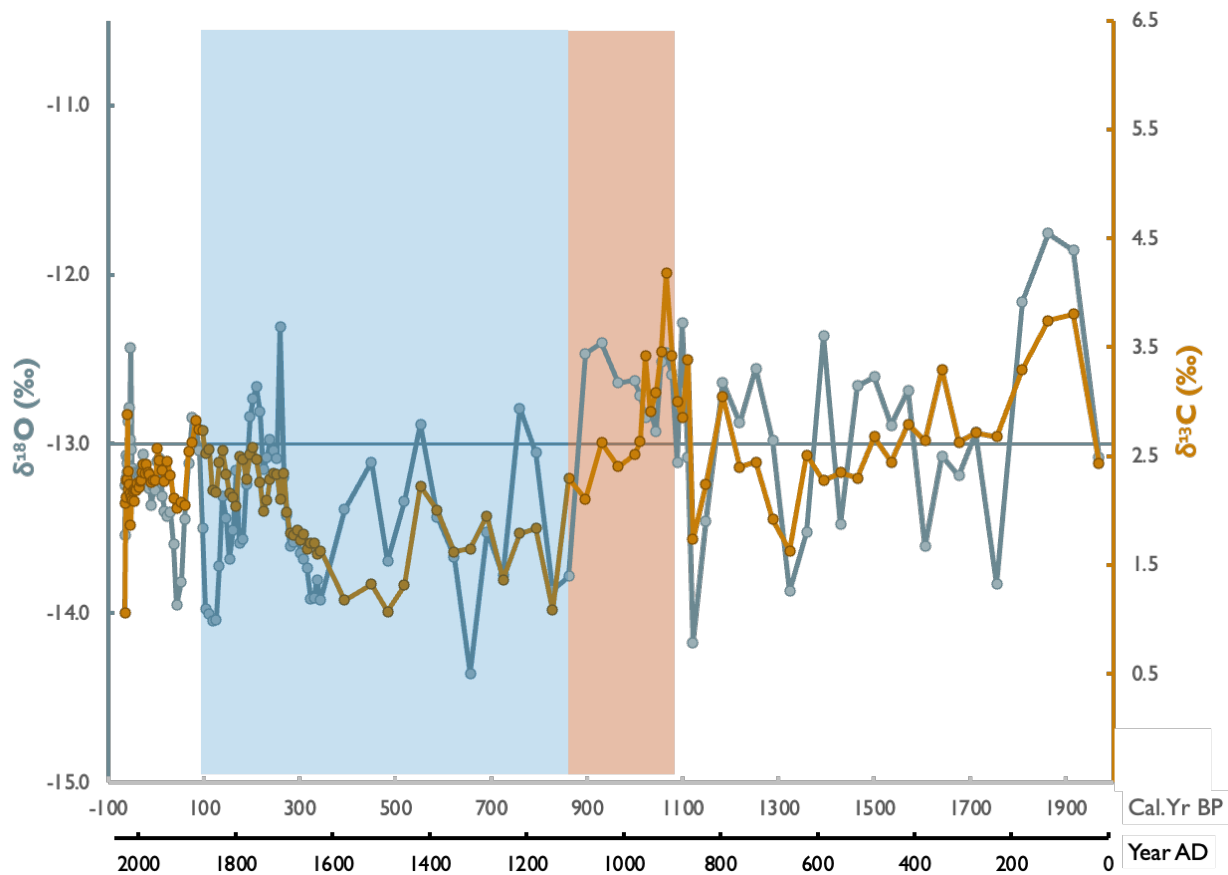


**Figure 7.**  $\delta^{18}\text{O}$  and  $\delta^{13}\text{C}_{\text{DIC}}$  during the Medieval Warm Period (red shading) and the Little Ice Age (blue shading). The record mean  $\delta^{18}\text{O}$  is represented by the blue horizontal.

### *1.8 References Cited in Chapter 1.*

- Abbott, M.B., Finney, B.P., Edwards, M.E., Kelts, K.R., 2000. Lake level reconstruction and paleohydrology of Birch Lake, central Alaska, based on seismic reflection profiles and core transects. *Quaternary Research* 53, p. 154–166.
- Addison, J. A., B. P. Finney, W. E. Dean, M. H. Davies, A. C. Mix, J. S. Stoner, and J. M. Jaeger, 2012, Productivity and sedimentary  $d^{15}N$  variability for the last 17,000 years along the northern Gulf of Alaska continental slope: *Paleoceanography*, v. 27, p. 1206, doi:10.1029/2011PA002161.
- Ager, T.A., 1983, Holocene vegetational history of Alaska. In: Wright Jr., H.E. (Ed.), *Late Quaternary Environments of the United States: The Holocene*, v. 2, University of Minnesota Press, Minneapolis, MN, p. 128–141.
- Ager, T.A., 1989, History of late Pleistocene and Holocene vegetation in the Copper River basin, south-central Alaska. In: Carter, L.D., Hamilton, T.D., Galloway, J.P. (Eds.), *Late Cenozoic History of the Interior Basins of Alaska and the Yukon: US Geological Survey Circular*, v. 1026, p. 89–92.
- Alaska Department of Fish and Game, 2013, <https://www.adfg.alaska.gov/static/fishing/pdfs/sport/byarea/southcentral/matsulakes.pdf> (accessed March 2022).
- Alley, R. B., 2000, The Younger Dryas cold interval as viewed from central Greenland: *Quaternary science reviews*, v. 19 (1-5), p. 213-226.
- Anderson, L., Abbott, M., Finney, B., and Burns, S., 2005, Regional atmospheric circulation change in the North Pacific during the Holocene inferred from lacustrine carbonate oxygen isotopes, Yukon Territory, Canada: *Quaternary Research*, doi: 10.1016/j.yqres.2005.03.008.
- Anderson, L., Berkelhammer, M., Barron, J.A., Steinman, B.A., Finney, B.P., and Abbott, M.B., 2016, Lake oxygen isotopes as recorders of North American Rocky Mountain hydroclimate: Holocene patterns and variability at multi-decadal to millennial time scales: *Global and Planetary Change*, v. 137, p. 131–148, doi:10.1016/j.gloplacha.2015.12.021.
- Bailey, H. L., et al., 2018, Holocene atmospheric circulation in the central North Pacific: A new terrestrial diatom and  $\delta^{18}O$  dataset from the Aleutian Islands: *Quaternary Science Reviews*, v. 194, p. 27-38, doi:10.1016/j.quascirev.2018.06.027.
- Bailey, H. L., Klein, E. S., & Welker, J. M., 2019, Synoptic and mesoscale mechanisms drive winter precipitation  $\delta^{18}O/\delta^2H$  in south-central Alaska: *Journal of Geophysical Research: Atmospheres*, v. 124 (7), p. 4252-4266.
- Barber, V.A., Finney, B.P., 2000, Late Quaternary paleoclimatic reconstructions for interior Alaska based on paleolake-level data and hydrologic models: *Journal of Paleolimnology*, v. 24, p. 29–41.
- Barclay, D. J., Wiles, G. C., & Calkin, P. E., 2009, Holocene glacier fluctuations in Alaska: *Quaternary Science Reviews*, v. 28(21-22), p. 2034-2048.

- Bartlein, P. J., Edwards, M. E., Hostetler, S. W., Shafer, S. L., Anderson, P. M., Brubaker, L. B., & Lozhkin, A. V., 2015, Early-Holocene warming in Beringia and its mediation by sea-level and vegetation changes: *Climate of the Past*, v. 11(9), p. 1197-1222.
- Berg, E. E., Kaufman, D. S., Anderson, R. S., Wiles, G. C., Lowell, T. V., Mitchell, E. A., ... & Werner, A., 2022, Late-Glacial and Holocene Lake-Level Fluctuations on the Kenai Lowland, Reconstructed from Satellite-Fen Peat Deposits and Ice-Shoved Ramparts, Kenai Peninsula, Alaska: *Quaternary*, v. 5(2), p. 23.
- Berger, A., 1978, A simple algorithm to compute long term variations of daily or monthly insolation. Contribution No. 18, Universite Catholique de Louvain, Institut d'Astronomie et de Geophysique, G. Lemaître: Louvain-la-Neuve, B-1348 Belgique.
- Bigelow, N.H., Edwards, M.E., 2001, A 14 000 yr paleoenvironmental record from Windmill Lake, central Alaska: evidence for high-frequency climatic and vegetation fluctuations: *Quaternary Science Reviews*, v. 20, p. 203–215.
- Bigelow, N.H., Reuther, J.D., Wallace, K.L., Saulnier-Talbot, É., Mulliken, K., and Wooller, M.J., 2019, Late-Glacial Paleoeology of the Middle Susitna Valley, Alaska: Environmental Context for Human Dispersal: *Frontiers in Earth Science*, v. 7, p. 43, doi:10.3389/feart.2019.00043.
- Bitz, C. M., & Battisti, D. S., 1999, Interannual to decadal variability in climate and the glacier mass balance in Washington, western Canada, and Alaska: *Journal of Climate*, v. 12(11), p. 3181-3196.
- Blaauw, M., & Christen, A. J., 2018, rbacon: Age-Depth Modelling using Bayesian Statistics. Retrieved from <https://CRAN.R-project.org/package=rbacon>
- Bond, G., Showers, W., Cheseby, M., Lotti, R., Almasi, P., deMenocal, P., Priore, P., Cullen, H., Hajdas, I., and Bonani, G., 1997, A pervasive millennial-scale cycle in North Atlantic Holocene and glacial climates: *Science*, v. 278, p. 1257–1266.
- Bova, S., Rosenthal, Y., Liu, Z., Godad, S. P., & Yan, M., 2021, Seasonal origin of the thermal maxima at the Holocene and the last interglacial: *Nature*, v. 589(7843), p. 548-553.
- Broadman, E., Kaufman, D. S., Henderson, A. C., Berg, E. E., Anderson, R. S., Leng, M. J., ... & Muñoz, S. E., 2020, Multi-proxy evidence for millennial-scale changes in North Pacific Holocene hydroclimate from the Kenai Peninsula lowlands, south-central Alaska: *Quaternary Science Reviews*, v. 241, p. 106420.
- Brubaker, L., Garfinkel, H., Edwards, M., 1983, A late Wisconsin and Holocene vegetation history from the central Brooks Range: implications for Alaskan paleoecology: *Quaternary Research*, v. 20, p. 194–214.
- Buizert, C., Gkinis, V., Severinghaus, J. P., He, F., Lecavalier, B. S., Kindler, P., Leuenberger, M., Carlson, A. E., Vinther, B., Masson-Delmotte, V., White, J. W. C., Liu, Z., Otto-Bliesner, B., & Brook, E. J., 2014, Greenland temperature response to climate forcing during the last Deglaciation: *Science*, v. 345(6201), p. 1177–1180.

- Dansgaard, W., Johnsen, S., Clausen, H. et al., 1993, Evidence for general instability of past climate from a 250-kyr ice-core record: *Nature* v. 364, p. 218–220, doi:10.1038/364218a0
- Caesar, L., Rahmstorf, S., Robinson, A., Feulner, G., and Saba, V., 2018, Observed fingerprint of a weakening Atlantic Ocean overturning circulation: *Nature*, v. 556(7700), p. 191-196, doi: 10.1038/s41586-018-0006-5.
- Calkin, P. E., Wiles, G. C., & Barclay, D. J., 2001, Holocene coastal glaciation of Alaska: *Quaternary Science Reviews*, v. 20(1-3), p. 449-461.
- Cohen, J., Screen, J., Furtado, J. et al., 2014, Recent Arctic amplification and extreme mid-latitude weather: *Nature Geoscience*, v. 7, p. 627–637.
- Davies, M. H., Mix, A. C., Stoner, J. S., Addison, J. A., Jaeger, J., Finney, B., & Wiest, J., 2011, The deglacial transition on the southeastern Alaska Margin: Meltwater input, sea level rise, marine productivity, and sedimentary anoxia: *Paleoceanography*, v. 26(2).
- Dean, W. E., & Schwalb, A., 2002, The lacustrine carbon cycle as illuminated by the waters and sediments of two hydrologically distinct headwater lakes in north-central Minnesota, USA: *Journal of Sedimentary Research*, v. 72(3), p. 416-431.
- Edwards, M.E., Anderson, P.M., Garfinkel, H.L., Brubaker, L.B., 1985, Late Wisconsin and Holocene vegetation history of the upper Koyukuk region, Brooks Range, Alaska: *Canadian Journal of Botany*, v. 63, p. 616–646.
- Finney, B. P., Bigelow, N. H., Barber, V. A., & Edwards, M. E., 2012, Holocene climate change and carbon cycling in a groundwater-fed, boreal forest lake: Dune Lake, Alaska: *Journal of paleolimnology*, v. 48(1), p. 43-54.
- Fisher, D., Osterberg, E., Dyke, A., Dahl-Jensen, D., Demuth, M., Zdanowicz, C., ... & Rupper, S., 2008, The Mt Logan Holocene—late Wisconsinan isotope record: tropical Pacific—Yukon connections: *The Holocene*, v. 18(5), p. 667-677.
- Fisher, D., Wake, C., Kreutz, K., Yalcin, K., Steig, E., Mayewski, P., ... & Burns, S., 2004, Stable isotope records from Mount Logan, Eclipse ice cores and nearby Jellybean Lake. Water cycle of the North Pacific over 2000 years and over five vertical kilometres: sudden shifts and tropical connections: *Géographie physique et Quaternaire*, v. 58(2-3), p. 337-352.
- Gaglioti, B. V., Mann, D. H., Wooller, M. J., Jones, B. M., Wiles, G. C., Groves, P., ... & Reanier, R. E., 2017, Younger-Dryas cooling and sea-ice feedbacks were prominent features of the Pleistocene-Holocene transition in Arctic Alaska: *Quaternary Science Reviews*, v. 169, p. 330-343.
- Gorham, E., Lehman, C., Dyke, A., Janssens, J., & Dyke, L., 2007, Temporal and spatial aspects of peatland initiation following deglaciation in North America: *Quaternary Science Reviews*, v. 26(3-4), p. 300-311.
- Graversen, R., Mauritsen, T., Tjernström, M. et al., 2008, Vertical structure of recent Arctic warming: *Nature*, v. 451, p. 53–56.

- Heusser, C. J., 1995, Late-Quaternary vegetation response to climatic-glacial forcing in North Pacific America: *Physical Geography*, v. 16(2), p. 118-149.
- Heusser, C.J., Heusser, L.E., Peteet, D.M., 1985, Late-Quaternary climatic change on the American North Pacific coast. *Nature*, v. 315, p. 485–487.
- Horton, T. W., Defliese, W. F., Tripathi, A. K., and Oze, C., 2016, Evaporation induced  $^{18}\text{O}$  and  $^{13}\text{C}$  enrichment in lake systems: A global perspective on hydrologic balance effects: *Quaternary Science Reviews*, v. 131, p. 365-379, doi:10.1016/j.quascirev.2015.06.030.
- Kaufman, D. S., Ager, T. A., Anderson, N. J., Anderson, P. M., Andrews, J. T., Bartlein, P. J., ... & Wolfe, B. B., 2004, Holocene thermal maximum in the western Arctic (0–180 W): *Quaternary Science Reviews*, v. 23(5-6), p. 529-560.
- Kaufman, D. S., Axford, Y., Anderson, R. S., Lamoureux, S. F., Schindler, D. E., Walker, I. R., & Werner, A., 2012, A multi-proxy record of the Last Glacial Maximum and last 14,500 years of paleoenvironmental change at Lone Spruce Pond, southwestern Alaska: *Journal of Paleolimnology*, v. 48(1), p. 9-26.
- Kikuchi, C.P., 2013, Shallow Groundwater in the Matanuska-Susitna Valley, Alaska—  
Conceptualization and Simulation of Flow: U.S. Geological Survey Scientific Investigations Report, v. 2013–5049.
- Kokorowski, H. D., Anderson, P. M., Mock, C. J., & Lozhkin, A. V., 2008, A re-evaluation and spatial analysis of evidence for a Younger Dryas climatic reversal in Beringia: *Quaternary Science Reviews*, v. 27(17-18), p. 1710-1722.
- Kopczynski, S. E., Kelley, S. E., Lowell, T. V., Evenson, E. B., & Applegate, P. J., 2017, Latest Pleistocene advance and collapse of the Matanuska–Knik glacier system, Anchorage Lowland, southern Alaska: *Quaternary Science Reviews*, v. 156, p. 121-134.
- Lasher, G. E., Abbott, M. B., Anderson, L., Yasarer, L., Rosenmeier, M., & Finney, B. P., 2021, Holocene hydroclimatic reorganizations in northwest Canada inferred from lacustrine carbonate oxygen isotopes: *Geophysical Research Letters*, v. 48(16), p. e2021GL092948.
- Leng, M. J., & Marshall, J. D., 2004, Palaeoclimate interpretation of stable isotope data from lake sediment archives: *Quaternary Science Reviews*, v. 23(7-8), p. 811-831.
- Mann, D.H., Peteet, D.M., Reanier, R.E., Kunz, M.L., 2002, Responses of an Arctic landscape to late glacial and early Holocene climatic changes: the importance of moisture: *Quaternary Science Reviews*, v. 21, p. 997–1021.
- McCulloch, D., Hopkins, D.M., 1966, Evidence for an early recent warm interval in northwestern Alaska: *Geological Society of America Bulletin*, v. 77, p. 1089–1108.
- McMillan, M.S., 2016, Spatial and temporal analysis of land cover, climate, and lake water quality in the Matanuska-Susitna, Valley, Alaska: Alaska Pacific University.

- Mock, C. J., Bartlein, P. J., & Anderson, P. M.. 1998, Atmospheric circulation patterns and spatial climatic variations in Beringia: *International Journal of Climatology: A Journal of the Royal Meteorological Society*, v. 18(10), p. 1085-1104.
- Moran, E.H., and Solin, G.L., 2006, Preliminary water-table map and water-quality data for part of the Matanuska-Susitna Valley, Alaska, 2005: U.S. Geological Survey Open-File Report, v. 2006-1209.
- Morrill, C., Overpeck, J. T., & Cole, J. E., 2003, A synthesis of abrupt changes in the Asian summer monsoon since the last deglaciation: *The Holocene*, v. 13(4), p. 465-476.
- Morrill, C., 2004, The influence of Asian summer monsoon variability on the water balance of a Tibetan lake: *Journal of Paleolimnology*, v. 32(3), p. 273-286.
- Moxham, R.M., and Eckhart, R.A., 1956, Marl Deposits in the Knik Arm Area Alaska: *Geological Survey Bulletin*, v. 1039-A, p. 4–17.
- Nelson, R.E., Carter, L.D., 1987, Paleoenvironmental analysis of insects and extralimital *Populus* from an early Holocene site on the Arctic Slope of Alaska: *Arctic and Alpine Research*, v. 19, p. 230–241.
- Pompeani, D. P., Steinman, B. A., & Abbott, M. B., 2012, A sedimentary and geochemical record of water-level changes from Rantin Lake, Yukon, Canada: *Journal of paleolimnology*, v. 48(1), p. 147-158.
- Praetorius, S. K., & Mix, A. C., 2014, Synchronization of North Pacific and Greenland climates preceded abrupt deglacial warming: *Science*, v. 345(6195), p. 444-448.
- Praetorius, S., Rugenstein, M., Persad, G., & Caldeira, K., 2018, Global and Arctic climate sensitivity enhanced by changes in North Pacific heat flux: *Nature communications*, v. 9(1), p. 1-12.
- Reimer PJ, Bard E, Bayliss A, Beck JW, Blackwell PG, Bronk Ramsey C, Buck CE, Cheng H, Edwards RL, Friedrich M, Grootes PM, Guilderson TP, Haflidason H, Hajdas I, Hatté C, Heaton TJ, Hoffmann DL, Hogg AG, Hughen KA, Kaiser KF, Kromer B, Manning SW, Niu M, Reimer RW, Richards DA, Scott EM, Southon JR, Staff RA, Turney CSM, van der Plicht J. 2013. IntCal13 and Marine13 radiocarbon age calibration curves 0–50,000 years cal BP. *Radiocarbon* 55(4):1869–1887.
- Rodionov, S., Bond, N., and Overland, J., 2007, The Aleutian Low, storm tracks, and winter climate variability in the Bering Sea: *Deep Sea Research Part II: Topical Studies in Oceanography*, v. 54, p. 2560–2577, doi: 10.1016/j.dsr2.2007.08.002.
- Rozanski, K., Araguás-Araguás, L., and Gonfiantini, R., 2013, Isotopic Patterns in Modern Global Precipitation: *Climate Change in Continental Isotopic Records Geophysical Monograph Series*, p.1–36, doi: 10.1029/gm078p0001.
- Shuman, B. N., & Serravezza, M., 2017, Patterns of hydroclimatic change in the Rocky Mountains and surrounding regions since the last glacial maximum: *Quaternary Science Reviews*, v. 173, p. 58-77.

- Stuiver, M., Grootes, P.M., and Braziunas, T.F., 1995, The GISP d18O climate record of the past 16 500 years and the role of the sun, ocean, and volcanoes: *Quaternary Research*, v. 44, p. 341–354.
- Stuiver, M., 1970, Oxygen and carbon isotope ratios of fresh-water carbonates as climatic indicators: *Journal of Geophysical Research*, v. 75(27), p. 5247-5257.
- Thomas, E. R., Wolff, E. W., Mulvaney, R., Steffensen, J. P., Johnsen, S. J., Arrowsmith, C., ... & Popp, T., 2007, The 8.2 ka event from Greenland ice cores: *Quaternary Science Reviews*, v. 26(1-2), p. 70-81.
- Trenberth, K. E., & Hurrell, J. W., 1994, Decadal atmosphere-ocean variations in the Pacific: *Climate Dynamics*, v. 9(6), p. 303-319.
- Wallace, K.L., Coombs, M.L., Hayden, L.A., and Waythomas, C.F., 2014, Insights from a proximal stratigraphic sequence from Hayes Volcano, south-central Alaska: U.S. Geological Survey Scientific Investigations Report, v. 2014- 5133, p. 32. doi: 10.3133/sir20145133.
- Wiles, G. C., D'Arrigo, R. D., Villalba, R., Calkin, P. E., & Barclay, D. J., 2004, Century-scale solar variability and Alaskan temperature change over the past millennium: *Geophysical Research Letters*, v. 31(15).
- Winski, D., Osterberg, E., Ferris, D., Kreutz, K., Wake, C., Campbell, S., ... & Handley, M., 2017, Industrial-age doubling of snow accumulation in the Alaska Range linked to tropical ocean warming: *Scientific reports*, v. 7(1), p. 1-12.
- Western Regional Climate Center, 2009, Anchorage Ted Stevens International Airport Alaska, Retrieved from <https://wrcc.dri.edu/cgi-bin/cliMAIN.pl?ak0280>
- Yu, Z., Walker, K.N., Evenson, E.B., and Hajdas, I., 2008, Lateglacial and early Holocene climate oscillations in the Matanuska Valley, south-central Alaska: *Quaternary Science Reviews*, v. 27, p. 148–161, doi:10.1016/j.quascirev.2007.02.020.

***Chapter 2: Ecological recovery in postglacial Alaska: a sedimentary isotope record of productivity and catchment processes following deglaciation of the Matanuska-Susitna Valley***

**2. Abstract.** Climate change can significantly influence nutrient supply to aquatic ecosystems, subsequently altering carbon and nitrogen cycling in lake catchments. With ocean-atmosphere processes resulting in significant alterations to moisture supply across Alaska, understanding the response of aquatic ecosystems to such drivers is becoming increasingly important. The application of sedimentary organic isotopes can reveal insights on these relationships and their changes through time. This study applies stable isotope analysis on sediment organic matter from Finger Lake in the Matanuska-Susitna Valley to provide an ~13.7 ka record of aquatic productivity and nutrient cycling throughout the postglacial period in south central Alaska. The isotopic record reveals the freshwater ecosystem established quickly after glacial disturbance and underwent significant changes in nutrient sourcing during intervals of wetter climate, beginning with an initial wetting event centered on ~10 ka. A close coupling of  $\delta^{13}\text{C}_{\text{org}}$  to changes in P–E water balance displays the likely control of lake inflow on the supply of respired carbon to limnic autotrophs, accounting for dramatic changes and overall trends in  $\delta^{13}\text{C}_{\text{org}}$ . Aquatic productivity continued to gradually rise with a more stable climate and generally increased moisture, and therefore nutrient supply, throughout the Holocene. Dramatic changes in carbon cycling occurred ~3 ka during a regional cooling and wetting event thought to represent the onset of the Neoglaciation. Throughout the record, loess input seems to contribute to sediment  $\text{CaCO}_3$  as well as carbonate and organic matter fluxes in the lake, producing a notable increase in sedimentation rate in recent millennia. Sustained enrichments in  $\delta^{13}\text{C}_{\text{org}}$  and  $\delta^{15}\text{N}$  initiated by ~2 ka reflect increasing aquatic productivity into the present, likely in response to a culmination of increased moisture supply, loess fertilization, and catchment nutrient inputs.

## ***2.1 Introduction.***

The responses of terrestrial and freshwater ecosystems of southern Alaska to climate transitions following glacial disturbance (Ager, 1983;1989; Heusser, 1985;1995) can be investigated with limnological records. These records can reveal unique insights on biological productivity and nutrient cycling throughout the postglacial interval. This study applies stable isotope and elemental analysis on sediment organic material from Finger Lake (61°36'18"N, 149°16'53"W), a glacier-formed lake in the Matanuska-Susitna Valley, to reconstruct ecological change over the last ~13.7 ka (13,700 cal. years before present (BP)) from the nutrient cycling perspective. Chlorophyll-a and phosphorus analysis of Finger Lake reveals a mesotrophic status, suggesting its aquatic ecosystem is highly productive relative to many other lakes in the valley (McMillan, 2016). Stable nitrogen and carbon isotope signals from this aquatic community reveal a strong relationship between regional moisture supply and nutrient sourcing from the lake catchment, providing new information on aquatic responses to climate variability of the postglacial era.

Organic and nutrient compounds carry source-specific isotopic signatures that are instrumental in tracing elemental flows and cycles in lake systems (Meyers & Ishiwatari, 1993). The deposition of organic matter in lakes archives stable isotopic compositions in a stratigraphic sequence where they can be sampled and quantified. Sediment organic carbon  $\delta^{13}\text{C}$  ( $\delta^{13}\text{C}_{\text{org}}$ ) may serve as an indicator of lake carbon sourcing, cycling, and primary productivity (Meyers, 2003; Finney et al., 2012; Woodward et al., 2012). Allochthonous dominance of the sediment isotope signal may indicate changes in terrestrial productivity or input and the preclusive climatic controls on such processes (Gu et al., 1996). In sediments where  $\delta^{13}\text{C}_{\text{org}}$  is dominated by aquatic plants, isotopic excursions can be driven by aquatic productivity and associated carbon

fractionation and limitation (Laws et al., 1995; Brenner et al., 1999; Aichner et al., 2010), and can therefore vary by lake trophic status (Gu et al., 1996; Finney et al., 2012). Evaluating changes in the  $\delta^{13}\text{C}$  through the lens of the dominant control on its signal can lend insights to carbon flows through the lake history, and the relative importance of terrestrial versus aquatic sources. Similar to organic carbon, sedimentary  $\delta^{15}\text{N}$  is instrumental as a tracer of relative contributions from distinctive nitrogen sources (Woodward et al., 2012; Botrel et al., 2014), and serves as an indication of lake trophic status, productivity, and nitrogen cycling including nitrogen limitation and loss by denitrification (Brenner et al., 1999; De Kluijver et al., 2017). Distinguishing the dominant organic source to lake sediment is aided by correlations with C/N ratio, which is governed by physiology and vascular structuring specific to the organic source (Müller, 1977; Meyers & Ishiwatari, 1993; Gu et al., 1996), but also nutrient limitation (Hecky, et al., 1993).

## **2.2 Methods.**

### *2.2.1 Study Location.*

The Matanuska-Susitna Valley in south-central Alaska separates the Talkeetna mountains to the north and Chugach mountains to the south, and lies within the interior boreal forest ecozone (Viereck and Little, 1975). The maritime climate (Stafford et al., 2000) receives mean annual precipitation of ~35 cm (WRCC, 2009) that supports a contemporary vegetation community consisting mainly of mixed spruce (*Picea*), alder (*Alnus*), and birch (*Betula*) forest stands, and willow (*Salix*) and sedge (*Cyperaceae*) riparian zones. Finger Lake is situated in Quaternary glacial and alluvial deposits (Kikuchi, 2013) and has a basin volume of 6,934,634 m<sup>3</sup> with an average depth of ~4.7 m (ADFG, 2013). The lake basin features a complex morphometry

with multiple bays (Figure 1), and is hydrologically closed at the surface, featuring groundwater recharge and prolonged water residence in its basin.

### *2.2.2 Sediment Sampling and Chronology.*

Finger lake was cored through the ice in April 2016, on a shallow carbonate-bearing shelf (Figure 1). The sediment-water interface and upper sediments were retrieved with a piston corer in polycarbonate tubing to avoid disturbance, and deeper sediments were cored with a Livingstone piston-corer in overlapping drives to obtain 664 cm of total sediment. Cores were scanned for magnetic susceptibility, sectioned, photographed, and described. The cores were then analyzed at 2-4 cm increments for compositional properties including water content, bulk density, and organic matter and calcite content quantified by the loss-on-ignition (LOI) method at 550 and 950°C. Age control for the sedimentary sequence places proxy expressions into a temporal context and is informed by  $^{210}\text{Pb}$  dating in the upper sediment profile and 10 AMS  $^{14}\text{C}$  dates on terrestrial macrofossils and charcoal sampled throughout the core, with calibrations based on IntCal 13 by Reimer et al. (2013) (Baxter, Chapter 1). Sediment ages were modeled to non-dated depths using interpolation from a linear regression model that was referenced with the Bayesian age-depth interpolation developed by Blaauw and Christen (2011).

### *2.2.3. Organic Isotope ( $\delta^{13}\text{C}$ , $\delta^{15}\text{N}$ ) Analysis.*

For organic C and sedimentary N isotopes, core segments were sampled at 2-8 cm increments and reacted with 1N HCl to remove carbonate material. The acidified residuals were well rinsed, freeze dried, and packed into tin capsules for %C, %N,  $\delta^{13}\text{C}$ , and  $\delta^{15}\text{N}$  analysis on a Costech ECS 4010 elemental analyzer with pneumatic autosampler coupled to a Delta V Advantage Stable Isotope Ratio Mass Spectrometer (IRMS) in the Idaho State University Stable Isotope Laboratory. Carbon to nitrogen ratios, or C/N, were determined from total C% and total

N‰ as quantified from combustion of organic samples in the elemental analyzer. Isotopic compositions are presented in delta notation ( $\delta$ ), given by the equation  $\delta \text{ element } (\text{‰}) = [(R \text{ sample} - R \text{ standard}) / R \text{ standard}] * 1000$  where, for the element of interest, “R” is the ratio of heavy to light isotopes (e.g.,  $^{15}\text{N}/^{14}\text{N}$ ), and “standard” is atmospheric  $\delta^{15}\text{N}$  for N and the Vienna Pee Dee Belemnite (VPDB) for C. Delta values are reported in deviations permil (‰) from the standards.

## **2.3 Results.**

### *2.3.1 Sediment Description.*

The Finger Lake sediments consist mainly of varying proportions of  $\text{CaCO}_3$  to organic matter, together accounting for ~28 to 87% of the total sediment composition with residual mineral content constituting ~13 to 72% throughout the lake record. Core stratigraphy features thinly bedded (3-10 cm) strata of white-pale yellow carbonate layers interleaved with gray-grayish brown to olive brown-black organic layers with diffuse to indistinct contacts throughout the core (0-664 cm). Some notable breaks in the layered bedding occur as more massive, homogeneous sections at 228-242 cm, 351-358 cm, and 380-387 cm, all ranging from dark gray to very dark grayish brown in color. A spike in magnetic susceptibility at 390 cm (Figure 2) likely represents a cryptotephra within a 7 cm dark gray band, with radiocarbon dating through this section of the core placing the tephra within the timing uncertainty of the Watana Tephra (~3900  $^{14}\text{C}$  yr BP; Wallace et al., 2014). The sediment color slowly transitions downcore from a general green-gray chroma from 37-201 cm, to darker grays down to 290 cm, below which the core transitions to gray-brown at 334 cm. Below this level, sediments darken to very dark gray above a transition to lighter shades of brown-tan from 509-557 cm where sediments continue to lighten downcore to tan-white and end in gray gravelly sand at the core base.

Throughout the core, variability in LOI data reveals compositional changes in coherence with the visual descriptions. Sediment organic composition ranges from 5 to 56.8% and correlates with intervals of darker color. The CaCO<sub>3</sub> content ranges from 5 to 80% and is highest on average in the lower 108 cm where color ranges from pale-yellow to white. Organic content is highest in the mid-core section (250 - 556 cm), averaging at 31.7%, but falls to 15.1% from 0-250 cm and 13.8% from 556-664 cm. Conversely, CaCO<sub>3</sub> content decreases from 50% at 0-250 cm, to 26.9% at 250-556 cm, before increasing to 53.3% from 556-664 cm. The transition to higher organic matter content in the mid-section of the core is reflected by darkened color and less evident layering contacts with carbonate laminations. The heightened CaCO<sub>3</sub> content above and below the organic-rich middle section are consistent with their overall lighter sediment color. Terrestrial macrofossils sampled throughout the Livingstone drives display the prevalence of *Alnus sp.*, *Betula sp.*, *Picea mariana*, and *Picea glauca* in the catchment, and aquatic macrofossils including leafy plant material, trace ostracode remains, and *Chara spp. oogonia* and stem casts.

### 2.3.2. Sedimentation and Geochronology.

The age model displays considerable changes in sedimentation rate downcore (Figure 3). Sedimentation rate is highest in the upper 200 cm (~1,900 years), with the most recent years dated by <sup>210</sup>Pb accumulation demonstrating the highest sedimentation rates averaging at 0.14 cm/year. Sedimentation rate decreases downcore to the lowest rates below 500 cm (~7 ka) ranging from 0.031 to 0.021 cm/year in the oldest sediments. Due to the low abundance of suitable macrofossils, the lake age was extrapolated to 13.7 ka (uncertainty range represented in Figure 3) from the nearest AMS date of 13,100 ± 220 cal. years BP to represent the latest time of deglaciation in this part of the valley.

### *2.3.3 Isotopic Compositions.*

Downcore variability in  $\delta^{13}\text{C}_{\text{org}}$  displays a broad range from -31‰ to -19.5‰ and sedimentary  $\delta^{15}\text{N}$  has a narrower range, from -1.2‰ to 2.9‰. The trend in  $\delta^{13}\text{C}_{\text{org}}$  demonstrates an overall prolonged increase from core base to ~4 ka, with a pronounced punctuation to this trend of a near 7.5‰ depletion excursion centered at ~3 ka (Figure 5).  $\delta^{15}\text{N}$  varies less dramatically at ~0.5‰ fluctuations around a mean of ~0.3‰ until ~2.5 ka where a seemingly gradual enrichment initiates and continues to the core top. Organic carbon content (%) of the carbonate-free material ranges from 1.7% at 13.7 ka to 38.3% at 7.4 ka (Figure 2). Organic nitrogen content displays less dramatic variability ranging from 0.1% at 13.7 ka to 3.1% at 7.4 ka. C/N ratios average at ~11 throughout the core but are generally higher in the deeper sediments.

### *2.4 Discussion.*

The Finger Lake organic isotope compositions reveal the dominance of aquatic-sourced organic matter in the sediment. The record average C/N of ~11 likely reflects the dominance of nonvascular plant tissue in sediment organic matter and falls within the higher end of the typical range for diatoms and phytoplankton (Müller, 1977; Meyers & Ishiwatari, 1993). Due to low relief catchment topography, and the lack of inlet or outlet streams, lake inputs of terrestrial organic matter are likely limited. Notable changes in C/N may therefore reflect periods of nitrogen limitation, increases caused by organic decomposition, or the presence of aquatic vascular plants with higher C/N. C/N is generally highest between ~8 and 10.2 ka, yielding values as high as 14.5 in the early Holocene (Figure 5), and likely reflects nitrogen limitation, namely where C/N elevates above 12. Regression analyses between record isotopic values and

C/N ratios (Figure 4) reveal the nature of isotopic variance as a factor of organic source, with  $\delta^{13}\text{C}_{\text{org}}$  demonstrating a weak negative correlation ( $r^2=0.24$ ). At high C/N,  $\delta^{13}\text{C}_{\text{org}}$  can have values similar to that expected from terrestrial C3 plants, and also the most depleted values of the record. The  $\delta^{15}\text{N}$  versus C/N relationships are not strong but may suggest a shift to a positive relationship prior to  $\sim 2$  ka and a negative relationship after (Figure 4). Comparison with the carbonate  $\delta^{18}\text{O}$  as a proxy of P–E water balance (Baxter, Chapter 1) reveals a climatic linkage to these relationships, as discussed below.

#### *2.4.1 Climatic Influence on Lake Carbon Cycling.*

Relationships between the respective proxies for the period of record (Figures 5 & 6) reveal the consistent negative correlation between  $\delta^{13}\text{C}_{\text{org}}$  and C/N. Major  $\delta^{13}\text{C}_{\text{org}}$  depletion events centered on  $\sim 10$ , 8, and 3 ka are correlative with increased C/N and times of significant declines in  $\delta^{18}\text{O}$  indicating periods of wetter climate (Baxter, Chapter 1). During intervals of increased P–E, surface runoff and groundwater recharge may be capable of transporting terrestrial material to the lake basin. However, as discussed, the low relief catchment topography and lack of inlet or outlet streams in the coring bay may generally limit the input of land-plant or soil detritus to Finger Lake. Furthermore, the depleted  $\delta^{13}\text{C}_{\text{org}}$  of  $\sim -30\text{‰}$  in these intervals is inconsistent with input of terrestrial vascular plant material (Meyers & Ishiwatari, 1993). Therefore, the  $\delta^{13}\text{C}_{\text{org}}$  may reflect aquatic plants under the influence of changes in carbon sourcing to the lake basin. Microbial respiration in organic-rich catchment soils produces  $\text{CO}_2$  with  $\delta^{13}\text{C}$  depleted from atmospheric levels (Kling et al., 1991) which, when supplied in abundance to the lake basin, can result in large fractionation to aquatic plants explaining deep  $\delta^{13}\text{C}_{\text{org}}$  depletions (Finney et al., 2012). Therefore, the negative  $\delta^{13}\text{C}_{\text{org}}$  versus C/N relationship is

likely driven by partial autotrophic uptake of respired carbon supplied from the catchment, the flux of which increases during periods of high lake inflow.

Conversely, enriched  $\delta^{13}\text{C}_{\text{org}}$  intervals may represent a higher  $\delta^{13}\text{C}_{\text{org}}$  baseline due to factors such as evaporative enrichment of  $\delta^{13}\text{C}_{\text{DIC}}$  (Figure 6) and increased productivity. Enrichment of dissolved inorganic carbon (DIC) via  $\text{CO}_2$  degassing during evaporation (Baxter, Chapter 1) may cascade to the enrichment of aquatic plant  $\delta^{13}\text{C}_{\text{org}}$  (Meyers & Ishiwatari, 1993; Laws et al., 1995; Aichner et al., 2010), with increasing productivity providing another cause of  $\delta^{13}\text{C}_{\text{org}}$  enrichment. Additionally,  $\delta^{13}\text{C}_{\text{org}}$  enrichment during decreased P–E may result from  $\text{CO}_2$  limitation under reduced supply from the catchment, and greater uptake of the DIC pool or plant usage of isotopically heavier bicarbonate.

#### *2.4.2 Nitrogen Cycling.*

$\delta^{15}\text{N}$  remains relatively stable and unchanged prior to  $\sim 2$  ka, with values ranging from  $\sim 0$  to  $1\text{‰}$ . The  $\delta^{15}\text{N}$  values are consistent with aquatic and terrestrial values in a relatively closed nitrogen system with recycled nitrogen retained, perhaps enabled by long water residence time in the lake basin, nitrogen limitation, or co-limitation, and therefore little to no net fractionation of bioavailable nitrogen. Subtle increases in  $\delta^{15}\text{N}$  ( $\sim 0.5$  to  $1\text{‰}$ ) correlate with inferred wet intervals and increased lake inflow, which are likely driven by input of isotopically enriched nitrogen sources from the catchment. Given the importance of groundwater for inflow to Finger Lake, the enriched  $\delta^{15}\text{N}$  and increased C/N during periods of wetter climate may be driven by input from a sub-oxic groundwater system creating denitrifying conditions during transitions to wetter climate periods. The influence of oxygen-depleted groundwater on lake nitrogen levels is twofold; (1) reducing conditions in oxygen-poor groundwater can result in the supply of dissolved nitrate that is isotopically enriched as the residual of denitrification, resulting in elevated  $\delta^{15}\text{N}$ ; (2) sub-oxic

groundwater may distribute across the lake basin during periods of high inflow, causing loss of bioavailable nitrogen in the lake basin and resulting in nitrogen limitation reflected in the elevated C/N. Groundwater supply of partially reduced nitrate to the lake basin may result from exchange with anoxic wetlands that persisted up-valley of Finger Lake during periods of wetter climate.

#### *2.4.3 Late-glacial Productivity.*

The presence of coarse, gray basal sediments in Finger Lake are interpreted as glaciolacustrine deposits, suggesting Finger Lake formed during deglaciation and received input from a proximal glacier. The age of Finger Lake is extrapolated to  $\sim 13.7$  ka (age uncertainty represented in Figure 3) and is generally consistent with radiocarbon constraints for the retreat of the Matanuska lobe of the inferred Matanuska-Knik valley glacier to the Matanuska Valley, between  $13,650 \pm 130$  cal. years BP and  $13,350 \pm 90$  cal. years BP (Ager, unpublished data; Kocczynski et al., 2017). Quickly following deglaciation, the organic isotope record reveals an active aquatic ecosystem with  $\delta^{13}\text{C}_{\text{org}}$  of  $-29.4\text{‰}$  and relatively low C/N (Figure 5) representing the prevalence of aquatic production. These  $\delta^{13}\text{C}_{\text{org}}$  values are similar to those observed in lakes of the Susitna Valley (Bigelow et al., 2019) and southwestern Alaska (Hu et al., 1995; Kaufman et al., 2012) and are interpreted to represent low aquatic productivity. This inference is supported by low  $\delta^{13}\text{C}$  of the inorganic carbon pool (Baxter, chapter 1), suggesting negligible isotopic enrichment of the DIC pool by photosynthetic uptake. Low basal  $\delta^{15}\text{N}$  of  $-0.6\text{‰}$  displays little overall fractionation from atmospheric nitrogen ( $0\text{‰}$ ), potentially representing early nitrogen limitation and the dominance of nitrogen-fixing cyanobacteria, or the potential recycling of low nitrogen sources and low net fractionation. The total organic content remained low in the oldest

sediments, with sediment organic content of ~10%, suggesting biomass production in the lake basin or sourcing from the catchment was initially low.

Soon after deglaciation and until ~10.7 ka, organic matter content, C/N,  $\delta^{13}\text{C}_{\text{org}}$ , and  $\delta^{15}\text{N}$  show subtle changes and little response to more abrupt signals in environment as inferred by  $\delta^{18}\text{O}$ , such as during the Younger Dryas chronozone or Holocene Thermal Maximum (HTM; Baxter, Chapter 1). Throughout this period,  $\delta^{13}\text{C}_{\text{org}}$  displays a gradual enrichment of ~3‰ from ~13 to 10.7 ka, which may reflect increasing productivity as the aquatic ecosystem developed, but alternatively, generally tracks enrichment of the DIC pool which could suggest the trend is caused by increasing evaporative enrichment (Baxter, Chapter 1). There are no obvious perturbations to this gradual  $\delta^{13}\text{C}_{\text{org}}$  enrichment, despite a depleted excursion in  $\delta^{18}\text{O}$  from ~12.3 to 11.6 ka that likely reflects a regional cooling concomitant with the Younger Dryas chronozone (Baxter, Chapter 1). This supports a cooling control on the  $\delta^{18}\text{O}$  depletion, as depletion caused by wetting climate should be reflected in  $\delta^{13}\text{C}_{\text{org}}$  by increasing carbon supply to the lake basin. Additionally, the sustained  $\delta^{15}\text{N}$  and C/N throughout this cooling interval indicates the event had no significant influence on the productivity of the freshwater ecosystem. Although proxies of lake productivity contain inherent warm-season bias, it seems unlikely that the organic isotope signal is insensitive to cool-season extremes given their general correlation with wetting events inferred from the carbonate isotope record, which is sensitive to changes in P–E mainly during the ice-free period.

The gradual increase in  $\delta^{13}\text{C}_{\text{org}}$  that initiated at ~13 ka reaches its maximum at ~10.7 ka, during the peak of the HTM expression in the  $\delta^{18}\text{O}$  record (Baxter, Chapter 1). The increase in  $\delta^{13}\text{C}_{\text{org}}$  correlates with, and may be driven by, enrichment of  $\delta^{13}\text{C}_{\text{DIC}}$  (Figure 6). Indications of aridity during the HTM are expressed throughout Alaska (Kaufman et al., 2004), including

decreased lake levels across interior Alaska (Abbott et al., 2000; Barber & Finney, 2000) and the Yukon (Pompeani et al., 2012), and potential evaporative enrichment of otherwise throughflow lake  $\delta^{18}\text{O}$  signals representing meteoric  $\delta^{18}\text{O}$  (Baxter, chapter 1) in the Matanuska Valley (Yu et al., 2008) and southwest Yukon (Lasher et al., 2021). However, a distinct transition is apparent in the early Holocene at  $\sim 10$  to 10.5 ka, where C/N abruptly elevates to the record maximum of 14.4. The shift in C/N is accompanied by a pronounced depletion of  $\sim 4\text{‰}$  in  $\delta^{13}\text{C}_{\text{org}}$  and an increase in  $\delta^{15}\text{N}$  of  $\sim 1\text{‰}$ . These changes are consistent with a period of significant climatic wetting, increasing groundwater inflow to the lake and supply of dissolved inorganic carbon and nitrogen from the catchment.

A regional alder rise likely occurred at this time (Ager, 1983; Heusser, 1995; Yu et al., 2008; Bigelow et al., 2019; Broadman et al., 2020), which supports regional wetting and may have altered terrestrial nitrogen cycling, further supporting the potential for nitrate reduction in wetlands and groundwater enabling  $\delta^{15}\text{N}$  enrichment. Furthermore, the occurrence of a regional wetting event centered on  $\sim 10$  ka is supported by depletion in  $\delta^{18}\text{O}$  (Baxter, Chapter 1). The significant change in regional moisture supply at  $\sim 10$  ka is reflected in other lake records (Lasher et al., 2021; Berg et al., 2022) and pollen records (Ager, 1983; Heusser, 1995; Broadman et al., 2020) across the North Pacific during an inferred shift to meridional circulation (Fisher et al., 2008), likely demonstrating initial strong Aleutian Low (AL) activity in the Holocene following the HTM (Baxter, Chapter 1). The  $\sim 10$  ka regional wetting demonstrates the initial coupling of nutrient sourcing to synoptic hydroclimate controls in the early Holocene, from relatively unaltered nutrient sourcing prior.

#### 2.4.4 Carbon and Nitrogen Cycling throughout the Holocene.

Following the initial period of increased inflow to Finger Lake at ~10 ka, cyclonic modulation of regional hydroclimate and associated nutrient sourcing to Finger Lake appears to continue until ~3.5 ka. After ~10 ka, gradual enrichment in  $\delta^{13}\text{C}_{\text{org}}$  is observed and mirrored by generally decreasing C/N, together reflecting increasing limnic productivity as the ecosystem developed and autochthonous biomass production increased. A few notable perturbations to the  $\delta^{13}\text{C}_{\text{org}}$  trend occurred when significant changes in nutrient sourcing occurred. The first perturbation signifies a regional wetting interval reflected in a notable  $\delta^{13}\text{C}_{\text{org}}$  depletion of ~4‰ centered on ~8 ka which correlates with a significant  $\delta^{18}\text{O}$  depletion (Baxter, Chapter 1). The relationships with C/N and  $\delta^{15}\text{N}$  noted above are held, consistent with a wetting event.

Quickly following this interval,  $\delta^{13}\text{C}_{\text{org}}$  continued on the enrichment trajectory until ~3.5 ka. The abrupt ~7‰ depletion in  $\delta^{13}\text{C}_{\text{org}}$  and concomitant rise in C/N support climatic wetting contributed to the  $\delta^{18}\text{O}$  depletion. This  $\delta^{18}\text{O}$  depletion correlates with atmospheric cooling (Baxter, Chapter 1) and increased glacial activity during the early Neoglaciation (Calkin et al., 2001; Barclay et al., 2009). These records collectively suggest a shift in climate state towards cooler and wetter conditions, likely enabling increased catchment inorganic carbon and nitrogen inputs through groundwater inflow. The magnitude of this  $\delta^{13}\text{C}_{\text{org}}$  depletion is the largest in the record, however, the depletion likely reflects aquatic utilization of respired carbon, not a decrease in productivity.

At ~3 ka,  $\delta^{13}\text{C}_{\text{org}}$  rapidly enriches to -23.3‰ by ~2.3 ka. A simultaneous  $\delta^{15}\text{N}$  enrichment trend ensues and continues into the late Holocene, with minor perturbations to the increase centered on 580 cal. years BP, potentially caused by minor adjustments in nitrogen cycling. These isotopic enrichments of the sediment organic matter concurrent with decreasing C/N

demonstrate increasing aquatic productivity in the late Holocene, and correlate with an increase in sedimentation rate (Figure 3) as organic matter flux and carbonate flux increase (Figure 7). The increase in freshwater productivity contrasts the expected pattern of nutrient supply exhaustion by the development of catchment soils over time (Engstrom et al., 2000), making an alternate supply of nutrients likely. The increase in productivity occurs during a period of higher precipitation but could be augmented by increased deposition of loess in the lake basin following Neoglacial retreats. Glacial activity during the Neoglacial and increased silt sources could result in fertilization and altered water chemistry, facilitating aquatic productivity. The presence of silty loams in lake catchments has been shown to influence lake chemistry in the Matanuska-Susitna Valley (McMillan, 2016), and may have played an important role in sediment compositions throughout the lake history, as explored in the following section.

The increasing  $\delta^{13}\text{C}_{\text{org}}$  trend in the late Holocene seems to peak at  $\sim 1.8$  ka, a time that correlates with a similar expression in southwestern Alaska with increased productivity and an inferred warm episode (Kaufman et al., 2012). Following this peak,  $\delta^{13}\text{C}_{\text{org}}$  declines, and fluctuates without any long-term trend to present. The lack of any  $\delta^{13}\text{C}_{\text{org}}$  depletion since the industrial revolution, and no signal corresponding to the Suess Effect, could be explained by an offset caused by increased aquatic productivity such that the degree of reduced carbon discrimination by higher productivity was similar in magnitude to  $\delta^{13}\text{C}$  depletion from fossil fuel burning. In the last century, an increase in aquatic productivity is likely driven by a culmination of factors, including climatic wetting (Baxter, Chapter 1) and the associated increase of nutrient input. Residential development of the lake catchment potentially provides new sources of bioavailable nitrogen, which is supported by the unprecedented enrichment of  $\delta^{15}\text{N}$  in the last  $\sim 75$  years, potentially representing an influx of enriched nitrogen from septic sources.

#### *2.4.5 Changes in Loess Supply Inferred from Sediment Lithology.*

Comparisons of core lithology with LOI results yield interesting paleoenvironmental insights in addition to the isotopic signals. A decrease in CaCO<sub>3</sub> abundance from a 53.5% average prior to ~9 ka, to an average of 28.7% between ~9-2.1 ka and the associated increase in organic matter, averaging 13.6% is represented by darker sediment colors (Figure 7). This alteration of carbonate deposition in the lake may have been caused by either decreased carbonate precipitation or dissolution of produced carbonate. A common explanation for changing carbonate abundance in lake sediment is thermal stratification as a control on the pH gradient in the water column (Dean & Schwalb, 2002). High CO<sub>2</sub> content in the hypolimnion may result in water undersaturated with respect to carbonate minerals, and thus dissolution inhibiting its preservation. The seasonal thermocline in Finger Lake appears in temperature profiles at ~5 m depth (McMillan, unpublished data). Assuming constant lake levels, sediment infill would have placed the coring location (~1.6 m modern depth) above the epilimnion by ~3 ka. This is nearly 1 ka before the marked rise in CaCO<sub>3</sub> content in the late Holocene, though the degree that hypolimnetic waters are undersaturated depends on organic flux, which is low in the middle Holocene. Therefore, thermal stratification control on low CaCO<sub>3</sub> in the mid-core is possible, but unlikely.

Preservation of carbonate is also dependent on sediment pore water chemistry, though aided by thermal stratification and hypolimnion chemistry, but where increased organic matter flux to sediments and subsequent decay increases CO<sub>2</sub> production by microbial respiration. Given the increase in sediment organic matter flux ~10 ka during early Holocene wetting, this may have contributed to reduced carbonate preservation throughout the middle Holocene (Figure 7). Interestingly, other limnological records in Alaska contain carbonate sediments early in their

records, but deposition does not continue throughout the Holocene. For example, carbonate sediments in Hundred Mile Lake ceased ~7.5 ka (Yu et al., 2008) and severely decreased in Birch Lake of the interior ~9.7 ka (Abbott et al., 2000; Finney et al., unpublished data). This early depletion in lacustrine carbonate may link to a common source, such as a regional control on the supply of carbonate forming ions to lake water.

In the Matanuska-Susitna Valley, loess is known to influence the specific conductivity of lakes containing silt loam in their catchments (McMillan, 2016). Eolian input of CaCO<sub>3</sub>-rich loess may therefore significantly load lake waters with carbonate forming ions. Similarly, the tendency of lakes across Alaska to cease carbonate deposition in the early Holocene may be driven by an eventual depletion of loess supplied from Wisconsinan glacial retreat or stabilization of silt deposits by increased vegetation. In these lakes, carbonate bedrock is lacking, necessitating an allochthonous supply of carbonate ions to enable carbonate precipitation. In Finger Lake, a ready supply of carbonate ions from groundwater-bedrock interactions (Moxham & Eckhart, 1956; Moran & Solin, 2006) allows carbonate precipitation regardless of eolian ion replenishment. Therefore, a decrease in loess deposition to Finger Lake ~9 ka concurrent with CaCO<sub>3</sub> diminishment in other lakes, would result in decreased CaCO<sub>3</sub> as is observed, but not total cessation of carbonate deposition. The overall low carbonate flux throughout the lateglacial does not support the high CaCO<sub>3</sub> content but may result from the low sedimentation rate (Figure 3).

A connection between glacial activity and carbonate loess supply to Finger Lake can explain the resumption of higher CaCO<sub>3</sub> abundance and flux in Finger Lake after ~2.1 ka. CaCO<sub>3</sub> increases from a 28.7% average to a 49.9% average from ~2.1 ka to present, concomitant with a significant rise in carbonate flux (Figure 7) which may have resulted from an increase in

CaCO<sub>3</sub>-rich loess deposition in Finger Lake. Increased loess sourced by heightened glacial activity at the onset of the Neoglacial (~3.6-3 ka, Calkin et al., 2001; Barclay et al., 2009) may have contributed to the carbonate ion load of Finger Lake, fueling increased carbonate precipitation. The exact timing of this increase, as inferred from the Finger Lake record, is ~2 ka. An additional or alternative control on increased carbonate flux in the recent millennia may source from increased groundwater input with climatic wetting (Baxter, Chapter 1), which may serve as an important supplement of carbonate ions to the lake basin (Shapley et al., 2002).

Most likely, a culmination the factors noted above drives the major thresholds in Holocene CaCO<sub>3</sub> accumulation at ~9 and 2.1 ka, including loess deposition, the maturation of soil in the catchment, progression of terrestrial vegetation communities influencing soil acidity, and carbonate flux rates driven by groundwater supply of ions and aquatic primary productivity.

## ***2.5 Conclusion.***

The organic isotope and elemental records of Finger Lake reveal an active freshwater ecosystem that established quickly after deglaciation and remained relatively stable throughout the lateglacial. During this early interval, high sediment CaCO<sub>3</sub> content likely resulted from lake input of carbonate loess, largely sourced from Wisconsinan glacial retreat. Following a period of initial climatic wetting ~10 ka the aquatic community underwent significant changes in nutrient sourcing which continued throughout the Holocene during shifts in regional water balance modulated by cyclonic activity over the North Pacific. Wetter climate throughout the middle Holocene likely resulted in overall lower sediment CaCO<sub>3</sub> content by reducing loess input and encouraging terrestrial vegetation productivity, and climatic warming reducing glacial activity. Throughout the record, a close coupling of  $\delta^{13}\text{C}_{\text{org}}$  to changes in P-E water balance displays the

likely control of lake inflow on the supply of respired carbon to limnic autotrophs, accounting for dramatic changes and overall trends in  $\delta^{13}\text{C}_{\text{org}}$ . Aquatic productivity continued to gradually rise with a stable climate and nutrient supply throughout the Holocene, with changes in carbon cycling centered on  $\sim 3$  ka during a regional cooling and wetting event thought to represent the onset of the Neoglaciation. Sustained enrichments in  $\delta^{13}\text{C}_{\text{org}}$  and  $\delta^{15}\text{N}$  initiated by  $\sim 2$  ka reflect increasing aquatic productivity into the present, likely in response to a culmination of increased moisture supply, loess fertilization, and catchment nutrient inputs. The increase in productivity and loess input likely contribute to carbonate flux in the lake, producing a notable increase in sedimentation rate in recent millennia.

2.6 Figures.

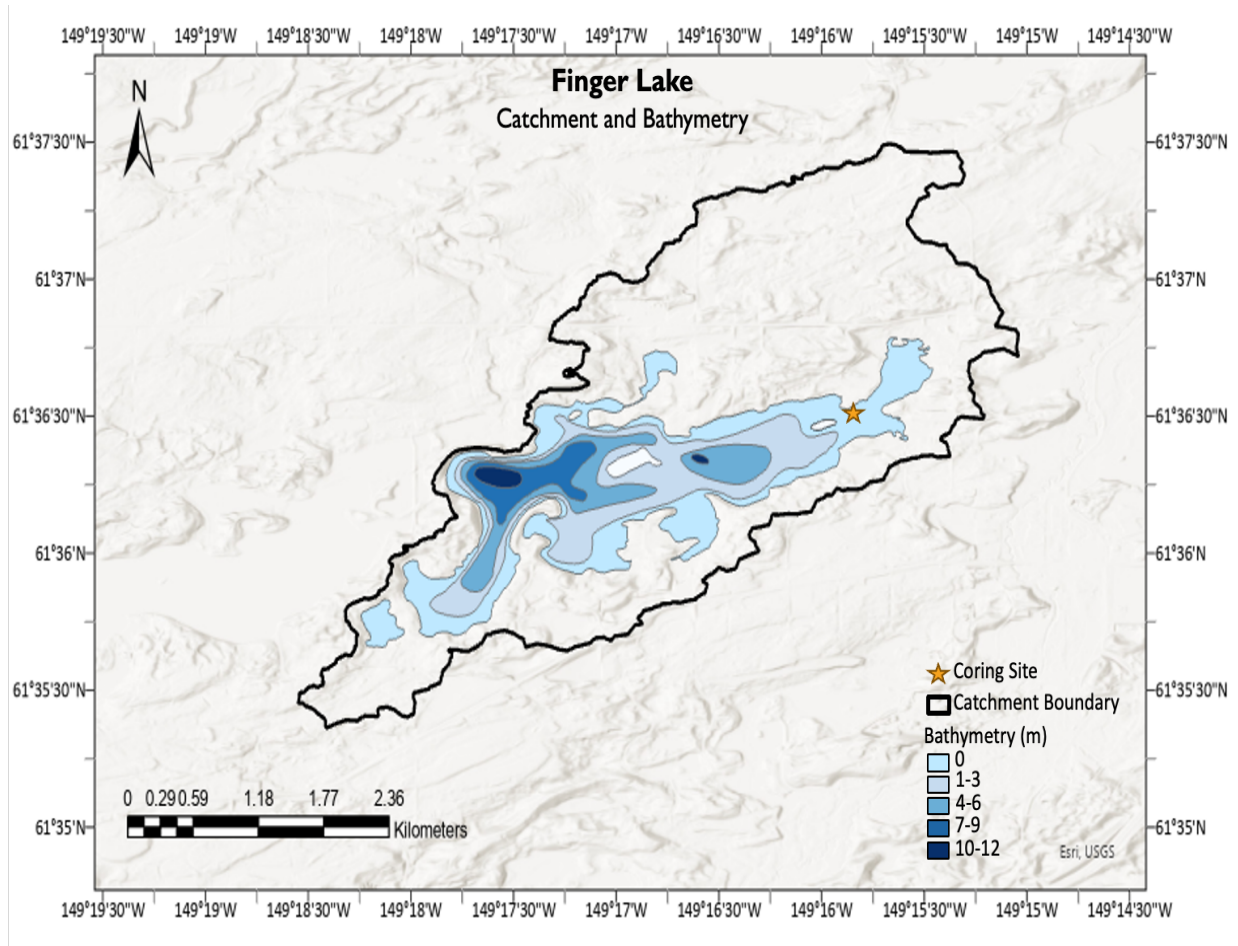


**Figure 1.** Map of the study location depicting the bathymetry of Finger Lake and the low-relief catchment. The coring site is depicted by an orange star (bathymetric contours and catchment boundary by R. T. Pelltier).

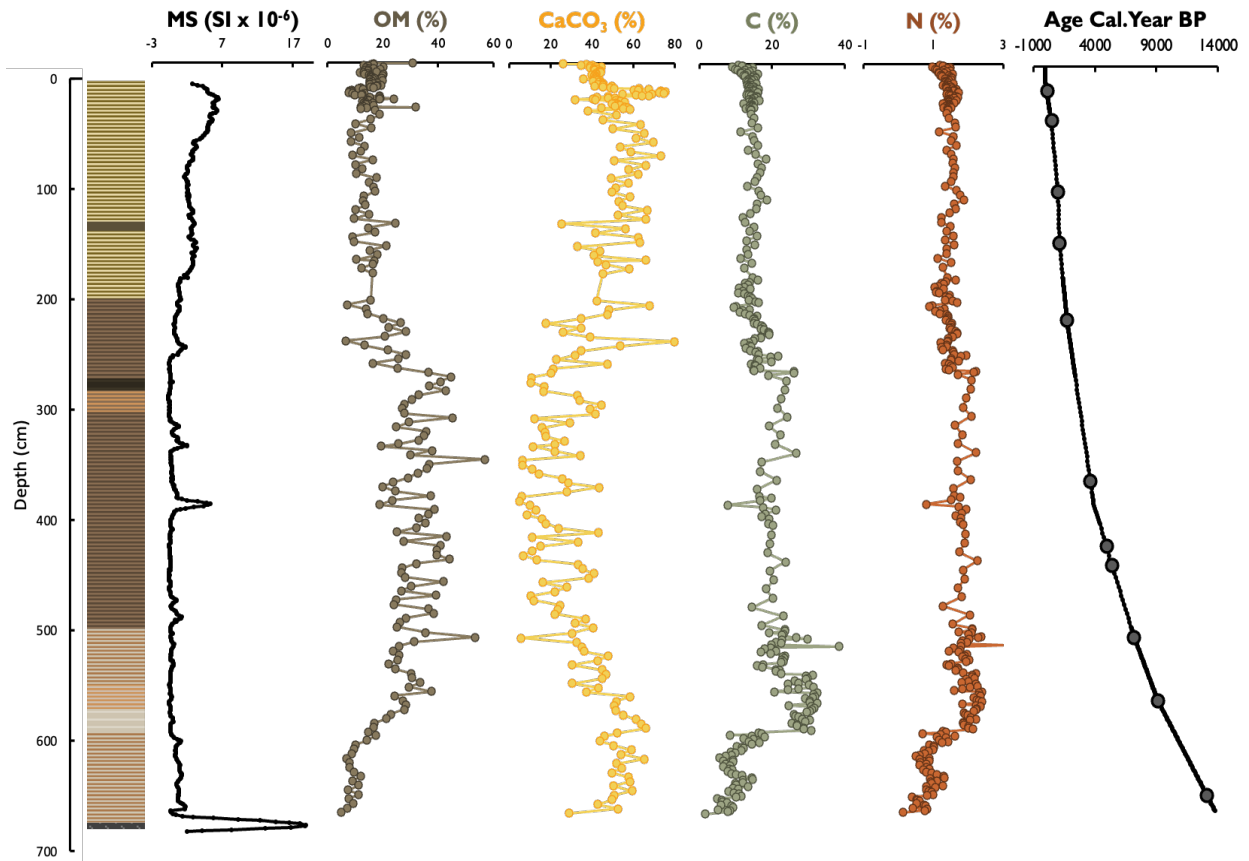


**Figure 2.** Initial sediment analyses with depth down core. (Left to right) simplified diagram of core lithology representing primary lithologic units and associated descriptions below, sediment magnetic susceptibility (SI), organic matter content (OM) in brown, calcium carbonate content (CaCO<sub>3</sub>) in yellow, %C in green, %N in red, and ages in calibrated years before present (1950 AD) with black dots representing the locations of dated samples and the black line representing the linear interpolation of ages to non-dated depths.

**Lithologic Key.**

Thin bedded (3-10 cm) marl, green-gray chroma	Gyttja, olive brown-black	Organic-rich, thin bedded (3-10 cm) sediments, gray-brown to very dark gray	Thin bedded (3-10 cm) marl, tan-white	Glaciolacustrine Gravelly Sand
---	---------------------------	---	---------------------------------------	--------------------------------

Core-Drive-Depth	Depth	Material	<sup>14</sup> C AGE	±	1-Sigma	Cal. Years	Error of	Lab/Date
	(cm)					BP	Mean	
A16-D2-29.0 cm	48	Bark fragments	430	15	494-506	500	6	WHOI 7/26/2021
A16-D2-93.0 cm	112	1 woody fragment, 1 bud, 4 broad-leaf type fragments	1100	25	958-1053	1000	47.5	WHOI 7/26/2021
A16-D2-138.5 cm	157.5	Numerous leaf fragments	1210	20	1075-1164	1126	44.5	WHOI 7/26/2021
A16-D3-52-53cm	226	Black tissue, possibly charcoal	1800	170	1535-1923	1730	388	LLNL 9/1/2018
A16-D5-36-37cm	370	Black tissue, possibly charcoal	3400	60	3568-3719	3650	151	LLNL 8/1/2018
A16-D5- 56 cm	390	Watana Tephra			3700-4085	3900	385	
A16-D5-94 cm	428	6 broadleaf fragments picked, 1 Alnus/Betula sp. seed	4400	40	4950-5040	4970	45	WHOI 7/26/2021
A16-D6-38 cm	445	1 Alnus/Betula sp. seed, 1 Picea sp. needle base, 1 Pinaceae needle fragment	4670	40	5321-5463	5400	70.5	WHOI 7/26/2021
A16-D7-14-15cm	509	Wood	6245	30	7162-7245	7200	83	LLNL 8/1/2018
A16-D7-72 cm	566	Woody leaf scar	8170	75	9013-9143	9130	65	WHOI 8/5/21
A16-D8-76 cm	650	Wood and leaf-type fragments	11200	220	12895-13303	13102	204	WHOI 8/5/21

*Table 1. Radiocarbon sample depths, dated material, and age uncertainties.*

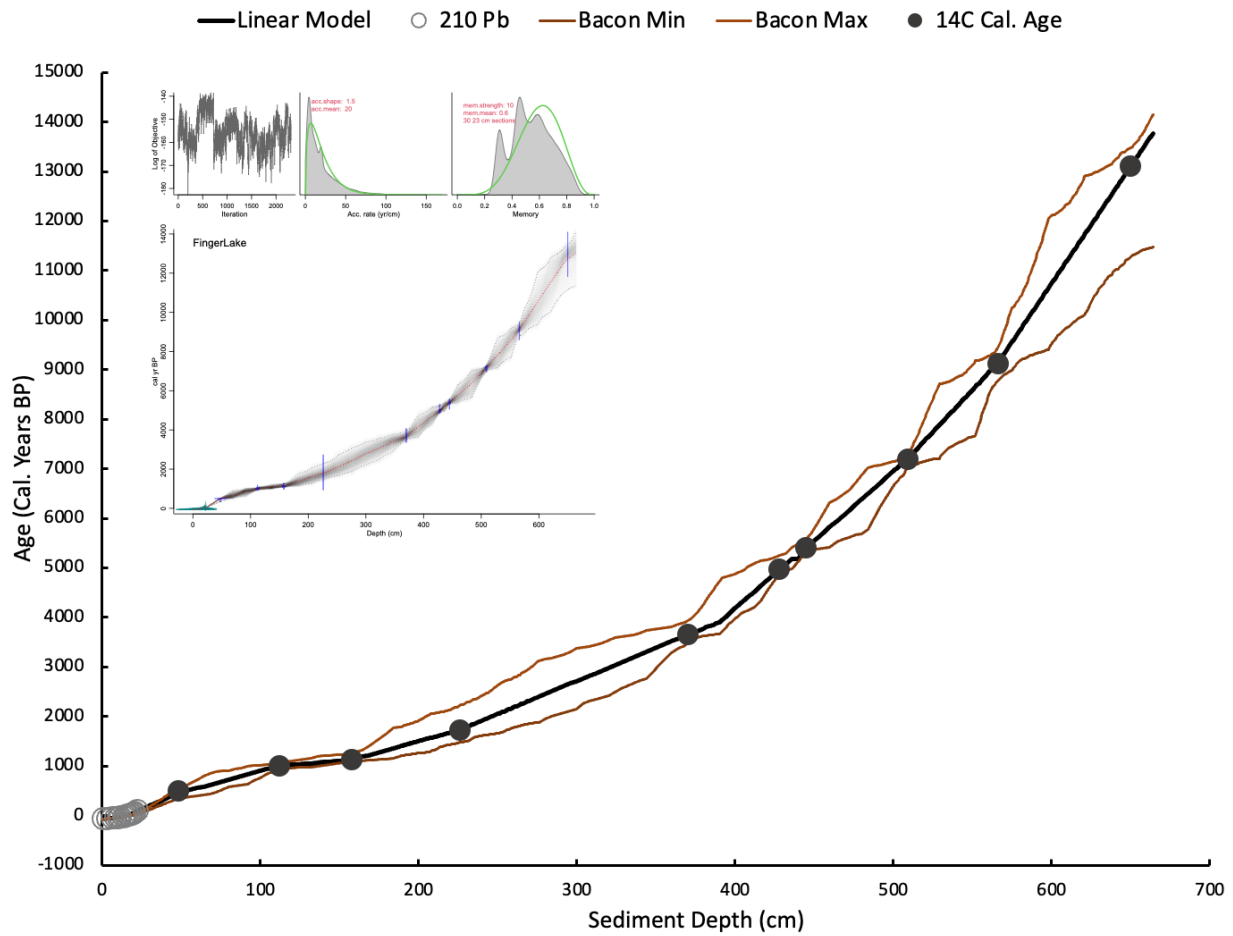


**Figure 3.** Sediment Age Model. Black-filled circles represent radiocarbon dated terrestrial macrofossils sampled throughout the sediment column. Gray hollow circles represent <sup>210</sup>Pb dated sediments in the upper core. The thick black curve represents the age model defined by linear interpolation. The red curves represent the maximum and minimum age models generated by Bayesian interpolation using the R package BACON by Blaauw and Christen (2011). The inset graph generated by BACON displays age uncertainty.

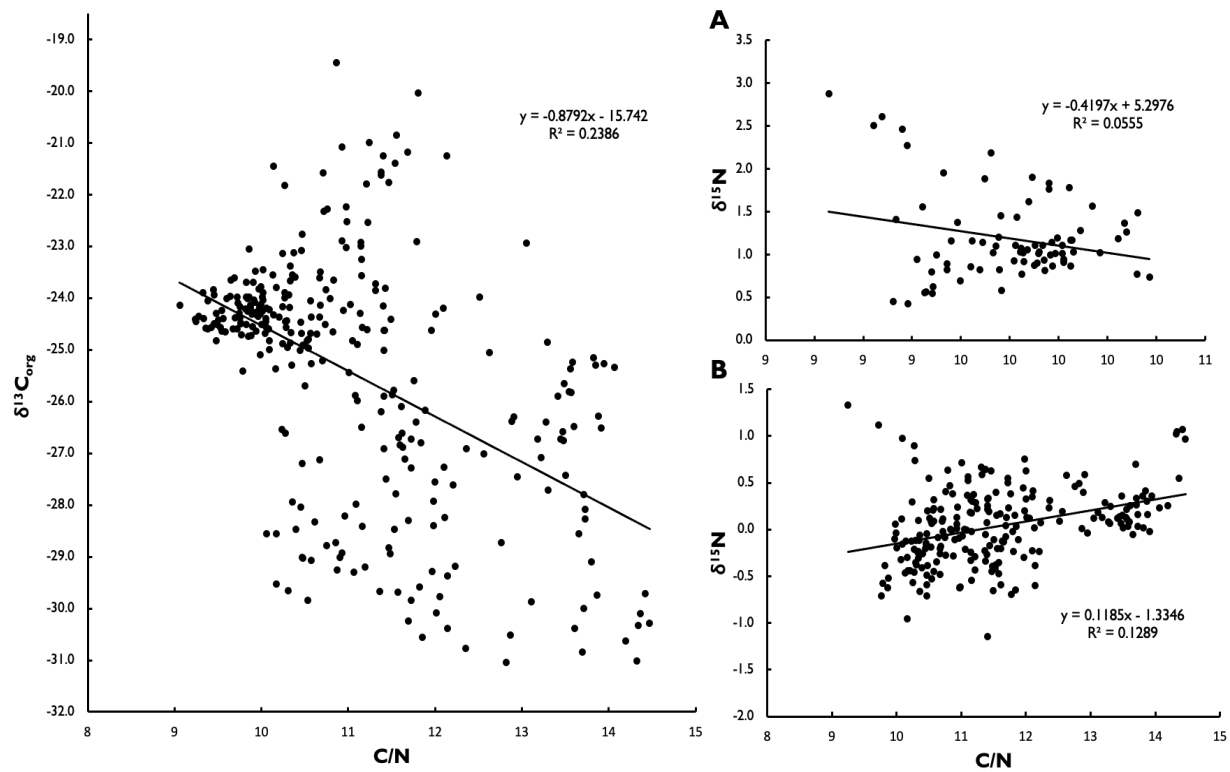


**Figure 4.** Regressions comparing C/N with  $\delta^{13}C_{org}$  (left) and  $\delta^{15}N$  (right) post 2 ka (A) and prior to 2 ka (B).

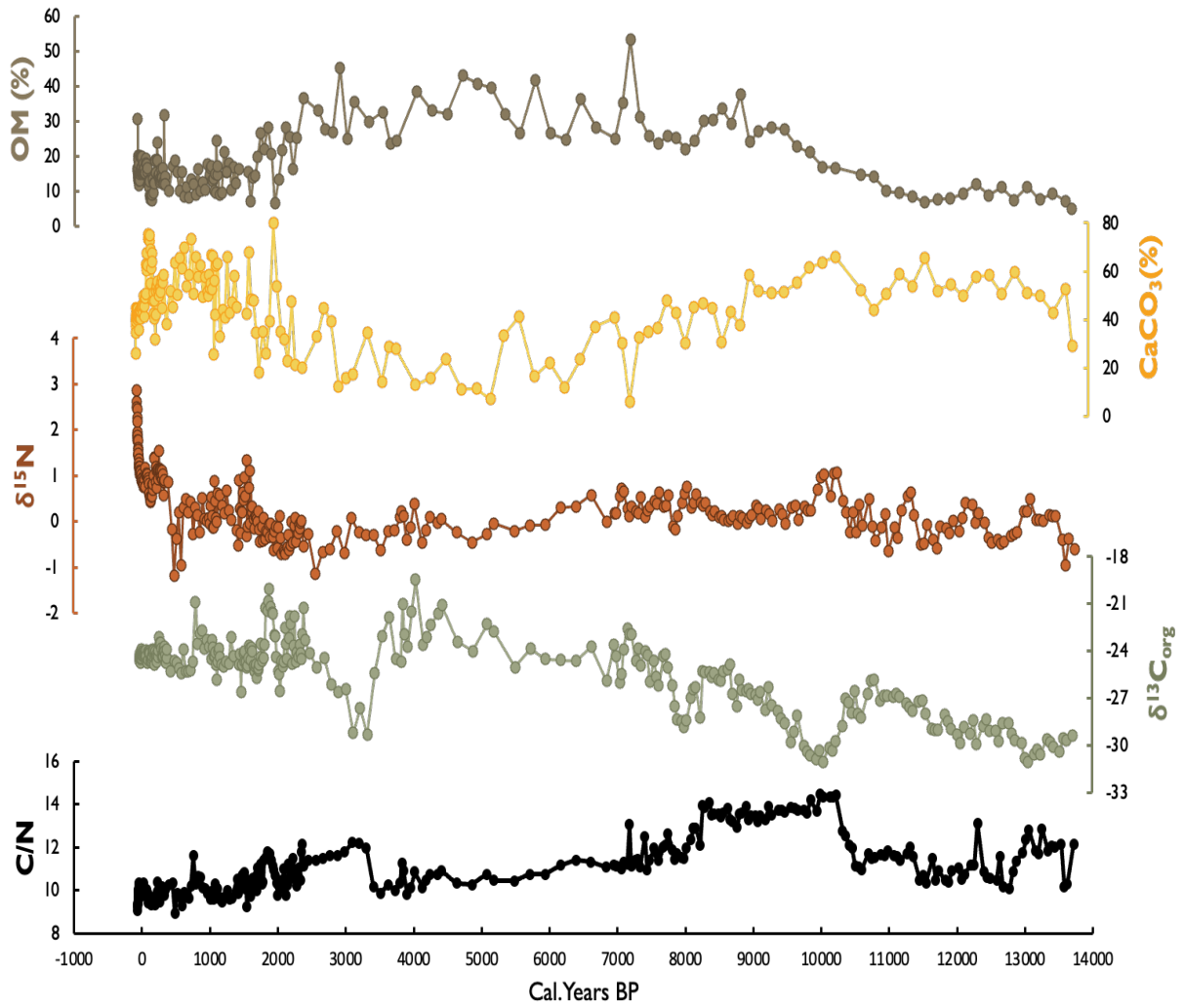


**Figure 5.** (Bottom to top/left to right) C/N ratio (black),  $\delta^{13}C_{org}$  (green), sediment organic  $\delta^{15}N$  (red), sediment  $CaCO_3$  content (yellow), and sedimentary organic matter content (brown) plotted with age in calibrated years before present.

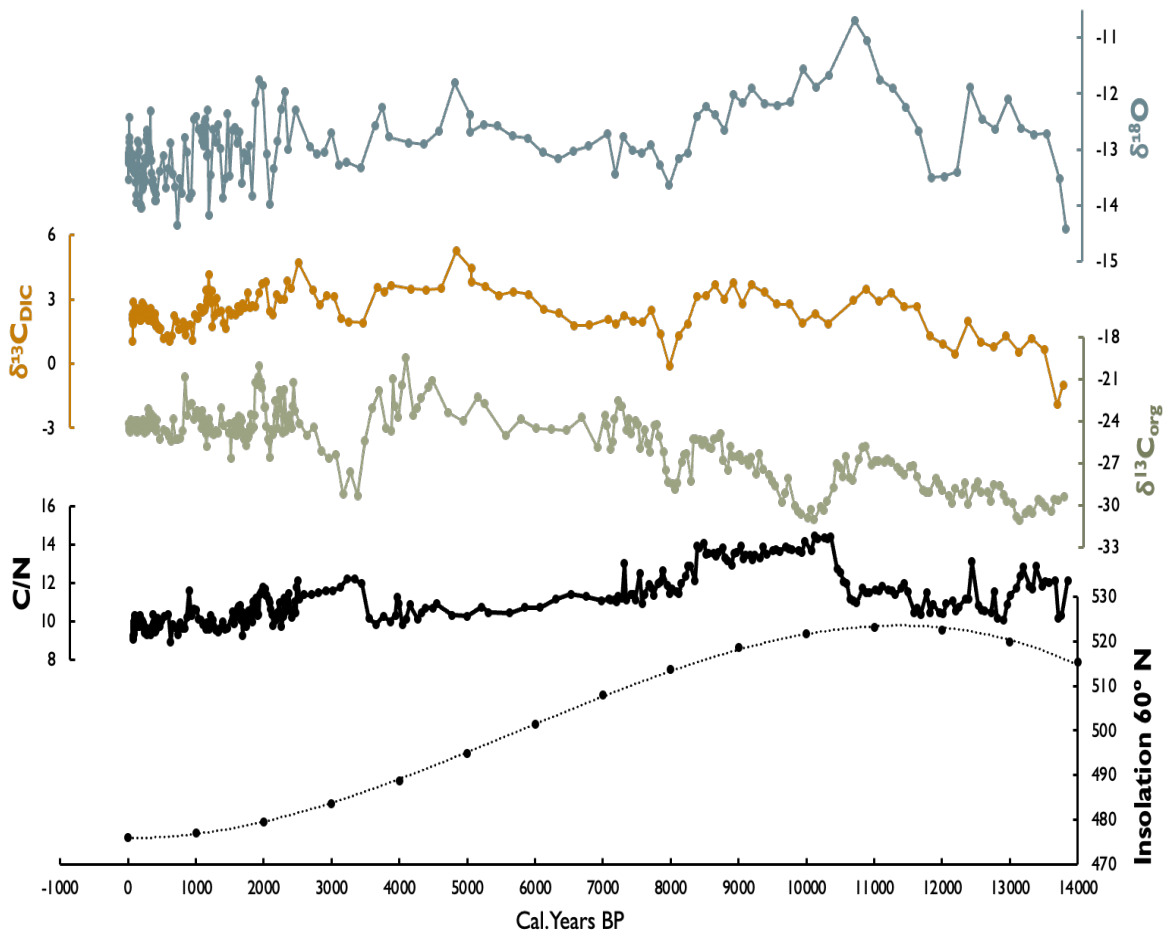


**Figure 6.** (Bottom to top/left to right) June insolation at 60° N by Berger (1978), sedimentary organic C/N (black),  $\delta^{13}\text{C}_{\text{org}}$  (green), and carbonate isotope compositions from Baxter, Chapter 1.

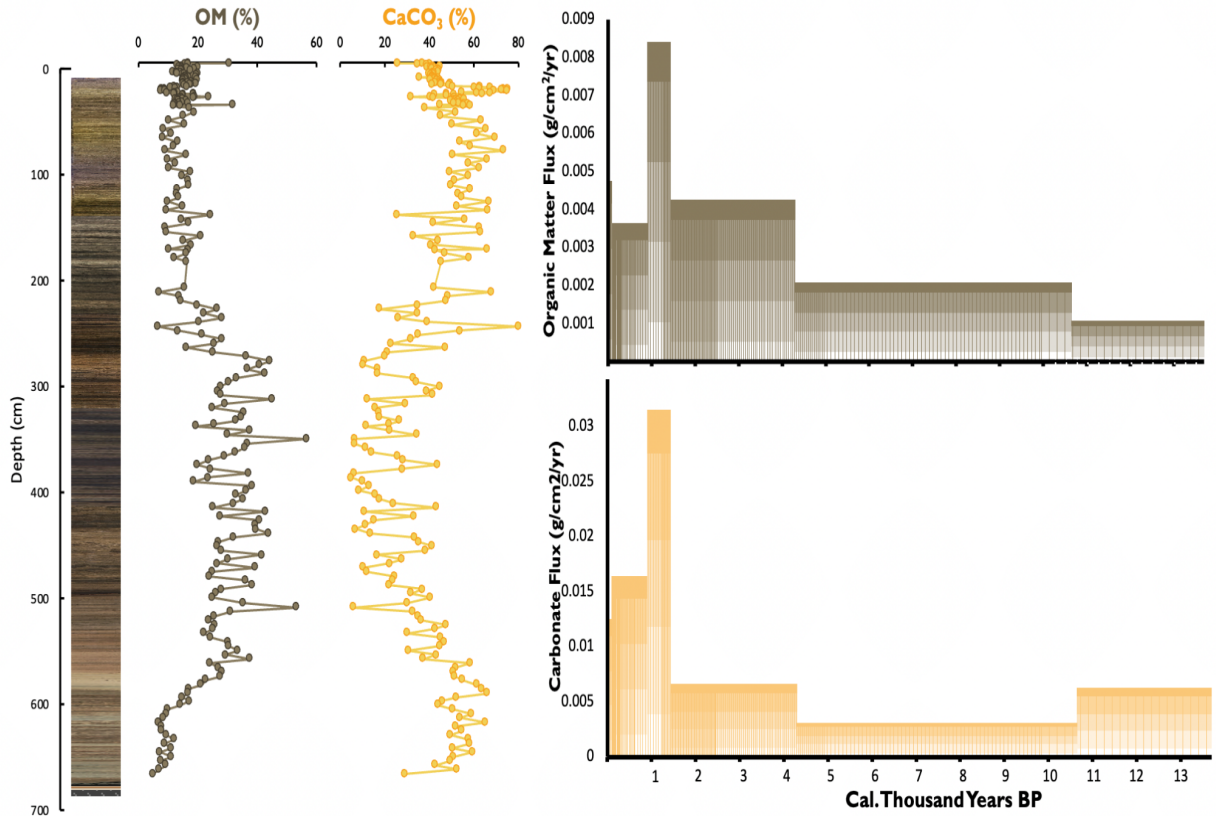


*Figure 7. A comparison of sediment color with organic matter content (OM in dark brown) and calcite content (CaCO<sub>3</sub> in yellow) on the left (top), and organic matter flux (brown bar graph) and carbonate flux (yellow bar graph) on the right (bottom).*

## 2.7 References Cited in Chapter 2.

- Abbott, M.B., Finney, B.P., Edwards, M.E., Kelts, K.R., 2000. Lakelevel reconstruction and paleohydrology of Birch Lake, central Alaska, based on seismic reflection profiles and core transects. *Quaternary Research* 53, p. 154–166.
- Addison, J. A., B. P. Finney, W. E. Dean, M. H. Davies, A. C. Mix, J. S. Stoner, and J. M. Jaeger, 2012, Productivity and sedimentary  $\delta^{15}\text{N}$  variability for the last 17,000 years along the northern Gulf of Alaska continental slope: *Paleoceanography*, v. 27, p. 1206, doi:10.1029/2011PA002161.
- Ager, T.A., 1983, Holocene vegetational history of Alaska. In: Wright Jr., H.E. (Ed.), *Late Quaternary Environments of the United States: The Holocene*, v. 2, University of Minnesota Press, Minneapolis, MN, p. 128–141.
- Ager, T.A., 1989, History of late Pleistocene and Holocene vegetation in the Copper River basin, south-central Alaska. In: Carter, L.D., Hamilton, T.D., Galloway, J.P. (Eds.), *Late Cenozoic History of the Interior Basins of Alaska and the Yukon: US Geological Survey Circular*, v. 1026, p. 89–92.
- Aichner, B., Wilkes, H., Herzs Schuh, U., Mischke, S., & Zhang, C., 2010, Biomarker and compound-specific  $\delta^{13}\text{C}$  evidence for changing environmental conditions and carbon limitation at Lake Koucha, eastern Tibetan Plateau: *Journal of Paleolimnology*, v. 43(4), p. 873-899.
- Alaska Department of Fish and Game, 2013, <https://www.adfg.alaska.gov/static/fishing/pdfs/sport/byarea/southcentral/matsulakes.pdf> (accessed March 2022).
- Alley, R. B., 2000, The Younger Dryas cold interval as viewed from central Greenland: *Quaternary science reviews*, v. 19 (1-5), p. 213-226.
- Barclay, D. J., Wiles, G. C., & Calkin, P. E., 2009, Holocene glacier fluctuations in Alaska: *Quaternary Science Reviews*, v. 28(21-22), p. 2034-2048.
- Berger, A., 1978, A simple algorithm to compute long term variations of daily or monthly insolation. Contribution No. 18, Universite Catholique de Louvain, Institut d'Astronomie et de Geophysique, G. Lemaitre: Louvain-la-Neuve, B-1348 Belgique.
- Bigelow, N.H., Reuther, J.D., Wallace, K.L., Saulnier-Talbot, É., Mulliken, K., and Wooller, M.J., 2019, Late-Glacial Paleocology of the Middle Susitna Valley, Alaska: Environmental Context for Human Dispersal: *Frontiers in Earth Science*, v. 7, p. 43, doi:10.3389/feart.2019.00043.
- Botrel, M., Gregory-Eaves, I. & Maranger, R., 2014, Defining drivers of nitrogen stable isotopes ( $\delta^{15}\text{N}$ ) of surface sediments in temperate lakes: *J Paleolimnology*, v. 52, p. 419–433, doi:10.1007/s10933-014-9802-6.
- Brenner, M., Whitmore, T. J., Curtis, J. H., Hodell, D. A., & Schelske, C. L., 1999, Stable isotope ( $\delta^{13}\text{C}$  and  $\delta^{15}\text{N}$ ) signatures of sedimented organic matter as indicators of historic lake trophic state: *Journal of Paleolimnology*, v. 22(2), p. 205-221.
- Broadman, E., Kaufman, D. S., Henderson, A. C., Berg, E. E., Anderson, R. S., Leng, M. J., ... & Muñoz, S. E., 2020, Multi-proxy evidence for millennial-scale changes in North Pacific

- Holocene hydroclimate from the Kenai Peninsula lowlands, south-central Alaska: *Quaternary Science Reviews*, v. 241, p. 106420.
- Buizert, C., Gkinis, V., Severinghaus, J. P., He, F., Lecavalier, B. S., Kindler, P., Leuenberger, M., Carlson, A. E., Vinther, B., Masson-Delmotte, V., White, J. W. C., Liu, Z., Otto-Bliesner, B., & Brook, E. J., 2014, Greenland temperature response to climate forcing during the last Deglaciation: *Science*, v. 345(6201), p. 1177–1180.
- Calkin, P. E., Wiles, G. C., & Barclay, D. J., 2001, Holocene coastal glaciation of Alaska: *Quaternary Science Reviews*, v. 20(1-3), p. 449-461.
- Dansgaard, W., Johnsen, S., Clausen, H. et al., 1993, Evidence for general instability of past climate from a 250-kyr ice-core record: *Nature* v. 364, p. 218–220, doi:10.1038/364218a0
- Davies, M. H., Mix, A. C., Stoner, J. S., Addison, J. A., Jaeger, J., Finney, B., & Wiest, J., 2011, The deglacial transition on the southeastern Alaska Margin: Meltwater input, sea level rise, marine productivity, and sedimentary anoxia: *Paleoceanography*, v. 26(2).
- Dean, W. E., & Schwalb, A., 2002, The lacustrine carbon cycle as illuminated by the waters and sediments of two hydrologically distinct headwater lakes in north-central Minnesota, USA: *Journal of Sedimentary Research*, v. 72(3), p. 416-431.
- De Kluijver, A., Schoon, P. L., Downing, J. A., Schouten, S., & Middelburg, J. J., 2014, Stable carbon isotope biogeochemistry of lakes along a trophic gradient: *Biogeosciences*, v. 11(22), p. 6265-6276.
- Engstrom, D. R., Fritz, S. C., Almendinger, J. E., & Juggins, S., 2000, Chemical and biological trends during lake evolution in recently deglaciated terrain: *Nature*, v. 408(6809), p. 161-166.
- Finney, B. P., Bigelow, N. H., Barber, V. A., & Edwards, M. E., 2012, Holocene climate change and carbon cycling in a groundwater-fed, boreal forest lake: Dune Lake, Alaska: *Journal of paleolimnology*, v. 48(1), p. 43-54.
- Gu, B., Schelske, C. L., & Brenner, M., 1996, Relationship between sediment and plankton isotope ratios ( $\delta^{13}\text{C}$  and  $\delta^{15}\text{N}$ ) and primary productivity in Florida lakes: *Canadian Journal of Fisheries and Aquatic Sciences*, v. 53(4), p. 875-883.
- Hecky, R. E., Campbell, P., & Hendzel, L. L., 1993, The stoichiometry of carbon, nitrogen, and phosphorus in particulate matter of lakes and oceans: *Limnology and Oceanography*, v. 38(4), p. 709-724.
- Heusser, C. J., 1995, Late-Quaternary vegetation response to climatic-glacial forcing in North Pacific America: *Physical Geography*, v. 16(2), p. 118-149.
- Heusser, C.J., Heusser, L.E., Peteet, D.M., 1985, Late-Quaternary climatic change on the American North Pacific coast. *Nature*, v. 315, p. 485–487.
- Hu FS, Brubaker LB, Anderson PM, 1995, Postglacial vegetation and climate change in the northern Bristol Bay region, southwestern Alaska: *Quaternary Research*, v. 43, p. 382–392.

- Kaufman, D. S., Ager, T. A., Anderson, N. J., Anderson, P. M., Andrews, J. T., Bartlein, P. J., ... & Wolfe, B. B., 2004, Holocene thermal maximum in the western Arctic (0–180 W): Quaternary Science Reviews, v. 23(5-6), p. 529-560.
- Kaufman, D. S., Axford, Y., Anderson, R. S., Lamoureux, S. F., Schindler, D. E., Walker, I. R., & Werner, A., 2012, A multi-proxy record of the Last Glacial Maximum and last 14,500 years of paleoenvironmental change at Lone Spruce Pond, southwestern Alaska: Journal of Paleolimnology, v. 48(1), p. 9-26.
- Kikuchi, C.P., 2013, Shallow Groundwater in the Matanuska-Susitna Valley, Alaska—Conceptualization and Simulation of Flow: U.S. Geological Survey Scientific Investigations Report, v. 2013–5049.
- Kling, G. W., Kipphut, G. W., & Miller, M. C., 1991, Arctic lakes and streams as gas conduits to the atmosphere: implications for tundra carbon budgets: Science, v. 251(4991), p. 298-301.
- Kokorowski, H. D., Anderson, P. M., Mock, C. J., & Lozhkin, A. V., 2008, A re-evaluation and spatial analysis of evidence for a Younger Dryas climatic reversal in Beringia: Quaternary Science Reviews, v. 27(17-18), p. 1710-1722.
- Kopczynski, S. E., Kelley, S. E., Lowell, T. V., Evenson, E. B., & Applegate, P. J., 2017, Latest Pleistocene advance and collapse of the Matanuska–Knik glacier system, Anchorage Lowland, southern Alaska: Quaternary Science Reviews, v. 156, p. 121-134.
- Lasher, G. E., Abbott, M. B., Anderson, L., Yasarer, L., Rosenmeier, M., & Finney, B. P., 2021, Holocene hydroclimatic reorganizations in northwest Canada inferred from lacustrine carbonate oxygen isotopes: Geophysical Research Letters, v. 48(16), p. e2021GL092948.
- Laws, E. A., Popp, B. N., Bidigare, R. R., Kennicutt, M. C., & Macko, S. A., 1995, Dependence of phytoplankton carbon isotopic composition on growth rate and [CO<sub>2</sub>] aq: theoretical considerations and experimental results: Geochimica et cosmochimica acta, v. 59(6), p. 1131-1138.
- McMillan, M.S., 2016, Spatial and temporal analysis of land cover, climate, and lake water quality in the Matanuska-Susitna, Valley, Alaska: Alaska Pacific University.
- Meyers, P. A., & Ishiwatari, R., 1993, Lacustrine organic geochemistry—an overview of indicators of organic matter sources and diagenesis in lake sediments: Organic geochemistry, v. 20(7), p. 867-900.
- Meyers, P.A., 2003, Applications of organic geochemistry to paleolimnological reconstructions: a summary of examples from the Laurentian Great Lakes: Organic geochemistry, v. 34(2), p. 261-289.
- Moran, E.H., and Solin, G.L., 2006, Preliminary water-table map and water-quality data for part of the Matanuska-Susitna Valley, Alaska, 2005: U.S. Geological Survey Open-File Report, v. 2006-1209.
- Morrill, C., Overpeck, J. T., & Cole, J. E., 2003, A synthesis of abrupt changes in the Asian summer monsoon since the last deglaciation: The Holocene, v. 13(4), p. 465-476.

- Morrill, C., 2004, The influence of Asian summer monsoon variability on the water balance of a Tibetan lake: *Journal of Paleolimnology*, v. 32(3), p. 273-286.
- Moxham, R.M., and Eckhart, R.A., 1956, Marl Deposits in the Knik Arm Area Alaska: *Geological Survey Bulletin*, v. 1039-A, p. 4-17.
- Müller, P. J., 1977, CN ratios in Pacific deep-sea sediments: Effect of inorganic ammonium and organic nitrogen compounds sorbed by clays: *Geochimica et Cosmochimica Acta*, v. 41(6), p. 765-776.
- Pompeani, D. P., Steinman, B. A., & Abbott, M. B., 2012, A sedimentary and geochemical record of water-level changes from Rantin Lake, Yukon, Canada: *Journal of paleolimnology*, v. 48(1), p. 147-158.
- Praetorius, S. K., & Mix, A. C., 2014, Synchronization of North Pacific and Greenland climates preceded abrupt deglacial warming: *Science*, v. 345(6195), p. 444-448.
- Reimer PJ, Bard E, Bayliss A, Beck JW, Blackwell PG, Bronk Ramsey C, Buck CE, Cheng H, Edwards RL, Friedrich M, Grootes PM, Guilderson TP, Haflidason H, Hajdas I, Hatté C, Heaton TJ, Hoffmann DL, Hogg AG, Hughen KA, Kaiser KF, Kromer B, Manning SW, Niu M, Reimer RW, Richards DA, Scott EM, Southon JR, Staff RA, Turney CSM, van der Plicht J. 2013. IntCal13 and Marine13 radiocarbon age calibration curves 0–50,000 years cal BP. *Radiocarbon* 55(4):1869–1887.
- Stafford, J. M., Wendler, G., & Curtis, J., 2000, Temperature and precipitation of Alaska: 50 year trend analysis: *Theoretical and Applied Climatology*, v. 67(1), p. 33-44.
- Verburg, P., 2007, The need to correct for the Suess effect in the application of  $\delta^{13}\text{C}$  in sediment of autotrophic Lake Tanganyika, as a productivity proxy in the Anthropocene: *Journal of Paleolimnology*, v. 37(4), p. 591-602.
- Viereck, L.A., Little Jr., E.L., 1975, Atlas of United States Trees, vol. 2, Alaska Trees and Common Shrubs. Miscellaneous Publication no. 1293: USDA Forest Service, Washington, DC, p. 85.
- Wallace, K.L., Coombs, M.L., Hayden, L.A., and Waythomas, C.F., 2014, Insights from a proximal stratigraphic sequence from Hayes Volcano, south-central Alaska: U.S. Geological Survey Scientific Investigations Report, v. 2014- 5133, p. 32. doi: 10.3133/sir20145133.
- Western Regional Climate Center, 2009, Anchorage Ted Stevens International Airport Alaska, Retrieved from <https://wrcc.dri.edu/cgi-bin/cliMAIN.pl?ak0280>
- Woodward, C.A., Potito, A.P. & Beilman, D.W., 2012, Carbon and nitrogen stable isotope ratios in surface sediments from lakes of western Ireland: implications for inferring past lake productivity and nitrogen loading: *J Paleolimnology*, v. 47, p. 167–184, doi: 10.1007/s10933-011-9568-z.
- Yu, Z., Walker, K.N., Evenson, E.B., and Hajdas, I., 2008, Lateglacial and early Holocene climate oscillations in the Matanuska Valley, south-central Alaska: *Quaternary Science Reviews*, v. 27, p.148–161, doi:10.1016/j.quascirev.2007.02.02.

## Appendix.

### A. LOI Tables

Sample	Depth (cm)	DBD g/cm2	%LOI 550	%OC	%LOI 950	%CO3	%CaCO3	Residual
FING-A16-D1	0.5	0.06	31	15.34	11.44	15.56	26	43.34
FING-A16-D1	1	0.11	17	8.34	16.40	22.30	37	46.09
FING-A16-D1	1.5	0.13	16	7.89	17.72	24.11	40	43.98
FING-A16-D1	2		17	8.37	15.31	20.82	35	48.52
FING-A16-D1	2.5	0.16	13	6.54	17.22	23.42	39	47.84
FING-A16-D1	3	0.17	14	7.15	19.66	26.74	45	41.07
FING-A16-D1	3.5	0.17	15	7.33	18.52	25.18	42	43.30
FING-A16-D1	4		20	10.03	17.32	23.55	39	40.64
FING-A16-D1	4.5	0.17	14	6.99	18.04	24.54	41	45.07
FING-A16-D1	5	0.18	15	7.47	18.16	24.70	41	43.84
FING-A16-D1	5.5	0.19	17	8.26	18.72	25.46	43	40.97
FING-A16-D1	6		19	9.48	18.20	24.76	41	39.71
FING-A16-D1	6.5	0.19	14	6.86	19.26	26.19	44	42.57
FING-A16-D1	7	0.21	15	7.39	19.54	26.58	44	40.86
FING-A16-D1	7.5	0.22	14	7.25	19.53	26.56	44	41.17
FING-A16-D1	8		18	8.87	18.96	25.78	43	39.22
FING-A16-D1	8.5	0.22	12	5.83	19.48	26.50	44	44.12
FING-A16-D1	9	0.22	13	6.52	18.52	25.18	42	44.93
FING-A16-D1	9.5	0.22	14	7.20	18.62	25.32	42	43.33
FING-A16-D1	10		20	10.11	17.61	23.95	40	39.82
FING-A16-D1	10.5	0.22	13	6.62	18.29	24.87	42	45.24
FING-A16-D1	11	0.22	15	7.55	18.35	24.95	42	43.26
FING-A16-D1	11.5	0.21	16	7.81	18.43	25.07	42	42.53
FING-A16-D1	12		20	9.88	18.07	24.57	41	39.22
FING-A16-D1	12.5	0.21	16	7.96	18.32	24.92	42	42.49
FING-A16-D1	13	0.22	16	8.04	18.19	24.73	41	42.64
FING-A16-D1	13.5	0.21	17	8.46	18.37	24.99	42	41.37
FING-A16-D1	14		20	9.78	15.82	21.52	36	44.54
FING-A16-D1	14.5	0.22	16	8.14	18.60	25.30	42	41.48
FING-A16-D1	15	0.23	15	7.71	19.38	26.35	44	40.59
FING-A16-D1	15.5	0.22	15	7.68	18.90	25.71	43	41.73
FING-A16-D1	16		20	10.00	17.83	24.24	40	39.53
FING-A16-D1	16.5	0.23	16	8.08	19.11	25.98	43	40.48
FING-A16-D1	17	0.23	15	7.56	19.17	26.07	44	41.36
FING-A16-D1	17.5	0.23	15	7.65	19.74	26.85	45	39.88
FING-A16-D1	18		18	9.05	19.92	27.09	45	36.68
FING-A16-D1	18.5	0.24	15	7.66	20.18	27.45	46	38.86
FING-A16-D1	19	0.23	17	8.34	18.89	25.69	43	40.43
FING-A16-D1	19.5	0.24	15	7.65	20.02	27.22	45	39.27
FING-A16-D1	20		19	9.69	21.91	29.80	50	30.89
FING-A16-D1	20.5	0.21	18	9.01	18.16	24.70	41	40.76
FING-A16-D1	21	0.23	18	8.81	20.00	27.20	45	36.99
FING-A16-D1	21.5	0.24	16	7.78	21.54	29.29	49	35.54
FING-A16-D1	22		17	8.29	22.32	30.35	51	32.76
FING-A16-D1	22.5	0.29	12	6.05	27.65	37.61	63	25.13
FING-A16-D1	23	0.28	11	5.56	29.76	40.47	68	21.33
FING-A16-D1	23.5	0.28	13	6.57	26.62	36.20	60	26.43
FING-A16-D1	24		13	6.37	27.53	37.44	62	24.78
FING-A16-D1	24.5	0.37	9	4.40	32.28	43.90	73	17.92
FING-A16-D1	25	0.39	8	3.92	33.21	45.17	75	16.76
FING-A16-D1	25.5	0.38	8	4.22	32.49	44.18	74	17.82
FING-A16-D1	26		9	4.37	31.98	43.50	73	18.65
FING-A16-D1	26.5	0.40	8	3.75	33.01	44.89	75	17.56
FING-A16-D1	27	0.36	9	4.52	30.46	41.42	69	21.82
FING-A16-D1	27.5	0.27	13	6.74	24.14	32.84	55	31.72
FING-A16-D1	28		12	6.21	27.03	36.76	61	26.22
FING-A16-D1	28.5	0.33	10	4.86	29.76	40.48	68	22.71
FING-A16-D1	29	0.30	12	6.15	28.24	38.40	64	23.61
FING-A16-D1	29.5	0.21	19	9.39	21.12	28.72	48	33.29
FING-A16-D1	30		19	9.40	18.76	25.51	43	38.62
FING-A16-D1	30.5	0.24	15	7.68	22.49	30.59	51	33.58
FING-A16-D1	31	0.25	15	7.60	21.10	28.69	48	36.91
FING-A16-D1	31.5	0.21	19	9.58	17.85	24.27	41	40.32
FING-A16-D1	32		24	11.92	14.01	19.05	32	44.35
FING-A16-D1	32.5	0.21	19	9.37	18.46	25.10	42	39.37
FING-A16-D1	33	0.26	15	7.25	22.76	30.95	52	33.84
FING-A16-D1	33.5	0.28	14	6.94	23.86	32.44	54	31.97

FING-A16-D1	34		15	7.50	23.64	32.16	54	31.33
FING-A16-D1	34.5	0.28	13	6.32	24.56	33.40	56	31.60
FING-A16-D1	35	0.27	14	6.83	22.75	30.94	52	34.70
FING-A16-D1	35.5	0.27	13	6.60	23.05	31.35	52	34.47
FING-A16-D1	36		16	8.13	21.97	29.88	50	33.87
FING-A16-D1	36.5	0.26	14	6.85	23.35	31.76	53	33.29
FING-A16-D1	37	0.26	15	7.44	22.97	31.24	52	32.99
FING-A16-D1	37.5	0.27	14	7.00	23.60	32.10	54	32.42
FING-A16-D1	38		17	8.34	22.61	30.76	51	31.99
FING-A16-D1	38.5	0.29	13	6.36	24.55	33.39	56	31.55
FING-A16-D1	39	0.30	12	6.05	25.22	34.31	57	30.64
FING-A16-D1	39.5	0.30	32	15.95	19.74	26.84	45	23.30
FING-A16-D1	40		14	7.05	24.35	33.12	55	30.63
FING-A16-D1	40.5	0.30	12	5.97	25.80	35.09	59	29.49
Fing A16-D2 42	0.27	17	8.59	16.80	22.85	38	44.70	
Fing A16-D2 46	0.20	19	9.44	22.84	31.06	52	29.28	
Fing A16-D2 50	0.25	15	7.72	19.93	27.10	45	39.33	
Fing A16-D2 54	0.37	10	5.09	27.96	38.02	63	26.36	
Fing A16-D2 58	0.25	16	7.83	22.13	30.10	50	34.10	
Fing A16-D2 62	0.42	9	4.27	28.86	39.25	66	25.95	
Fing A16-D2 66	0.33	11	5.67	27.03	36.76	61	27.30	
Fing A16-D2 70	0.40	8	4.16	30.68	41.73	70	22.03	
Fing A16-D2 74	0.31	13	6.69	23.66	32.17	54	32.91	
Fing A16-D2 78	0.34	12	6.02	25.82	35.12	59	29.35	
Fing A16-D2 82	0.41	9	4.49	32.37	44.03	73	17.53	
Fing A16-D2 86	0.28	16	8.20	22.33	30.37	51	32.91	
Fing A16-D2 90	0.36	10	5.01	29.11	39.59	66	23.89	
Fing A16-D2 94	0.33	13	6.32	25.40	34.55	58	29.69	
Fing A16-D2 98	0.38	10	5.16	27.46	37.35	62	27.34	
Fing A16-D2 102	0.28	18	8.83	21.73	29.56	49	33.01	
Fing A16-D2 106	0.30	15	7.43	25.35	34.47	58	27.61	
Fing A16-D2 110	0.28	17	8.35	22.71	30.89	52	31.74	
Fing A16-D2 114	0.28	17	8.54	21.94	29.84	50	33.13	
Fing A16-D2 118	0.35	13	6.55	25.80	35.09	59	28.33	
Fing A16-D2 122	0.32	13	6.46	23.41	31.84	53	33.93	
Fing A16-D2 126	0.29	14	6.77	24.13	32.82	55	31.68	
Fing A16-D2 130	0.39	10	5.02	29.45	40.05	67	23.10	
Fing A16-D2 134	0.29	15	7.49	23.17	31.51	53	32.42	
Fing A16-D2 138	0.40	10	4.76	29.17	39.68	66	24.26	
Fing A16-D2 142	0.21	25	12.30	11.23	15.28	26	49.89	
Fing A16-D2 146	0.31	15	7.34	24.72	33.63	56	29.19	
Fing A16-D2 150	0.29	17	8.53	18.45	25.09	42	41.06	
Fing A16-D2 154	0.46	9	4.49	27.49	37.38	62	28.63	
Fing A16-D2 158	0.42	9	4.75	27.77	37.77	63	27.46	
Fing A16-D2 162	0.22	21	10.61	14.50	19.72	33	45.87	
Fing A16-D2 166	0.32	15	7.66	19.41	26.39	44	40.64	
Fing A16-D2 170	0.28	18	9.02	18.03	24.52	41	41.03	
Fing A16-D2 174	0.39	10	5.18	29.04	39.49	66	23.73	
Fing A16-D3 175	0.30	17	8.43	18.93	25.74	43	40.17	
Fing A16-D2 178	0.30	16	8.19	20.67	28.10	47	36.72	
Fing A16-D2 182	0.37	12	6.11	25.57	34.77	58	29.74	
Fing A16-D2 186	0.30	16	8.16	19.96	27.15	45	38.37	
Fing A16-D3 210	0.33	16	7.83	18.65	25.37	42	42.01	
Fing A16-D3 214	0.51	7	3.53	29.87	40.62	68	25.14	
Fing A16-D3 218	0.35	14	6.96	21.25	28.90	48	37.85	
Fing A16-D3 222	0.32	14	7.23	21.01	28.57	48	37.84	
Fing A16-D3 226	0.21	20	10.01	15.28	20.78	35	45.28	
Fing A16-D3 230	0.21	27	13.27	7.90	10.74	18	55.53	
Fing A16-D3 234	0.24	22	11.08	15.32	20.84	35	43.06	
Fing A16-D3 238	0.19	28	14.19	11.48	15.61	26	45.57	
Fing A16-D3 242	0.23	21	10.34	17.34	23.58	39	39.96	
Fing A16-D3 246	0.57	7	3.30	35.22	47.90	80	13.45	
Fing A16-D3 250	0.36	13	6.67	23.72	32.26	54	32.80	
Fing A16-D3 254	0.23	22	10.83	15.42	20.97	35	43.34	
Fing A16-D3 258	0.21	28	14.15	14.10	19.18	32	39.70	
Fing A16-D3 262	0.24	26	12.82	10.04	13.66	23	51.57	
Fing A16-D3 266	0.34	16	8.16	20.93	28.46	48	36.18	
Fing A16-D3 270	0.22	25	12.66	9.39	12.77	21	53.37	
Fing A16-D4 274	0.17	37	18.31	8.87	12.06	20	43.26	
Fing A16-D4 278	0.14	45	22.27	4.84	6.58	11	44.47	
Fing A16-D4 282	0.17	41	20.47	4.62	6.29	10	48.55	
Fing A16-D4 286	0.19	37	18.36	7.48	10.17	17	46.30	
Fing A16-D4 290	0.16	43	21.37	7.40	10.07	17	40.46	
Fing A16-D4 294	0.20	33	16.53	14.49	19.70	33	34.06	
Fing A16-D4 298	0.21	31	15.27	15.02	20.43	34	35.36	

Fing A16-D4 302	0.22	28	13.89	19.67	26.75	45	27.57
Fing A16-D4 306	0.25	27	13.45	17.23	23.43	39	34.00
Fing A16-D4 310	0.22	28	13.88	18.38	24.99	42	30.52
Fing A16-D4 314	0.16	45	22.60	5.37	7.30	12	42.60
Fing A16-D4 318	0.23	29	14.64	12.99	17.67	29	41.23
Fing A16-D4 322	0.25	25	12.45	7.02	9.55	16	59.16
Fing A16-D4 326	0.21	36	17.83	7.70	10.48	17	46.85
Fing A16-D4 330	0.20	35	17.39	7.79	10.59	18	47.55
Fing A16-D4 334	0.21	33	16.43	11.81	16.06	27	40.33
Fing A16-D4 337	0.24	26	12.83	9.72	13.21	22	52.28
Fing A16-D4 339	0.31	19	9.70	5.14	6.99	12	68.93
Fing A16-D4 343	0.18	38	18.88	9.76	13.27	22	40.09
Fing A16-D4 347	0.22	30	14.98	15.16	20.62	34	35.61
Fing A16-D4 351	0.14	57	28.41	2.89	3.94	7	36.62
Fing A16-D5 355	0.18	37	18.40	2.87	3.90	7	56.68
Fing A16-D5 359	0.18	36	18.02	4.94	6.72	11	52.74
Fing A16-D5 363	0.19	33	16.37	6.33	8.60	14	52.90
Fing A16-D5 367	0.21	29	14.52	11.37	15.46	26	45.14
Fing A16-D5 371	0.24	24	11.90	12.57	17.10	29	47.67
Fing A16-D5 375	0.29	20	9.92	19.25	26.18	44	36.45
Fing A16-D5 379	0.23	24	12.24	12.32	16.76	28	47.53
Fing A16-D5 383	0.17	37	18.62	2.78	3.78	6	56.45
Fing A16-D5 387	0.26	23	11.72	2.19	2.98	5	71.59
Fing A16-D5 391	0.30	19	9.36	4.43	6.02	10	71.23
Fing A16-D5 395	0.17	39	19.28	5.72	7.78	13	48.46
Fing A16-D5 399	0.16	37	18.31	3.79	5.15	9	54.80
Fing A16-D5 403	0.20	33	16.52	7.03	9.57	16	51.00
Fing A16-D5 407	0.19	35	17.65	7.84	10.67	18	46.90
Fing A16-D5 411	0.20	32	16.05	10.47	14.23	24	44.13
Fing A16-D5 415	0.23	25	12.57	19.05	25.91	43	31.62
Fing A16-D5 419	0.16	43	21.56	4.93	6.71	11	45.68
Fing A16-D5 423	0.21	28	13.79	14.63	19.90	33	39.20
Fing A16-D5 427	0.16	41	20.38	6.76	9.19	15	43.90
Fing A16-D5 431	0.16	39	19.73	5.02	6.83	11	49.14
Fing A16-D6 435	0.16	40	19.81	3.09	4.20	7	53.38
Fing A16-D6 439	0.15	44	22.00	5.94	8.08	13	42.51
Fing A16-D6 443	0.20	32	16.04	14.77	20.08	34	34.39
Fing A16-D6 447	0.22	27	13.53	15.64	21.27	36	37.44
Fing A16-D6 451	0.22	27	13.35	18.13	24.66	41	32.14
Fing A16-D6 455	0.22	28	14.02	16.94	23.04	38	33.50
Fing A16-D6 459	0.15	42	20.94	7.23	9.84	16	41.69
Fing A16-D6 463	0.19	30	15.08	12.27	16.68	28	41.99
Fing A16-D6 467	0.22	27	13.31	9.79	13.32	22	51.15
Fing A16-D6 471	0.17	39	19.68	4.57	6.22	10	50.27
Fing A16-D6 475	0.24	25	12.43	5.29	7.20	12	63.13
Fing A16-D6 479	0.25	24	11.95	10.81	14.70	25	51.58
Fing A16-D6 483	0.19	36	18.20	10.37	14.10	24	40.07
Fing A16-D6 487	0.19	38	19.24	9.68	13.17	22	39.54
Fing A16-D6 491	0.23	28	14.11	16.33	22.21	37	34.71
Fing A16-D6 495	0.24	26	13.04	14.08	19.14	32	41.96
Fing A16-D6 499	0.26	25	12.54	17.92	24.37	41	34.25
Fing A16-D7 504	0.20	35	17.71	13.35	18.15	30	34.29
Fing A16-D7 508	0.15	54	26.75	2.56	3.49	6	40.67
Fing A16-D7 512	0.23	31	15.64	14.41	19.60	33	36.01
Fing A16-D7 516	0.24	26	12.90	15.46	21.03	35	39.09
Fing A16-D7 520	0.28	24	11.83	16.01	21.77	36	40.00
Fing A16-D7 524	0.26	26	12.98	21.04	28.61	48	26.28
Fing A16-D7 528	0.26	25	12.60	18.81	25.58	43	32.09
Fing A16-D7 532	0.28	22	11.04	13.35	18.16	30	47.60
Fing A16-D7 536	0.26	24	12.21	19.87	27.03	45	30.47
Fing A16-D7 540	0.24	30	15.10	20.63	28.05	47	22.98
Fing A16-D7 544	0.24	30	15.22	19.79	26.92	45	24.64
Fing A16-D7 548	0.23	34	16.81	13.44	18.28	31	35.88
Fing A16-D7 552	0.24	29	14.73	18.98	25.82	43	27.44
Fing A16-D7 556	0.21	38	18.84	16.52	22.47	38	24.80
Fing A16-D7 560	0.28	24	12.08	25.76	35.03	58	17.37
Fing A16-D7 564	0.27	27	13.62	22.79	30.99	52	21.02
Fing A16-D7 568	0.27	28	14.15	22.41	30.47	51	20.84
Fing A16-D7 572	0.26	28	13.86	22.72	30.90	52	20.69
Fing A16-D7 576	0.29	23	11.42	24.30	33.04	55	22.01
Fing A16-D7 580	0.31	21	10.60	27.09	36.85	61	17.29
Fing A16-D7 584	0.37	17	8.48	28.06	38.16	64	19.33
Fing A16-D7 588	0.40	17	8.33	29.10	39.57	66	17.28
Fing A16-D7 592	0.45	15	7.39	22.99	31.27	52	33.04
Fing A16-D8 595	0.36	17	8.68	20.35	27.68	46	36.44

Fing A16-D8 599	0.40	14	7.12	19.38	26.36	44	41.77
Fing A16-D8 603	0.45	10	5.05	22.30	30.33	51	39.28
Fing A16-D8 607	0.47	10	4.79	26.00	35.37	59	31.39
Fing A16-D8 611	0.53	9	4.31	23.75	32.30	54	37.47
Fing A16-D8 615	0.57	7	3.44	28.83	39.21	65	27.67
Fing A16-D8 619	0.61	8	3.89	22.89	31.13	52	40.25
Fing A16-D8 623	0.60	8	3.96	24.05	32.71	55	37.47
Fing A16-D8 627	0.58	9	4.73	21.92	29.81	50	40.80
Fing A16-D8 631	0.48	12	6.05	25.41	34.56	58	30.22
Fing A16-D8 635	0.55	9	4.45	25.73	35.00	58	32.69
Fing A16-D8 639	0.51	11	5.59	22.23	30.23	50	38.37
Fing A16-D8 643	0.63	7	3.74	26.20	35.63	59	33.05
Fing A16-D8 647	0.52	11	5.62	22.45	30.53	51	37.80
Fing A16-D8 651	0.70	8	3.80	21.91	29.79	50	42.67
Fing A16-D8 655	0.63	9	4.69	18.85	25.64	43	47.82
Fing A16-D8 659	0.73	7	3.60	23.18	31.53	53	40.18
Fing A16-D8 663	0.99	5	2.46	12.79	17.40	29	66.05

## B. Carbonate $\delta^{18}\text{O}$ and $\delta^{13}\text{C}$ Tables

Sample	Depth (cm)	Year AD	Age BP	$\delta^{13}\text{C}$ DIC	$\delta^{18}\text{O}$
FING-A16-D1	0.5	2015.3	-65.3	1.1	-13.5
FING-A16-D1	1.0	2014.2	-64.2	2.1	-13.2
FING-A16-D1	1.5	2013.1	-63.1	2.1	-13.2
FING-A16-D1	2.0	2012.0	-62.0	2.3	-13.1
FING-A16-D1	2.5	2010.9	-60.9	2.3	-13.1
FING-A16-D1	3.0	2009.8	-59.8	2.9	-13.2
FING-A16-D1	3.5	2008.5	-58.5	2.4	-13.1
FING-A16-D1	4.0	2007.1	-57.1	2.2	-12.9
FING-A16-D1	4.5	2005.8	-55.8	2.2	-12.8
FING-A16-D1	5.0	2004.4	-54.4	2.2	-13.0
FING-A16-D1	5.5	2003.0	-53.0	1.9	-12.4
FING-A16-D1	6.0	2001.6	-51.6	2.1	-13.0
FING-A16-D1	6.5	2000.0	-50.0	2.1	-13.1
FING-A16-D1	7.0	1998.2	-48.2	2.2	-13.2
FING-A16-D1	7.5	1996.4	-46.4	2.1	-13.2
FING-A16-D1	8.0	1994.5	-44.5	2.2	-13.2
FING-A16-D1	8.5	1992.5	-42.5	2.2	-13.2
FING-A16-D1	9.0	1990.4	-40.4	2.2	-13.2
FING-A16-D1	9.5	1988.3	-38.3	2.2	-13.2
FING-A16-D1	10.0	1986.0	-36.0	2.2	-13.2
FING-A16-D1	10.5	1983.7	-33.7	2.3	-13.2
FING-A16-D1	11.0	1981.4	-31.4	2.3	-13.2
FING-A16-D1	11.5	1978.9	-28.9	2.3	-13.1
FING-A16-D1	12.0	1976.0	-26.0	2.4	-13.1
FING-A16-D1	12.5	1973.2	-23.2	2.3	-13.1
FING-A16-D1	13.0	1970.4	-20.4	2.4	-13.2
FING-A16-D1	13.5	1967.1	-17.1	2.3	-13.2
FING-A16-D1	14.0	1963.5	-13.5	2.3	-13.3
FING-A16-D1	14.5	1959.9	-9.9	2.3	-13.4
FING-A16-D1	15.0	1955.9	-5.9	2.3	-13.3
FING-A16-D1	15.5	1951.6	-1.6	2.3	-13.3
FING-A16-D1	16.0	1947.3	2.7	2.6	-13.1
FING-A16-D1	16.5	1943.0	7.0	2.5	-13.1
FING-A16-D1	17.0	1937.3	12.7	2.4	-13.3
FING-A16-D1	17.5	1932.5	17.5	2.3	-13.4
FING-A16-D1	18.0	1926.0	24.0	2.5	-13.4
FING-A16-D1	18.5	1920.5	29.5	2.3	-13.4
FING-A16-D1	19.0	1913.1	36.9	2.1	-13.6
FING-A16-D1	19.5	1906.8	43.2	2.0	-14.0
FING-A16-D1	20.0	1897.3	52.7	2.1	-13.8
FING-A16-D1	20.5	1889.7	60.3	2.0	-13.4
FING-A16-D1	21.0	1881.4	68.6	2.5	-13.1
FING-A16-D1	21.5	1874.3	75.7	2.6	-12.8
FING-A16-D1	22.0	1867.2	82.8	2.8	-12.9
FING-A16-D1	22.5	1860.2	89.8	2.7	-13.0
FING-A16-D1	23.0	1853.1	96.9	2.7	-13.5
FING-A16-D1	23.5	1846.0	104.0	2.5	-14.0
FING-A16-D1	24.0	1839.0	111.0	2.6	-14.0
FING-A16-D1	24.5	1831.9	118.1	2.2	-14.0
FING-A16-D1	25.0	1824.9	125.1	2.2	-14.0
FING-A16-D1	25.5	1817.8	132.2	2.4	-13.7
FING-A16-D1	26.0	1810.7	139.3	2.6	-13.3
FING-A16-D1	26.5	1803.7	146.3	2.3	-13.4
FING-A16-D1	27.0	1796.6	153.4	2.2	-13.7
FING-A16-D1	27.5	1789.5	160.5	2.1	-13.5
FING-A16-D1	28.0	1782.5	167.5	2.0	-13.2
FING-A16-D1	28.5	1775.4	174.6	2.5	-13.6
FING-A16-D1	29.0	1768.4	181.6	2.5	-13.6
FING-A16-D1	29.5	1761.3	188.7	2.3	-13.2
FING-A16-D1	30.0	1754.2	195.8	2.5	-12.8
FING-A16-D1	30.5	1747.2	202.8	2.6	-12.7
FING-A16-D1	31.0	1740.1	209.9	2.5	-12.7
FING-A16-D1	31.5	1733.1	216.9	2.3	-12.8
FING-A16-D1	32.0	1726.0	224.0	2.0	-13.2
FING-A16-D1	32.5	1718.9	231.1	2.1	-13.1
FING-A16-D1	33.0	1711.9	238.1	2.3	-13.0
FING-A16-D1	33.5	1704.8	245.2	2.3	-13.0
FING-A16-D1	34.0	1697.7	252.3	2.3	-13.1
FING-A16-D1	34.5	1690.7	259.3	2.1	-12.3
FING-A16-D1	35.0	1683.6	266.4	2.3	-13.2

FING-A16-D1	35.5	1676.6	273.4	2.0	-13.4
FING-A16-D1	36.0	1669.5	280.5	1.8	-13.6
FING-A16-D1	36.5	1662.4	287.6	1.8	-13.6
FING-A16-D1	37.0	1655.4	294.6	1.8	-13.5
FING-A16-D1	37.5	1648.3	301.7	1.7	-13.6
FING-A16-D1	38.0	1641.2	308.8	1.8	-13.7
FING-A16-D1	38.5	1634.2	315.8	1.6	-13.7
FING-A16-D1	39.0	1627.1	322.9	1.7	-13.9
FING-A16-D1	39.5	1620.1	329.9	1.7	-13.9
FING-A16-D1	40.0	1613.0	337.0	1.6	-13.8
FING-A16-D1	40.5	1605.9	344.1	1.6	-13.9
Fing A16-D2 44.0	1556.5	393.5	1.2	-13.4	
Fing A16-D2 48.0	1500.0	450.0	1.3	-13.1	
Fing A16-D2 52.0	1465.6	484.4	1.1	-13.7	
Fing A16-D2 56.0	1431.3	518.8	1.3	-13.3	
Fing A16-D2 60.0	1396.9	553.1	2.2	-12.9	
Fing A16-D2 64.0	1362.5	587.5	2.0	-13.4	
Fing A16-D2 68.0	1328.1	621.9	1.6	-13.7	
Fing A16-D2 72.0	1293.8	656.3	1.6	-14.4	
Fing A16-D2 76.0	1259.4	690.6	1.9	-13.5	
Fing A16-D2 80.0	1225.0	725.0	1.4	-13.8	
Fing A16-D2 84.0	1190.6	759.4	1.8	-12.8	
Fing A16-D2 88.0	1156.3	793.8	1.8	-13.1	
Fing A16-D2 92.0	1121.9	828.1	1.1	-13.9	
Fing A16-D2 96.0	1087.5	862.5	2.3	-13.8	
Fing A16-D2 100.0	1053.1	896.9	2.1	-12.5	
Fing A16-D2 104.0	1018.8	931.3	2.6	-12.4	
Fing A16-D2 108.0	984.4	965.6	2.4	-12.6	
Fing A16-D2 112.0	950.0	1000.0	2.5	-12.6	
Fing A16-D2 116.0	938.9	1011.1	2.6	-12.7	
Fing A16-D2 120.0	927.8	1022.2	3.4	-12.8	
Fing A16-D2 124.0	916.8	1033.2	2.9	-12.8	
Fing A16-D2 128.0	905.7	1044.3	3.1	-12.9	
Fing A16-D2 132.0	894.6	1055.4	3.5	-12.5	
Fing A16-D2 136.0	883.5	1066.5	4.2	-12.5	
Fing A16-D2 140.0	872.5	1077.5	3.4	-12.6	
Fing A16-D2 144.0	861.4	1088.6	3.0	-13.1	
Fing A16-D2 148.0	850.3	1099.7	2.9	-12.3	
Fing A16-D2 152.0	839.2	1110.8	3.4	-13.1	
Fing A16-D2 156.0	828.2	1121.8	1.7	-14.2	
Fing A16-D2 160.0	802.0	1148.0	2.2	-13.5	
Fing A16-D2 164.0	766.7	1183.3	3.0	-12.6	
Fing A16-D2 168.0	731.4	1218.6	2.4	-12.9	
Fing A16-D2 172.0	696.1	1253.9	2.4	-12.6	
Fing A16-D2 176.0	660.9	1289.1	1.9	-13.0	
Fing A16-D2 180.0	625.6	1324.4	1.6	-13.9	
Fing A16-D2 184.0	590.3	1359.7	2.5	-13.5	
Fing A16-D2 188.0	555.1	1394.9	2.3	-12.4	
Fing A16-D3 192.0	519.8	1430.2	2.3	-13.5	
Fing A16-D3 196.0	484.5	1465.5	2.3	-12.7	
Fing A16-D3 200.0	449.3	1500.7	2.7	-12.6	
Fing A16-D3 204.0	414.0	1536.0	2.4	-12.9	
Fing A16-D3 208.0	378.7	1571.3	2.8	-12.7	
Fing A16-D3 212.0	343.4	1606.6	2.6	-13.6	
Fing A16-D3 216.0	308.2	1641.8	3.3	-13.1	
Fing A16-D3 220.0	272.9	1677.1	2.6	-13.2	
Fing A16-D3 224.0	237.6	1712.4	2.7	-12.9	
Fing A16-D3 228.0	193.3	1756.7	2.7	-13.8	
Fing A16-D3 232.0	140.0	1810.0	3.3	-12.2	
Fing A16-D3 236.0	86.7	1863.3	3.7	-11.8	
Fing A16-D3 240.0	33.3	1916.7	3.8	-11.9	
Fing A16-D3 244.0		1970.0	2.4	-13.1	
Fing A16-D3 248.0		2023.3	2.3	-14.0	
Fing A16-D3 252.0		2076.7	3.2	-13.3	
Fing A16-D3 256.0		2130.0	3.0	-12.8	
Fing A16-D3 260.0		2183.3	3.0	-12.3	
Fing A16-D3 264.0		2236.7	3.9	-12.0	
Fing A16-D3 268.0		2290.0	3.5	-13.0	
Fing A16-D4 276.0		2396.7	4.7	-12.3	
Fing A16-D4 292.0		2610.0	3.4	-12.9	
Fing A16-D4 300.0		2716.7	2.8	-13.1	
Fing A16-D4 308.0		2823.3	3.2	-13.0	
Fing A16-D4 316.0		2930.0	3.1	-12.7	
Fing A16-D4 324.0		3036.7	2.1	-13.3	
Fing A16-D4 332.0		3143.3	2.0	-13.2	

Fing A16-D4 348.0	3356.7	1.9	-13.3
Fing A16-D5 364.0	3570.0	3.6	-12.6
Fing A16-D5 372.0	3675.0	3.4	-12.2
Fing A16-D5 380.0	3775.0	3.7	-12.8
Fing A16-D5 396.0	4068.9	3.5	-12.9
Fing A16-D5 404.0	4294.2	3.4	-12.9
Fing A16-D5 412.0	4519.5	3.5	-12.7
Fing A16-D5 420.0	4744.7	5.3	-11.8
Fing A16-D5 428.0	4970.0	4.5	-12.4
Fing A16-D6 428.0	4970.0	3.8	-12.7
Fing A16-D6 436.0	5172.4	3.6	-12.6
Fing A16-D6 444.0	5374.7	3.2	-12.6
Fing A16-D6 452.0	5596.9	3.4	-12.8
Fing A16-D6 460.0	5821.9	3.2	-12.8
Fing A16-D6 468.0	6046.9	2.5	-13.1
Fing A16-D6 476.0	6271.9	2.4	-13.2
Fing A16-D6 484.0	6496.9	1.8	-13.0
Fing A16-D6 492.0	6721.9	1.8	-12.9
Fing A16-D7 502.0	7003.1	2.1	-12.7
Fing A16-D7 506.0	7115.6	1.8	-13.4
Fing A16-D7 510.0	7233.9	2.3	-12.8
Fing A16-D7 514.0	7369.3	2.0	-13.0
Fing A16-D7 518.0	7504.7	1.9	-13.1
Fing A16-D7 522.0	7640.2	2.5	-12.9
Fing A16-D7 526.0	7775.6	1.4	-13.3
Fing A16-D7 530.0	7911.1	-0.1	-13.6
Fing A16-D7 534.0	8046.5	1.3	-13.2
Fing A16-D7 538.0	8181.9	1.9	-13.1
Fing A16-D7 542.0	8317.4	3.1	-12.4
Fing A16-D7 546.0	8452.8	3.2	-12.2
Fing A16-D7 550.0	8588.2	3.7	-12.4
Fing A16-D7 554.0	8723.7	3.0	-12.7
Fing A16-D7 558.0	8859.1	3.8	-12.0
Fing A16-D7 562.0	8994.6	2.8	-12.2
Fing A16-D7 566.0	9130.0	3.7	-11.9
Fing A16-D7 570.0	9319.1	3.3	-12.2
Fing A16-D7 574.0	9508.3	2.8	-12.2
Fing A16-D7 578.0	9697.4	2.8	-12.2
Fing A16-D7 582.0	9886.6	1.9	-11.6
Fing A16-D7 586.0	10075.7	2.3	-11.9
Fing A16-D7 590.0	10264.9	1.9	-11.7
Fing A16-D8 598.0	10643.1	2.9	-10.7
Fing A16-D8 602.0	10832.3	3.5	-11.1
Fing A16-D8 606.0	11021.4	2.9	-11.8
Fing A16-D8 610.0	11210.6	3.3	-11.9
Fing A16-D8 614.0	11399.7	2.7	-12.2
Fing A16-D8 618.0	11588.9	2.7	-12.7
Fing A16-D8 622.0	11778.0	1.3	-13.5
Fing A16-D8 626.0	11967.1	0.9	-13.5
Fing A16-D8 630.0	12156.3	0.5	-13.4
Fing A16-D8 634.0	12345.4	2.0	-11.9
Fing A16-D8 638.0	12534.6	1.0	-12.5
Fing A16-D8 642.0	12723.7	0.8	-12.6
Fing A16-D8 646.0	12912.9	1.3	-12.1
Fing A16-D8 650.0	13102.0	0.6	-12.6
Fing A16-D8 654.0	13291.1	1.2	-12.7
Fing A16-D8 658.0	13480.3	0.7	-12.7
Fing A16-D8 662.0	13669.4	-1.9	-13.5
Fing A16-D8 664.0	13764.0	-1.0	-14.4

## C. Sediment Organic $\delta^{15}\text{N}$ and $\delta^{13}\text{C}$ Tables

Sample	Depth(cm)	$\delta^{15}\text{N}$	$\delta^{13}\text{C}$ ORG	% N	% C	C/N	Age BP
FING-A16-D1 1	1.0	2.9	-24.1	1.2	10.7	9.1	-64.2
FING-A16-D1 1.5	1.5	2.6	-24.3	1.3	12.1	9.3	-63.1
FING-A16-D1 2	2.0	2.5	-24.4	1.3	11.8	9.2	-62.0
FING-A16-D1 2.5	2.5	2.5	-24.6	1.0	9.1	9.4	-60.9
FING-A16-D1 3	3.0	1.9	-24.3	1.5	14.7	9.9	-59.8
FING-A16-D1 3.5	3.5	1.8	-24.3	1.5	14.5	10.0	-58.5
FING-A16-D1 4	4.0	2.0	-24.6	1.4	13.3	9.5	-57.1
FING-A16-D1 4.5	4.5	2.3	-24.6	1.1	9.9	9.4	-55.8
FING-A16-D1 5	5.0	2.2	-24.6	1.3	12.6	9.7	-54.4
FING-A16-D1 5.5	5.5	1.9	-24.4	1.1	10.6	9.7	-53.0
FING-A16-D1 6	6.0	1.8	-24.3	1.5	14.7	10.0	-51.6
FING-A16-D1 6.5	6.5	1.8	-24.7	1.4	13.9	10.0	-50.0
FING-A16-D1 7	7.0	1.5	-24.5	1.2	11.9	9.8	-48.2
FING-A16-D1 7.5	7.5	1.6	-24.7	1.2	11.4	9.9	-46.4
FING-A16-D1 8	8.0	1.4	-24.5	1.2	11.5	9.8	-44.5
FING-A16-D1 8.5	8.5	1.6	-24.3	1.3	13.3	10.1	-42.5
FING-A16-D1 9	9.0	1.5	-24.2	1.6	16.0	10.3	-40.4
FING-A16-D1 9.5	9.5	1.3	-24.4	1.2	12.5	10.3	-38.3
FING-A16-D1 10	10.0	1.2	-24.5	1.2	12.2	10.0	-36.0
FING-A16-D1 10.5	10.5	1.4	-23.9	1.5	14.9	10.3	-33.7
FING-A16-D1 11	11.0	1.3	-24.2	1.3	12.6	10.1	-31.4
FING-A16-D1 11.5	11.5	1.2	-24.2	1.5	15.6	10.2	-28.9
FING-A16-D1 12	12.0	1.1	-24.0	1.5	14.6	9.8	-26.0
FING-A16-D1 12.5	12.5	1.2	-24.1	1.5	15.4	10.0	-23.2
FING-A16-D1 13	13.0	1.1	-24.2	1.4	13.7	10.0	-20.4
FING-A16-D1 13.5	13.5	1.0	-24.2	1.3	13.4	10.1	-17.1
FING-A16-D1 14	14.0	1.0	-24.2	1.5	15.0	9.9	-13.5
FING-A16-D1 14.5	14.5	1.0	-24.3	1.4	14.4	10.0	-9.9
FING-A16-D1 15	15.0	1.1	-24.3	1.3	13.0	9.7	-5.9
FING-A16-D1 15.5	15.5	1.0	-24.1	1.4	13.7	9.9	-1.6
FING-A16-D1 16	16.0	0.9	-24.3	1.4	13.5	9.9	2.7
FING-A16-D1 16.5	16.5	0.9	-24.0	1.4	14.0	10.0	7.0
FING-A16-D1 17	17.0	0.9	-24.2	1.4	13.9	9.8	12.7
FING-A16-D1 17.5	17.5	0.9	-24.2	1.6	15.7	10.0	17.5
FING-A16-D1 18	18.0	0.8	-24.2	1.4	13.7	9.8	24.0
FING-A16-D1 18.5	18.5	0.8	-23.9	1.3	13.2	10.3	29.5
FING-A16-D1 19	19.0	0.8	-24.3	1.4	14.3	9.9	36.9
FING-A16-D1 19.5	19.5	0.9	-24.6	1.4	13.5	9.9	43.2
FING-A16-D1 20	20.0	0.8	-24.7	1.4	13.6	9.8	52.7
FING-A16-D1 20.5	20.5	1.2	-24.6	1.5	15.1	10.1	60.3
FING-A16-D1 21	21.0	1.0	-24.0	1.4	14.1	10.0	68.6
FING-A16-D1 21.5	21.5	1.0	-24.0	1.6	15.5	9.9	75.7
FING-A16-D1 22	22.0	1.1	-24.1	1.4	13.7	9.9	82.8
FING-A16-D1 22.5	22.5	1.0	-24.1	1.7	16.3	9.7	89.8
FING-A16-D1 23	23.0	0.9	-24.6	1.6	15.0	9.4	96.9
FING-A16-D1 23.5	23.5	0.9	-24.6	1.6	15.1	9.5	104.0
FING-A16-D1 24	24.0	0.8	-24.6	1.4	13.7	9.7	111.0
FING-A16-D1 24.5	24.5	0.6	-24.5	1.4	13.5	9.5	118.1
FING-A16-D1 25	25.0	0.5	-24.3	1.7	16.1	9.5	125.1
FING-A16-D1 25.5	25.5	0.4	-24.1	1.7	16.1	9.4	132.2
FING-A16-D1 26	26.0	0.5	-23.9	1.5	13.5	9.3	139.3
FING-A16-D1 26.5	26.5	0.6	-23.9	1.5	13.8	9.5	146.3
FING-A16-D1 27	27.0	0.6	-24.5	1.4	13.1	9.5	153.4
FING-A16-D1 27.5	27.5	0.8	-24.8	1.4	13.7	9.5	160.5
FING-A16-D1 28	28.0	0.7	-24.0	1.5	14.3	9.6	167.5
FING-A16-D1 28.5	28.5	0.8	-24.2	1.7	15.8	9.5	174.6
FING-A16-D1 29	29.0	1.0	-24.4	1.6	15.4	9.5	181.6
FING-A16-D1 29.5	29.5	1.4	-24.4	1.7	16.0	9.3	188.7
FING-A16-D1 30	30.0	1.4	-24.7	1.6	15.2	9.6	195.8
FING-A16-D1 31	31.0	1.2	-24.4	1.5	14.3	9.8	209.9
FING-A16-D1 31.5	31.5	0.9	-24.0	1.4	13.7	9.6	216.9
FING-A16-D1 32	32.0	0.7	-23.1	1.4	14.5	10.4	224.0
FING-A16-D1 32.5	32.5	1.1	-23.5	1.7	16.5	9.9	231.1
FING-A16-D1 33	33.0	1.1	-23.6	1.5	14.1	9.7	238.1
FING-A16-D1 33.5	33.5	1.2	-23.6	1.4	13.6	9.6	245.2
FING-A16-D1 34	34.0	0.9	-23.4	1.4	14.4	10.0	252.3
FING-A16-D1 34.5	34.5	1.6	-23.8	1.6	15.1	9.4	259.3
FING-A16-D1 35	35.0	1.2	-24.4	1.3	12.1	9.6	266.4
FING-A16-D1 35.5	35.5	1.1	-24.2	1.4	14.4	10.0	273.4
FING-A16-D1 36	36.0	1.0	-24.3	1.4	14.4	10.0	280.5

FING-A16-D1 36.5	36.5	1.1	-24.0	1.5	14.3	9.8	287.6
FING-A16-D1 37	37.0	1.0	-23.8	1.4	13.8	10.2	294.6
FING-A16-D1 37.5	37.5	1.1	-23.7	1.5	14.4	9.9	301.7
FING-A16-D1 38	38.0	0.9	-24.0	1.5	14.5	9.9	308.8
FING-A16-D1 38.5	38.5	1.0	-24.3	1.5	15.0	9.8	315.8
FING-A16-D1 39	39.0	0.9	-24.5	1.3	12.8	9.9	322.9
FING-A16-D1 39.5	39.5	0.6	-24.7	1.4	13.8	9.8	329.9
FING-A16-D1 40	40.0	0.9	-24.4	1.4	14.3	10.0	337.0
FING-A16-D1 40.5	40.5	0.9	-23.9	1.4	14.3	10.0	344.1
Fing A16-D2 25	44.0	0.9	-25.3	1.4	14.2	10.3	393.5
Fing A16-D2 29	48.0	-0.2	-24.6	1.5	15.0	10.4	450.0
Fing A16-D2 33	52.0	-1.2	-24.7	1.6	14.5	8.9	484.4
Fing A16-D2 37	56.0	-0.4	-25.1	1.6	16.1	9.8	518.8
Fing A16-D2 41	60.0	0.2	-25.4	1.2	11.2	9.7	553.1
Fing A16-D2 45	64.0	-0.9	-23.9	1.6	14.7	9.3	587.5
Fing A16-D2 49	68.0	0.3	-25.3	1.5	15.1	9.9	621.9
Fing A16-D2 53	72.0	0.5	-25.2	1.7	16.1	9.7	656.3
Fing A16-D2 57	76.0	0.2	-25.2	1.4	13.4	9.6	690.6
Fing A16-D2 61	80.0	0.4	-24.6	1.5	15.5	10.2	725.0
Fing A16-D2 65	84.0	-0.3	-20.9	1.6	18.3	11.6	759.4
Fing A16-D2 69	88.0	0.3	-23.5	1.6	16.1	10.3	793.8
Fing A16-D2 73	92.0	0.1	-22.9	1.6	17.1	10.6	828.1
Fing A16-D2 77	96.0	-0.2	-22.7	1.6	16.8	10.6	862.5
Fing A16-D2 81	100.0	0.5	-23.8	1.6	16.0	10.1	896.9
Fing A16-D2 85	104.0	0.1	-23.3	1.5	15.2	10.1	931.3
Fing A16-D2 89	108.0	0.0	-23.7	1.3	13.2	9.8	965.6
Fing A16-D2 93	112.0	0.1	-24.5	1.7	16.4	9.9	1000.0
Fing A16-D2 97	116.0	0.0	-23.3	1.8	17.0	9.6	1011.1
Fing A16-D2 101	120.0	0.3	-23.8	1.9	18.6	9.9	1022.2
Fing A16-D2 105	124.0	0.5	-24.3	1.6	15.8	9.9	1033.2
Fing A16-D2 109	128.0	0.1	-24.3	1.6	15.7	9.6	1044.3
Fing A16-D2 113	132.0	-0.1	-24.0	1.5	14.1	9.6	1055.4
Fing A16-D2 117	136.0	-0.1	-24.9	1.2	12.0	9.7	1066.5
Fing A16-D2 121	140.0	0.9	-25.8	1.2	12.7	10.3	1077.5
Fing A16-D2 125	144.0	0.4	-24.7	1.5	15.0	10.1	1088.6
Fing A16-D2 129	148.0	0.1	-24.0	1.4	13.7	10.0	1099.7
Fing A16-D2 133	152.0	0.0	-23.8	1.6	15.9	10.1	1110.8
Fing A16-D2 137	156.0	0.6	-24.4	1.3	12.9	9.7	1121.8
Fing A16-D2 141	160.0	0.6	-24.8	1.6	15.3	9.6	1148.0
Fing A16-D2 145	164.0	0.3	-25.0	1.4	13.0	9.5	1183.3
Fing A16-D2 149	168.0	0.2	-24.7	1.4	13.3	9.7	1218.6
Fing A16-D2 153	172.0	0.7	-24.8	1.1	11.3	10.0	1253.9
Fing A16-D2 157	176.0	0.2	-23.1	1.5	14.5	9.6	1289.1
Fing A16-D2 161	180.0	0.0	-24.3	1.3	12.3	9.6	1324.4
FING-A16-D3 14.5	189.0	-0.2	-24.8	1.4	14.7	10.5	1403.8
FING-A16-D3 16.5	191.0	-0.5	-24.2	1.6	16.1	9.9	1421.4
FING-A16-D3 18.5	193.0	0.9	-26.6	1.4	13.9	10.3	1439.0
FING-A16-D3 19.5	194.0	0.3	-24.9	1.2	12.6	10.2	1447.8
FING-A16-D3 20.5	195.0	-0.2	-24.9	1.3	13.4	10.3	1456.7
FING-A16-D3 22.5	197.0	0.2	-24.1	1.2	12.3	10.7	1474.3
FING-A16-D3 23.5	198.0	0.2	-24.7	1.0	10.9	10.6	1483.1
FING-A16-D3 24.5	199.0	0.6	-24.0	1.3	13.9	10.8	1491.9
FING-A16-D3 26.5	201.0	0.5	-24.7	1.1	12.0	10.8	1509.6
FING-A16-D3 27.5	202.0	1.0	-25.0	1.1	10.8	10.1	1518.4
FING-A16-D3 28.5	203.0	0.6	-24.9	1.2	12.3	10.5	1527.2
FING-A16-D3 30.5	205.0	1.3	-24.4	1.5	13.5	9.2	1544.8
FING-A16-D3 31.5	206.0	-0.3	-23.7	1.4	14.0	10.3	1553.6
FING-A16-D3 32.5	207.0	-0.1	-23.8	1.5	14.5	10.0	1562.5
FING-A16-D3 34.5	209.0	0.7	-24.6	1.3	13.7	10.3	1580.1
FING-A16-D3 35.5	210.0	0.0	-23.8	1.6	15.5	10.0	1588.9
FING-A16-D3 36.5	211.0	1.1	-24.0	1.7	16.3	9.7	1597.7
FING-A16-D3 39.5	214.0	0.2	-24.9	1.0	10.2	10.5	1624.2
FING-A16-D3 40.5	215.0	0.3	-25.3	0.9	9.4	10.6	1633.0
FING-A16-D3 42.5	217.0	0.1	-25.0	1.3	13.8	10.5	1650.6
FING-A16-D3 43.5	218.0	-0.2	-24.8	1.2	12.0	10.1	1659.5
FING-A16-D3 44.5	219.0	0.1	-25.7	1.1	11.0	10.5	1668.3
FING-A16-D3 46.5	221.0	0.1	-25.2	1.2	12.6	10.7	1685.9
FING-A16-D3 47.5	222.0	0.1	-25.1	1.4	13.9	10.0	1694.7
FING-A16-D3 48.5	223.0	0.0	-24.8	1.4	15.8	11.0	1703.5
FING-A16-D3 50.5	225.0	0.2	-24.4	1.4	15.0	10.6	1721.2
FING-A16-D3 51.5	226.0	-0.2	-23.5	1.4	15.0	10.7	1730.0
FING-A16-D3 52.5	227.0	-0.4	-24.6	1.4	15.3	11.2	1743.3
FING-A16-D3 54.5	229.0	-0.1	-24.4	1.5	15.1	10.3	1770.0
FING-A16-D3 55.5	230.0	-0.4	-23.6	1.5	15.9	10.4	1783.3
Fing A16-D3 56.5	231.0	0.1	-21.2	1.5	17.1	11.4	1796.7

Fing A16-D3 58.5	233.0	-0.4	-21.4	1.5	17.5	11.5	1823.3
Fing A16-D3 59.5	234.0	-0.2	-20.8	1.5	17.0	11.6	1836.7
Fing A16-D3 60.5	235.0	-0.2	-20.0	1.5	17.7	11.8	1850.0
Fing A16-D3 62.5	237.0	-0.1	-21.2	1.6	19.1	11.7	1876.7
Fing A16-D3 63.5	238.0	-0.3	-21.6	1.7	19.1	11.4	1890.0
Fing A16-D3 64.5	239.0	-0.1	-21.6	1.7	19.1	11.4	1903.3
Fing A16-D3 66.5	241.0	-0.3	-23.0	1.5	16.8	11.1	1930.0
Fing A16-D3 67.5	242.0	-0.6	-23.0	1.6	17.0	11.0	1943.3
Fing A16-D3 68.5	243.0	-0.2	-24.4	1.4	15.3	10.7	1956.7
Fing A16-D3 70.5	245.0	-0.1	-25.3	1.4	14.8	10.3	1983.3
Fing A16-D3 71.5	246.0	-0.6	-25.4	1.4	13.7	9.8	1996.7
Fing A16-D3 72.5	247.0	-0.1	-26.5	1.2	12.3	10.2	2010.0
Fing A16-D3 74.5	249.0	0.1	-24.6	1.4	13.8	10.1	2036.7
Fing A16-D3 75.5	250.0	-0.4	-24.9	1.4	14.2	10.3	2050.0
Fing A16-D3 76.5	251.0	-0.7	-24.7	1.2	12.9	10.5	2063.3
Fing A16-D3 78.5	253.0	-0.6	-22.5	1.3	14.1	11.0	2090.0
Fing A16-D3 79.5	254.0	-0.7	-23.6	1.6	16.2	10.4	2103.3
Fing A16-D3 80.5	255.0	-0.7	-24.5	1.6	15.4	9.8	2116.7
Fing A16-D3 82.5	257.0	-0.6	-23.1	1.6	16.3	10.2	2143.3
Fing A16-D3 83.5	258.0	-0.3	-21.8	1.9	21.6	11.2	2156.7
Fing A16-D3 84.5	259.0	-0.6	-22.2	1.8	19.5	11.0	2170.0
Fing A16-D3 86.5	261.0	-0.5	-24.8	1.5	15.9	10.5	2196.7
Fing A16-D3 87.5	262.0	0.0	-23.7	1.5	16.4	10.8	2210.0
Fing A16-D3 88.5	263.0	-0.4	-21.8	1.7	19.8	11.5	2223.3
Fing A16-D3 90.5	265.0	-0.1	-24.7	1.3	14.3	10.6	2250.0
Fing A16-D3 91.5	266.0	0.1	-24.1	1.4	15.2	10.6	2263.3
Fing A16-D3 92.5	267.0	-0.4	-24.4	1.5	15.5	10.2	2276.7
Fing A16-D3 94.5	269.0	-0.3	-23.6	1.6	16.6	10.7	2303.3
Fing A16-D3 95.5	270.0	-0.1	-24.1	1.4	14.9	11.0	2316.7
Fing A16-D3 96.5	271.0	-0.2	-24.5	1.4	15.1	10.5	2330.0
Fing A16-D4 17.5	272.0	0.0	-22.9	2.2	26.1	11.8	2343.3
Fing A16-D4 18.5	273.0	0.0	-21.3	2.2	26.1	12.1	2356.7
Fing A16-D4 20.5	275.0	-0.5	-23.3	1.7	19.0	11.2	2383.3
Fing A16-D4 25.5	280.0	-0.3	-24.2	2.1	23.9	11.4	2450.0
Fing A16-D4 33.5	288.0	-1.1	-25.0	2.1	23.5	11.4	2556.7
Fing A16-D4 41.5	296.0	-0.7	-24.4	2.0	22.4	11.5	2663.3
Fing A16-D4 49.5	304.0	-0.6	-26.1	1.9	21.5	11.6	2770.0
Fing A16-D4 57.5	312.0	-0.2	-26.6	2.1	24.2	11.6	2876.7
Fing A16-D4 65.5	320.0	-0.7	-26.4	1.6	19.1	11.8	2983.3
Fing A16-D4 73.5	328.0	0.1	-29.2	1.8	22.4	12.2	3090.0
Fing A16-D4 81.5	336.0	-0.2	-27.6	1.7	20.9	12.2	3196.7
Fing A16-D4 89.5	344.0	-0.3	-29.3	2.2	26.7	12.0	3303.3
Fing A16-D5 17.5	352.0	-0.3	-25.4	1.7	17.1	10.2	3410.0
Fing A16-D5 25.5	360.0	-0.6	-23.1	1.7	16.7	9.9	3516.7
Fing A16-D5 33.5	368.0	-0.2	-21.8	2.1	21.2	10.3	3623.3
Fing A16-D5 41.5	376.0	-0.2	-24.5	1.6	15.9	10.0	3725.0
Fing A16-D5 47.5	382.0	0.1	-24.7	1.6	16.6	10.3	3800.0
Fing A16-D5 49.5	384.0	0.2	-21.0	1.8	19.8	11.2	3825.0
Fing A16-D5 51.5	386.0	0.1	-22.9	1.5	16.6	10.9	3850.0
Fing A16-D5 55.5	390.0	-0.4	-23.7	0.8	7.8	9.8	3900.0
Fing A16-D5 57.5	392.0	-0.1	-21.5	1.7	17.6	10.1	3956.3
Fing A16-D5 59.5	394.0	0.4	-19.5	1.9	21.0	10.9	4012.6
Fing A16-D5 63.5	398.0	-0.5	-23.6	1.8	18.2	10.1	4125.3
Fing A16-D5 65.5	400.0	-0.2	-23.1	1.6	17.1	10.5	4181.6
Fing A16-D5 67.5	402.0	0.1	-22.3	1.8	19.2	10.7	4237.9
Fing A16-D5 71.5	406.0	0.0	-21.6	1.8	19.0	10.7	4350.5
Fing A16-D5 73.5	408.0	0.1	-21.1	1.9	20.3	10.9	4406.8
Fing A16-D5 81.5	416.0	-0.2	-23.4	1.9	19.8	10.3	4632.1
Fing A16-D5 89.5	424.0	-0.5	-24.0	1.9	19.5	10.3	4857.4
Fing A16-D6 17.5	432.0	-0.3	-22.3	1.7	18.7	10.8	5071.2
Fing A16-D6 25.5	440.0	0.0	-22.8	2.3	23.6	10.5	5172.4
Fing A16-D6 33.5	448.0	-0.2	-25.0	1.8	19.3	10.4	5484.4
Fing A16-D6 41.5	456.0	-0.1	-23.8	1.9	20.5	10.7	5709.4
Fing A16-D6 49.5	464.0	-0.1	-24.5	1.7	18.3	10.7	5934.4
Fing A16-D6 57.5	472.0	0.3	-24.6	1.8	20.2	11.2	6159.4
Fing A16-D6 65.5	480.0	0.3	-24.6	1.3	14.5	11.4	6384.4
Fing A16-D6 73.5	488.0	0.6	-23.7	2.0	23.1	11.3	6609.4
Fing A16-D6 81.5	496.0	0.0	-25.9	1.6	17.2	11.1	6834.4
Fing A16-D7 5.5	500.0	0.2	-23.6	2.1	23.4	11.2	6946.9
Fing A16-D7 6.5	501.0	0.2	-24.3	2.1	23.5	11.1	6975.0
Fing A16-D7 8.5	503.0	0.6	-26.0	1.7	19.2	11.1	7031.3
Fing A16-D7 9.5	504.0	0.7	-25.4	2.1	23.1	11.0	7059.4
Fing A16-D7 10.5	505.0	0.7	-23.9	2.0	22.8	11.3	7087.5
Fing A16-D7 12.5	507.0	0.3	-22.5	2.4	26.6	11.2	7143.8
Fing A16-D7 13.5	508.0	0.1	-22.9	2.3	29.7	13.1	7171.9

Fing A16-D7 14.5	509.0	0.3	-22.9	2.0	22.6	11.1	7200.0
Fing A16-D7 16.5	511.0	0.2	-24.6	1.8	21.0	11.4	7267.7
Fing A16-D7 17.5	512.0	0.2	-23.8	2.0	22.5	11.4	7301.6
Fing A16-D7 18.5	513.0	0.5	-24.9	1.8	19.9	11.1	7335.4
Fing A16-D7 20.5	515.0	0.1	-24.0	3.1	38.3	12.5	7403.2
Fing A16-D7 21.5	516.0	0.2	-24.2	1.8	19.7	10.9	7437.0
Fing A16-D7 22.5	517.0	0.3	-25.9	1.6	18.0	11.4	7470.9
Fing A16-D7 24.5	519.0	0.4	-24.6	1.8	21.0	12.0	7538.6
Fing A16-D7 25.5	520.0	0.4	-25.6	1.4	17.0	11.8	7572.5
Fing A16-D7 26.5	521.0	0.6	-26.2	1.7	19.5	11.4	7606.3
Fing A16-D7 28.5	523.0	0.3	-24.3	2.0	23.5	12.0	7674.0
Fing A16-D7 29.5	524.0	0.4	-24.2	1.9	23.0	12.1	7707.9
Fing A16-D7 30.5	525.0	0.6	-25.1	1.8	23.2	12.6	7741.8
Fing A16-D7 32.5	527.0	-0.1	-26.2	1.9	22.7	11.9	7809.5
Fing A16-D7 33.5	528.0	-0.2	-27.5	2.0	23.1	11.4	7843.3
Fing A16-D7 34.5	529.0	0.1	-28.3	1.9	22.6	11.7	7877.2
Fing A16-D7 36.5	531.0	0.4	-28.5	1.5	17.5	11.5	7944.9
Fing A16-D7 37.5	532.0	0.6	-28.8	1.4	15.8	11.5	7978.8
Fing A16-D7 38.5	533.0	0.8	-28.4	1.4	17.3	12.0	8012.6
Fing A16-D7 40.5	535.0	0.3	-26.9	1.7	21.1	12.4	8080.4
Fing A16-D7 41.5	536.0	0.4	-26.4	1.7	22.0	12.9	8114.2
Fing A16-D7 42.5	537.0	0.6	-26.3	1.6	21.0	12.9	8148.1
Fing A16-D7 44.5	539.0	0.4	-28.2	1.9	22.5	12.1	8215.8
Fing A16-D7 45.5	540.0	0.4	-25.3	2.2	31.1	13.9	8249.6
Fing A16-D7 46.5	541.0	0.4	-25.3	2.1	29.2	13.8	8283.5
Fing A16-D7 48.5	543.0	0.2	-25.3	2.1	29.7	14.1	8351.2
Fing A16-D7 49.5	544.0	0.2	-25.7	2.2	29.3	13.5	8385.1
Fing A16-D7 50.5	545.0	0.2	-25.4	1.9	26.2	13.6	8418.9
Fing A16-D7 52.5	547.0	0.1	-25.8	2.0	27.3	13.6	8486.7
Fing A16-D7 53.5	548.0	0.1	-25.9	1.8	24.4	13.4	8520.5
Fing A16-D7 54.5	549.0	0.0	-25.2	2.2	30.2	13.6	8554.4
Fing A16-D7 56.5	551.0	0.0	-25.2	2.3	31.4	13.8	8622.1
Fing A16-D7 57.5	552.0	0.1	-24.9	2.1	27.3	13.3	8656.0
Fing A16-D7 58.5	553.0	0.1	-26.7	1.8	24.3	13.2	8689.8
Fing A16-D7 60.5	555.0	0.0	-27.5	1.6	20.7	13.0	8757.5
Fing A16-D7 61.5	556.0	0.1	-25.8	2.4	32.4	13.5	8791.4
Fing A16-D7 62.5	557.0	0.1	-26.5	2.3	31.3	13.6	8825.3
Fing A16-D7 64.5	559.0	0.0	-26.5	2.3	31.7	13.9	8893.0
Fing A16-D7 65.5	560.0	0.1	-26.4	2.3	31.1	13.3	8926.8
Fing A16-D7 66.5	561.0	0.1	-26.7	2.2	29.0	13.4	8960.7
Fing A16-D7 68.5	563.0	0.4	-26.8	2.3	30.3	13.5	9028.4
Fing A16-D7 69.5	564.0	0.3	-27.1	2.3	30.4	13.2	9062.3
Fing A16-D7 70.5	565.0	0.1	-26.6	2.4	32.3	13.5	9096.1
Fing A16-D7 72.5	567.0	0.2	-27.7	1.8	24.5	13.3	9177.3
Fing A16-D7 73.5	568.0	0.2	-26.3	2.2	30.8	13.9	9224.6
Fing A16-D7 74.5	569.0	0.0	-27.4	2.3	31.6	13.5	9271.9
Fing A16-D7 76.5	571.0	0.3	-27.8	2.3	30.9	13.7	9366.4
Fing A16-D7 77.5	572.0	0.2	-28.3	2.2	30.3	13.7	9413.7
Fing A16-D7 78.5	573.0	-0.1	-28.6	2.2	29.5	13.7	9461.0
Fing A16-D7 80.5	575.0	0.3	-29.7	1.9	25.9	13.9	9555.6
Fing A16-D7 81.5	576.0	0.4	-29.1	1.9	26.5	13.8	9602.9
Fing A16-D7 82.5	577.0	0.0	-28.1	2.0	27.3	13.7	9650.1
Fing A16-D7 84.5	579.0	0.3	-30.0	2.1	28.2	13.7	9744.7
Fing A16-D7 85.5	580.0	0.3	-30.4	2.2	30.3	13.6	9792.0
Fing A16-D7 86.5	581.0	0.3	-30.6	2.1	29.1	14.2	9839.3
Fing A16-D7 88.5	583.0	0.7	-30.8	1.9	25.5	13.7	9933.9
Fing A16-D7 89.5	584.0	1.0	-30.3	1.9	26.9	14.5	9981.1
Fing A16-D7 90.5	585.0	1.0	-31.0	1.9	26.9	14.3	10028.4
Fing A16-D7 92.5	587.0	0.5	-30.1	2.0	28.7	14.4	10123.0
Fing A16-D7 93.5	588.0	1.0	-30.3	2.0	28.7	14.3	10170.3
Fing A16-D7 94.5	589.0	1.1	-29.7	2.1	30.7	14.4	10217.6
Fing A16-D8 16.5	591.0	0.5	-28.7	1.3	16.3	12.8	10312.1
Fing A16-D8 17.5	592.0	0.2	-27.0	1.4	17.1	12.6	10359.4
Fing A16-D8 18.5	593.0	-0.2	-27.3	0.7	8.5	12.1	10406.7
Fing A16-D8 19.5	594.0	0.2	-27.9	1.2	14.5	12.0	10454.0
Fing A16-D8 20.5	595.0	-0.2	-26.5	1.6	18.0	11.1	10501.3
Fing A16-D8 21.5	596.0	0.4	-28.0	1.1	12.1	11.1	10548.6
Fing A16-D8 22.5	597.0	-0.1	-28.2	1.4	14.8	11.0	10595.9
Fing A16-D8 24.5	599.0	0.5	-26.7	1.2	13.6	11.7	10690.4
Fing A16-D8 25.5	600.0	-0.1	-25.9	1.4	16.5	11.5	10737.7
Fing A16-D8 26.5	601.0	-0.4	-25.8	1.3	14.5	11.5	10785.0
Fing A16-D8 28.5	603.0	-0.1	-27.1	0.9	10.4	11.7	10879.6
Fing A16-D8 29.5	604.0	0.2	-26.8	1.0	11.8	11.6	10926.9
Fing A16-D8 30.5	605.0	-0.6	-26.8	1.0	12.1	11.8	10974.1
Fing A16-D8 32.5	607.0	-0.1	-26.9	1.0	11.6	11.6	11068.7

Fing A16-D8 33.5	608.0	-0.4	-26.7	0.7	8.6	11.6	11116.0
Fing A16-D8 34.5	609.0	0.3	-26.9	0.9	9.8	11.4	11163.3
Fing A16-D8 36.5	611.0	0.5	-27.3	0.8	8.9	11.7	11257.9
Fing A16-D8 37.5	612.0	0.6	-27.6	0.6	7.2	12.0	11305.1
Fing A16-D8 38.5	613.0	0.2	-27.8	0.5	5.7	11.6	11352.4
Fing A16-D8 40.5	615.0	-0.5	-27.2	0.9	9.3	10.5	11447.0
Fing A16-D8 41.5	616.0	-0.5	-27.1	0.6	6.5	10.7	11494.3
Fing A16-D8 42.5	617.0	-0.1	-27.9	0.9	9.2	10.4	11541.6
Fing A16-D8 44.5	619.0	-0.4	-28.9	0.6	7.1	11.5	11636.1
Fing A16-D8 45.5	620.0	-0.6	-29.0	0.8	8.5	10.5	11683.4
Fing A16-D8 46.5	621.0	-0.1	-29.0	0.6	6.5	10.9	11730.7
Fing A16-D8 48.5	623.0	-0.1	-28.0	0.8	8.3	10.5	11825.3
Fing A16-D8 49.5	624.0	-0.3	-28.5	0.9	9.2	10.4	11872.6
Fing A16-D8 50.5	625.0	0.0	-28.9	0.7	7.8	10.9	11919.9
Fing A16-D8 52.5	627.0	-0.2	-29.3	0.8	8.9	11.1	12014.4
Fing A16-D8 53.5	628.0	0.1	-29.8	1.0	10.1	10.5	12061.7
Fing A16-D8 54.5	629.0	0.4	-28.8	1.1	11.8	10.8	12109.0
Fing A16-D8 56.5	631.0	0.4	-29.2	1.3	14.4	11.2	12203.6
Fing A16-D8 57.5	632.0	0.0	-28.4	1.3	14.7	11.2	12250.9
Fing A16-D8 58.5	633.0	0.2	-29.9	0.9	11.9	13.1	12298.1
Fing A16-D8 60.5	635.0	0.0	-28.7	1.1	11.9	10.9	12392.7
Fing A16-D8 61.5	636.0	-0.3	-28.3	0.9	9.9	10.6	12440.0
Fing A16-D8 62.5	637.0	-0.4	-29.1	1.0	10.2	10.6	12487.3
Fing A16-D8 64.5	639.0	-0.4	-29.0	1.3	13.4	10.5	12581.9
Fing A16-D8 65.5	640.0	-0.5	-29.7	0.8	9.3	11.6	12629.1
Fing A16-D8 66.5	641.0	-0.4	-28.5	1.1	10.7	10.2	12676.4
Fing A16-D8 68.5	643.0	-0.3	-28.6	0.8	8.1	10.1	12771.0
Fing A16-D8 69.5	644.0	-0.3	-29.2	0.9	9.5	10.9	12818.3
Fing A16-D8 70.5	645.0	-0.2	-29.7	1.0	10.9	11.4	12865.6
Fing A16-D8 72.5	647.0	0.2	-29.8	1.0	11.6	11.7	12960.1
Fing A16-D8 73.5	648.0	0.2	-30.8	0.8	10.1	12.4	13007.4
Fing A16-D8 74.5	649.0	0.5	-31.0	0.4	5.0	12.8	13054.7
Fing A16-D8 76.5	651.0	0.0	-30.6	0.5	6.3	11.8	13149.3
Fing A16-D8 77.5	652.0	0.0	-30.2	0.6	6.4	11.7	13196.6
Fing A16-D8 78.5	653.0	0.0	-30.5	0.6	7.7	12.9	13243.9
Fing A16-D8 80.5	655.0	0.1	-29.6	0.5	6.0	11.8	13338.4
Fing A16-D8 81.5	656.0	0.1	-29.8	0.7	8.8	12.1	13385.7
Fing A16-D8 82.5	657.0	0.1	-30.1	0.8	9.3	12.0	13433.0
Fing A16-D8 84.5	659.0	-0.4	-30.4	0.4	5.1	12.1	13527.6
Fing A16-D8 85.5	660.0	-1.0	-29.5	0.8	8.4	10.2	13574.9
Fing A16-D8 86.5	661.0	-0.4	-29.7	0.8	7.7	10.3	13622.1
Fing A16-D8 88.5	663.0	-0.6	-29.4	0.1	1.7	12.1	13716.7

## D. Age Data Tables

### LEAD-210

Top(cm)	Base(cm)	Mid(cm)	Age: Base(yr)	Error(±s.d.)	Date Base(AD)	Date Mid(AD)	DMAR(g/cm <sup>2</sup> yr)	DMAR Error(±s.d.)
0	0.5	0.25	0.75	2.68	2015.5	2015.9	0.0399	0.0034
3	3.5	3.25	7.68	2.14	2008.6	2009.2	0.0679	0.0037
6	6.5	6.25	16.08	2.11	2000.2	2001.0	0.0653	0.0037
8	8.5	8.25	23.73	2.21	1992.5	1993.6	0.0487	0.0026
9.5	10	9.75	30.10	2.26	1986.1	1987.2	0.0519	0.0033
11	11.5	11.25	37.26	2.44	1979.0	1980.3	0.0410	0.0028
13	13.5	13.25	48.82	2.74	1967.4	1969.0	0.0341	0.0028
14.5	15	14.75	60.36	3.35	1955.9	1958.1	0.0265	0.0026
15.5	16	15.75	68.91	4.00	1947.3	1949.5	0.0266	0.0033
16.5	17	16.75	79.23	5.18	1937.0	1939.8	0.0210	0.0033
17.5	18	17.75	90.22	6.86	1926.0	1928.8	0.0224	0.0047
18.5	19	18.75	103.67	10.13	1912.6	1916.2	0.0157	0.0046
19.5	20	19.75	119.12	15.95	1897.1	1901.1	0.0148	0.0067
20	20.5	20.25	129.41	21.82	1886.8	1892.0	0.0103	0.0061
21.5	22	21.75	165.03	58.98	1851.2	1857.0	0.0111	0.0179

### CARBON-14

Sample	Depth	14C AGE	±	1-Sigma	Mean	Error of Mean	Lab/Date
FingA16-D2-29.0 cm	48	430	15	494-506	500	6	WHOI 7/26/2021
FingA16-D2-93.0 cm	112	1100	25	958-1053	1000	47.5	WHOI 7/26/2021
FingA16-D2-138.5 cm	157.5	1210	20	1075-1164	1126	44.5	WHOI 7/26/2021
FingA16-D3-52-53cm	226	1800	170	1535-1923	1730	388	LLNL 9/1/2018
FingA16-D5-36-37cm	370	3400	60	3568-3719	3650	151	LLNL 8/1/2018
FingA16-D5-94 cm	428	4400	40	4950-5040	4970	45	WHOI 7/26/2021
FingA16-D6-38 cm	445	4670	40	5321-5463	5400	70.5	WHOI 7/26/2021
FingA16-D7-14-15cm	509	6245	30	7162-7245	7200	83	LLNL 8/1/2018
FingA16-D7-72 cm	566	8170	75	9013-9143	9130	65	WHOI 8/5/21
FingA16-D8-76 cm	650	11200	220	12895-13303	13102	204	WHOI 8/5/21